Generalized Frequency Modulation

by

Wade P. Torres

B.S., Electrical Engineering and Mathematics (1995)
Southern Illinois University

M.S. Electrical Engineering (1997)
Massachusetts Institute of Technology

Submitted to the Department of Electrical Engineering and Computer Science
in partial fulfillment of the requirements for the degree of

Doctor of Philosophy

at the

MASSACHUSETTS INSTITUTE OF TECHNOLOGY

September 2001

Author .....
Department of Electrical Engineering and Computer Science
August 24, 2001

Certified by .....
Alan V. Oppenheim
Ford Professor of Engineering
Thesis Supervisor

Accepted by .....
Arthur C. Smith
Chairman, Department Committee on Graduate Students

Generalized Frequency Modulation

by

Wade P. Torres

Submitted to the Department of Electrical Engineering and Computer Science
on August 24, 2001, in partial fulfillment of the
requirements for the degree of
Doctor of Philosophy

Abstract

In frequency modulation (FM) systems, a continuous-time information signal is modulated onto a sinusoidal carrier wave by using the information signal to modulate the frequency of the carrier wave. In this thesis, a more general type of modulation is developed, of which FM is a special case, that we refer to as rate modulation. A rate modulation system consists of a dynamical system whose rate of evolution is varied in proportion to an information signal. The rate-modulated carrier wave is a scalar function of the state variables of the modulator.

The thesis is focused on three aspects of rate modulation and demodulation systems. First, explicit expressions are derived for the power density spectrum of the rate modulated carrier wave for sinusoidal modulation. Second, a systematic procedure is derived for constructing demodulators. This procedure requires that the dynamical system used in the modulator has a known exponentially convergent observer. Assuming such an observer is known, a systematic procedure for constructing demodulators is given that depends on the underlying dynamical system in a simple manner. Finally, the quasi-moment neglect closure technique is used to approximate the signal-to-noise ratio when the carrier wave is corrupted by additive white-noise.

Thesis Supervisor: Alan V. Oppenheim
Title: Ford Professor of Engineering

Acknowledgments

I would like to first thank Professor Alan Oppenheim for taking me under his wing, then shoving me out of the nest, guiding me while I flailed and flapped about frantically, and then helping me land gracefully. The Ph.D. experience involves much more than just research, and I was very fortunate that I could turn to him as a friend.

I would also like to thank Professor R. Ruben Rosales. He has had a tremendous impact on how I think about research and engineering. Working closely with him has made my graduate studies extremely rewarding.

Many people have helped me along the way. Professor Anantha Chandrakasan served on my thesis committee and as a thesis reader. Professor George Verghese and Professor John Wyatt helped me formulate and think about aspects of this thesis, as did members of the Digital Signal Processing Group - Nick Laneman, Andrew Russell, Stark Draper, Kathleen Wage, and Chris Hadjicostis. Of course, as all graduate students eventually realize, the non-technical benefits of being in a research group outweigh the technical benefits. For those other things, I would like to thank, in addition to those already mentioned, Matt Secor, Yonina Eldar, Maya Said, Charles Sestok, Emin Martinian, Everest Huang, Micheal Lopez, Li Lee, Albert Chan, Petros Boufounos, Huan Yao, Brian Chen, Richard Barron, and, of course, Giovanni Aliberti. Thanks also to Darla Secor and Dianne Wheeler for administrative support and mediating the informal DSPG chat forums held in 36-615.

I would like to thank the National Science Foundation and AT&T Laboratories for supporting me throughout my graduate studies. I would like also like to thank Dr. Rick Rose for being my mentor in the AT&T Laboratories program.

None of this would have been possible without my mother, father, grandmother, and great-grandmother keeping me pointed in more or less the right direction as I was growing up. I owe all my success to them.

Finally, I would like to thank my family, Donna and Xavier, for supporting me through all of this. I am truly lucky to have both of you in my life, and I love you more than anything.

In loving memory of my great-grandmother, Ethel Porter.

Contents

List of Figures

List of Tables

Chapter 1

Introduction

Frequency modulation (FM) systems modulate a continuous-time information signal onto a sinusoidal carrier wave by varying the frequency of the carrier wave in a manner proportional to the information signal. FM is a special case of a more general type of modulation developed in this thesis that is referred to as rate modulation. A rate modulated system is a dynamical system whose rate of evolution is modulated proportional to an information signal. The carrier wave is a scalar function, possibly nonlinear, of the state of the modulated dynamical system. Our approach to demodulation requires that the dynamical system used in the modulator have a known exponentially convergent observer. From such an observer, a demodulator is systematically constructed. The focus of this thesis is on the fundamental aspects of rate modulation and demodulation. In particular, the effect that modulation has on the bandwidth of the carrier wave is analyzed, a systematic procedure for the construction of demodulators is developed, and the robustness of the demodulator with respect to additive noise is analyzed.

The potential advantages of our rate modulation scheme result from the ability to use nonlinear systems and to choose the carrier wave from a large class of signals. For example, chaotic systems are nonlinear systems that are among the class of systems to which our approach to rate modulation and demodulation can be applied. Chaotic systems are potentially advantageous for communications because they produce naturally spread-spectrum signals. Also, chaotic signals are difficult to predict, which

suggests that they are less susceptible to eavesdropping. Also among the class of potential rate modulation systems are simple nonlinear oscillators, such as the Duffing oscillator and the van der Pol oscillator. Many of these nonlinear oscillators are appealing because they have very simple circuit implementations.

1.1 Outline of the Thesis

In Chapter 2, rate modulation of dynamical systems is described along with its relation to FM. The power density spectrum of the modulated carrier wave is shown to be related to the power density spectrum of the unmodulated carrier wave through a linear integral transform. For certain types of modulation, it is possible to determine the kernel of the integral transform and determine the power density spectrum of the modulated carrier wave from the power density spectrum of the unmodulated carrier wave.

In Chapter 3, a general procedure for constructing demodulators is described. The dynamical system used in the modulator is assumed to have a known exponentially convergent observer. Based on a new perturbation technique developed in this thesis, the observer is systematically modified so that it recovers the information signal from the modulated carrier waveform. Examples of demodulators are presented based on the van der Pol oscillator and the chaotic Lorenz system. The remainder of the chapter covers three ways in which the demodulator can be enhanced. First, the demodulator is modified to track signals that vary at a higher rate. Second, a filter is added to smooth the rate estimate and potentially improve performance of the demodulator in the presence of noise. Finally, the demodulator is approximated in a manner that reduces the number of nonlinearities. This approximation is shown to be equivalent to a least squares solution for tracking the modulating signal.

Chapter 4 presents a technique for approximately analyzing the effects of additive noise on the demodulator for the high signal-to-noise ratio (SNR) case. The technique is called the quasi-moment neglect closure (QMNC) technique and is a method for approximating the probability distributions of the state variables of dynamical sys-

tems that are driven by white noise [8]. From these distributions, the signal-to-noise ratio at the output of the demodulator is computed. Three systems are analyzed with the QMNC technique. The first system is based on a nonlinear oscillator that can be used to demodulate FM signals. The next system is based on the Van der Pol oscillator and the last is based on the chaotic Lorenz system.

In Chapter 5, a hardware implementation of the Lorenz based modulator and demodulator is described. The circuit is built using operational amplifiers, analog multipliers, capacitors, and resistors. The chapter contains discussion on some of the design issues that were encountered in building the system, such as the circuit board layout, building materials, shielding of sensitive traces, and component selection. The chapter concludes with examples of the modulation and demodulation of a pure sine wave and a speech signal.

Chapter 6 summarizes the contributions of the thesis an suggests directions for further study.

Chapter 2

Modulation

Traditional FM signals are sinusoids whose frequency varies proportional to an information signal. An FM signal can be generated by using an information signal to modulate the rate at which a harmonic oscillator evolves. The FM signal is then obtained by taking a linear combination of the state variables of the modulated harmonic oscillator. Interpreting FM in this manner leads to the more general concept, which is referred to as rate modulation, that is developed in this thesis. A rate modulated signal is a scalar function of the state variables of a dynamical system whose rate of evolution is modulated by an information signal.

In the first half of this chapter, rate modulation is described in detail. In the second half of this chapter, the effect that modulation has on the power density spectrum of the carrier wave is explored, and the conditions are described under which the power density spectrum of the modulated signal can be determined explicitly in terms of the power density spectrum of the unmodulated carrier wave.

2.1 Rate Modulation

An FM signal has the form

$$y_m(t) = A\cos(\omega_c t + \beta\int_0^t m(\tau)d\tau) \qquad t > 0, \tag{2.1}$$

where $m(t)$ is the information signal, ω_c is the carrier frequency, A is a gain constant, and β is the modulation index. The instantaneous frequency of the FM signal is $\omega_c + \beta m(t)$, which is assumed to be positive, that is, $\omega_c > |\beta m(t)|$ for all $t > 0$. The unmodulated carrier wave, $y(t) = A\cos(\omega_c t)$, can be generated by a harmonic oscillator,

$$\begin{aligned} \dot{x}_1 &= -\omega_c x_2, \\ \dot{x}_2 &= \omega_c x_1. \end{aligned} \tag{2.2}$$

If $x_1(0) = 1$ and $x_2(0) = 0$, then $x_1(t) = \cos(\omega_c t)$ and $x_2(t) = \sin(\omega_c t)$. In this case, the carrier is a linear combination of the state variables, $y = a_1 x_1 + a_2 x_2$, with $a_1 = A$ and $a_2 = 0$. To produce the FM signal in (2.1), the gradient vector of the harmonic oscillator in (2.2) is scaled proportional to the information signal, that is,

$$\begin{aligned} \dot{x}_1 &= -\big(\omega_c + \beta m(t)\big)x_2, \\ \dot{x}_2 &= \big(\omega_c + \beta m(t)\big)x_1. \end{aligned} \tag{2.3}$$

With $x_1(0) = 1$ and $x_2(0) = 0$, the solution to (2.3) is

$$\begin{aligned} x_1(t) &= \cos\big(\omega_c t + \beta \int_0^t m(\tau)d\tau\big), \\ x_2(t) &= \sin\big(\omega_c t + \beta \int_0^t m(\tau)d\tau\big). \end{aligned} \tag{2.4}$$

To verify that (2.4) is a solution to (2.3), $x_1(t)$ and $x_2(t)$ are differentiated to get

$$\begin{aligned} \dot{x}_1 &= -(\omega_c + \beta m(t)) \sin\big(\omega_c t + \beta \int_0^t m(\tau)d\tau\big) = -(\omega_c + \beta m(t))x_2, \\ \dot{x}_2 &= (\omega_c + \beta m(t)) \cos\big(\omega_c t + \beta \int_0^t m(\tau)d\tau\big) = (\omega_c + \beta m(t))x_1. \end{aligned} \tag{2.5}$$

Assuming $m(t)$ is continuous, the solution to (2.3) is unique [6], and since (2.2) and (2.3) have the same initial conditions, (2.4) is the unique solution to (2.3).

In Figure 2-1, the state-space trajectory of the harmonic oscillator is shown. The gradient vector points in the direction of the trajectory that the states of the dynamical system follow. The length of the gradient vector determines the rate at which the system travels along its trajectory. Since an FM signal can be generated by scaling the gradient vector of a harmonic oscillator as in (2.3), FM can be interpreted as rate modulation of a harmonic oscillator.

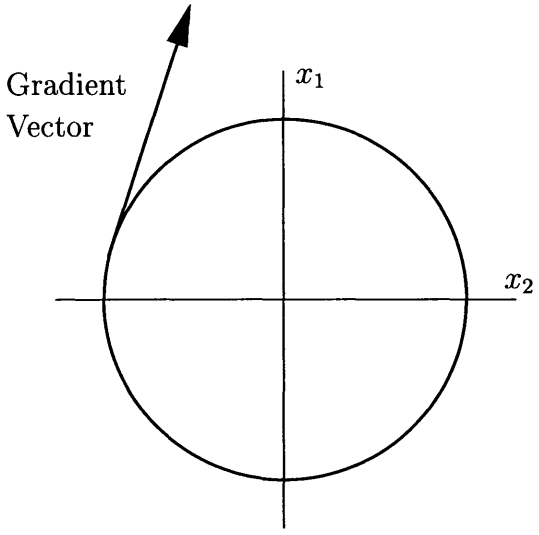

Figure 2-1: A state-space perspective of frequency modulation.

The rate modulation interpretation of FM can be extended to any dynamical system[1]. For example, consider an arbitrary dynamical system given by

$$\dot{\mathbf{x}}_{\text{nom}} = \mathbf{f}(\mathbf{x}_{\text{nom}}), \tag{2.6}$$

where $\mathbf{x}_{\text{nom}}$ and $\mathbf{f}(\mathbf{x}_{\text{nom}})$ are both N-dimensional vectors. Modulation is introduced

[1] However, for the class of demodulators discussed in Chapter 3, the dynamical system must have a known exponentially convergent observer.

by scaling the gradient vector,

$$\dot{\mathbf{x}}_{\text{mod}} = \big(\omega_c + \beta m(t)\big)\mathbf{f}(\mathbf{x}_{\text{mod}}), \tag{2.7}$$

where $\omega_c > |\beta m(t)|$ for all t. Similar to FM, the carrier wave is a scalar function of the state variables. Specifically, the transmitted signal is

$$y = h(\mathbf{x}), \tag{2.8}$$

where $h(\cdot)$ is a possibly nonlinear function that maps the N-dimensional state-space vector to a scalar function. The demodulators discussed in Chapter 3 require that $h(\mathbf{x})$ be chosen so that $\nabla h(\mathbf{x}) = 0$ only at isolated points along the orbit of the dynamical system[2].

The state variables of the modulated system can be expressed in terms of the nominal system in (2.6) in a manner similar to that of FM. Let $\mathbf{x}_{\text{mod}}(t)$ be the solution of the modulated system in (2.7) with $\mathbf{x}_{\text{mod}} = \mathbf{c}_0$, and let $\mathbf{x}_{\text{nom}}(t)$ be the solution of the nominal system in (2.6) with $\mathbf{x}_{\text{nom}}(0) = \mathbf{x}_{\text{mod}}(0)$. Then $\mathbf{x}_{\text{mod}}(t)$ is related to $\mathbf{x}_{\text{nom}}(t)$ by

$$\mathbf{x}_{\text{mod}}(t) = \mathbf{x}_{\text{nom}}\big(\omega_c t + \beta \int_0^t m(\tau)d\tau\big). \tag{2.9}$$

This relationship is verified by showing that $\mathbf{x}_{\text{nom}}(\omega_c t + \beta \int_0^t m(\tau)d\tau)$ satisfies (2.7). Taking the derivative of $\mathbf{x}_{\text{nom}}(\omega_c t + \beta \int_0^t m(\tau)d\tau)$ with respect to time gives

$$\frac{d}{dt}\Big\{\mathbf{x}_{\text{nom}}\big(\omega_c t + \beta \int_0^t m(\tau)d\tau\big)\Big\} = \big(\omega_c + \beta m(t)\big)\mathbf{f}\big(\mathbf{x}_{\text{nom}}\big(\omega_c t + \beta \int_0^t m(\tau)d\tau\big)\big). \tag{2.10}$$

Substituting (2.9) into (2.10) gives the relationship in (2.7). Therefore, $\mathbf{x}_{\text{mod}}(t) =$

[2] $\nabla h(\mathbf{x})$ is the gradient of $h(\mathbf{x})$, that is,

$$\nabla h(\mathbf{x}) = \left[\frac{\partial h(\mathbf{x})}{\partial x_1} \quad \cdots \quad \frac{\partial h(\mathbf{x})}{\partial x_n}\right].$$

$\mathbf{x}_{\text{nom}}\big(\omega_c t + \beta \int_0^t m(\tau)d\tau\big)$ is a solution to (2.7). If the solution to (2.6) is unique and $m(t)$ is continuous and bounded, then the solution to (2.7) is also unique [6]. Since $\mathbf{x}_{\text{mod}}(0) = \mathbf{x}_{\text{nom}}(0)$, $\mathbf{x}_{\text{mod}}(t) = \mathbf{x}_{\text{nom}}\big(\omega_c t + \beta \int_0^t m(\tau)d\tau\big)$ is the unique solution to (2.7).

Returning to FM, any dynamical system that has a sinusoidal solution for at least one state variable can be used to generate an FM signal. Suppose that state variable $x_1(t)$ of (2.6) is a sinusoid, for example $x_1(t) = \sin(t)$. Applying the result given in (2.9), the modulated system produces a signal

$$x_1(t) = \sin\big(\omega_c t + \beta \int_0^t m(\tau)d\tau\big), \tag{2.11}$$

which is an FM signal.

As an example of using a different dynamical system for carrier wave generation, the rate modulation procedure is applied to the Lorenz system. The Lorenz system is a simplified model of fluid convection [7] and is given by

$$\begin{aligned} \dot{x_1} &= \sigma(x_2 - x_1), \\ \dot{x_2} &= r x_1 - x_1 x_3 - x_2, \\ \dot{x_3} &= x_1 x_2 - b x_3, \end{aligned} \tag{2.12}$$

For appropriate choices of the constants σ, r, and b, the Lorenz system is chaotic. Chaotic systems are generally defined as those with bounded solutions that exhibit long-term aperiodic behavior and have a sensitive dependence on initial conditions. Applying the modulation procedure to these equations results in

$$\begin{aligned} \dot{x_1} &= \big(\omega_c + \beta m(t)\big)\sigma(x_2 - x_1) \\ \dot{x_2} &= \big(\omega_c + \beta m(t)\big)(r x_1 - x_1 x_3 - x_2) \\ \dot{x_3} &= \big(\omega_c + \beta m(t)\big)(x_1 x_2 - b x_3) \end{aligned} \tag{2.13}$$

Figure 2-2 shows a comparison between the trajectories of the Lorenz system without modulation, as given in (2.12), and the trajectories of the Lorenz system with modulation, as given in (2.13), when the modulating signal is $m(t) = \sin(0.2t)$. Just

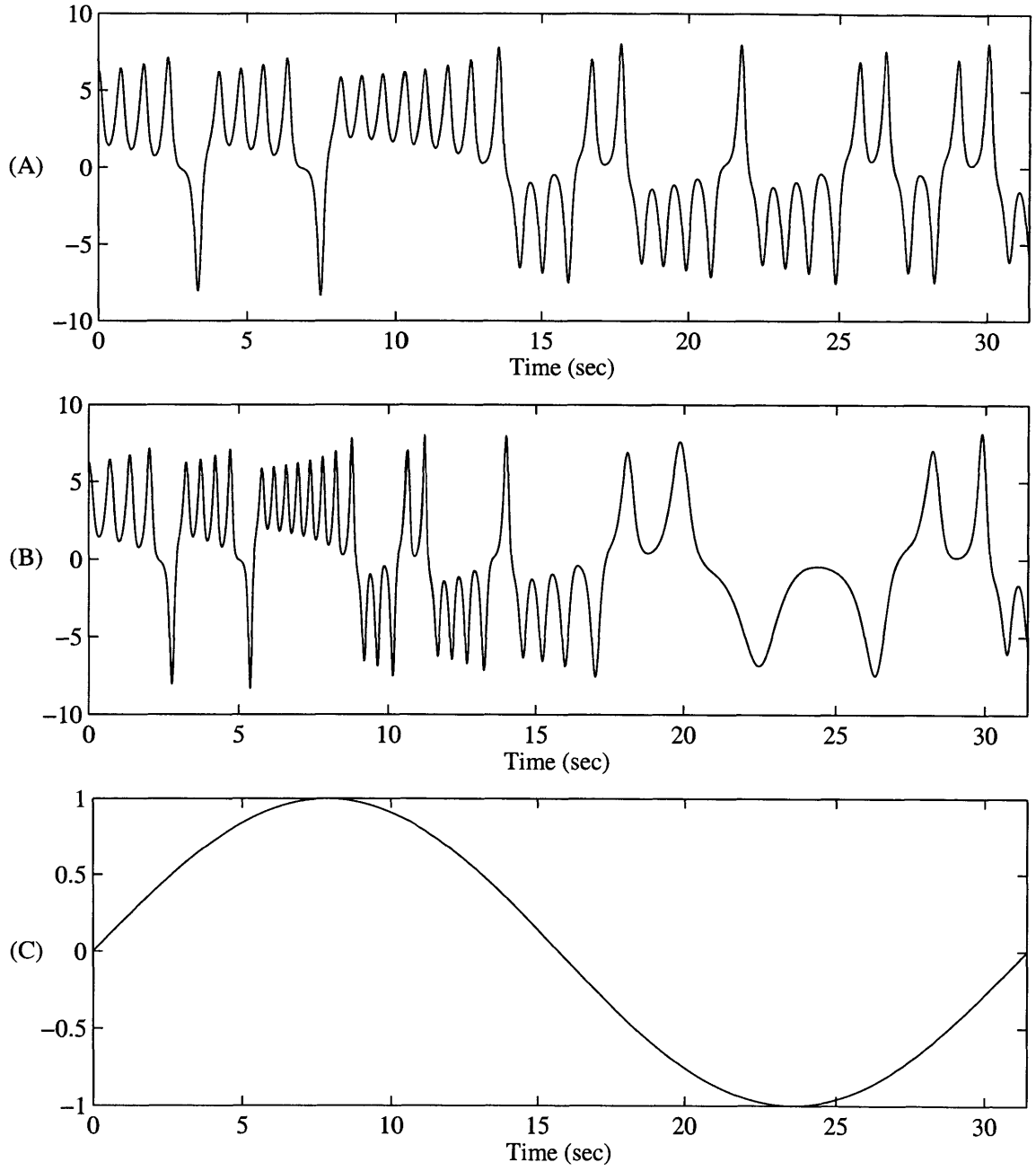

Figure 2-2: The effect of sinusoidal modulation on the Lorenz system: (A) $x_1(t)$ without modulation, (B) $x_1(t)$ with $\omega_c = 1$, $m(t) = \sin(0.2t)$, and $\beta = 0.8$, and (C) $m(t)$.

as with FM, the carrier wave is dilated and compressed in time proportional to $m(t)$, while the amplitude remains unaltered.

2.2 Power Density Spectrum of Rate-Modulated Carrier Waves

Although the bandwidth of an FM signal is infinite, most of its power lies within a finite frequency range and, for practical purposes, any signal power outside of this range is negligible. For example, Carson's rule states that ninety-eight percent of the power of an FM signal lies within a spectral range of $2(\beta + 1)\omega_m$ when $m(t) = \omega_m \sin(\omega_m t)$. In this section, the power density spectrums of rate modulated signals are analyzed.

In this section, the usual definitions of the autocorrelation function and the power density spectrum are used. Specifically, the time-average autocorrelation function of a finite power deterministic signal, $y(t)$, is defined as

$$R_y(\tau) = \lim_{T\to\infty} \frac{1}{2T} \int_{-T}^{T} y(t)y(t+\tau)dt. \tag{2.14}$$

The ensemble-average autocorrelation function of a stochastic process, $y_m(t)$, is defined as

$$R_{y_m}(t,\tau) = E[y_m(t)y_m(t+\tau)], \tag{2.15}$$

and the time-average autocorrelation function is

$$R_{y_m}(\tau) = \lim_{T\to\infty} \frac{1}{2T} \int_{-T}^{T} R_{y_m}(t,\tau)dt. \tag{2.16}$$

If $y_m(t)$ is a wide-sense stationary stochastic process, then (2.15) and (2.16) are equivalent. The power density spectrum is defined as the Fourier transform of the time-

average autocorrelation function, that is,

$$S_{y_m}(\omega) = \int_{-\infty}^{\infty} R_{y_m}(\tau) e^{-j\omega\tau} d\tau. \tag{2.17}$$

From the Wiener-Khintchine Theorem [3], if

$$\int_{-\infty}^{\infty} |\tau R_{y_m}(\tau)| d\tau < \infty, \tag{2.18}$$

then

$$S_{y_m}(\omega) = \lim_{T\to\infty} \left(\frac{E\left[|Y_{m,T}(\omega)|^2\right]}{2T} \right), \tag{2.19}$$

where

$$Y_{m,T}(\omega) = \int_{-T}^{T} y_m(t) e^{-j\omega t} dt. \tag{2.20}$$

In terms of the unmodulated carrier wave, the modulated carrier wave is

$$\begin{aligned} y_m(t) &= y\big(\omega_c t + \beta \int_0^t m(\tau) d\tau\big) \\ &= y\big(\omega_c t + \beta M(t)\big). \end{aligned} \tag{2.21}$$

When $M(t)$ is a stochastic process, the autocorrelation of $y_m(t)$ is, from (2.15),

$$R_{y_m}(t,\tau) = E[y\big(\omega_c(t+\tau) + \beta M(t+\tau)\big) y\big(\omega_c t + \beta M(t)\big)]. \tag{2.22}$$

Assuming $M(t)$ is a stationary process, (2.22) becomes

$$R_{y_m}(t,\tau) = E[y\big(\omega_c(t+\tau) + \beta M(\tau)\big) y\big(\omega_c t + \beta M(0)\big)]. \tag{2.23}$$

From (2.16), the time-average autocorrelation of $y_m(t)$ is

$$\begin{aligned} R_{y_m}(\tau) &= \lim_{T\to\infty} \frac{1}{2T} \int_{-T}^{T} E\big[y\big(\omega_c(t+\tau)+\beta M(\tau)\big)y\big(\omega_c t+\beta M(0)\big)\big]dt \\ &= E\Big[\lim_{T\to\infty} \frac{1}{2T} \int_{-T}^{T} y\big(\omega_c(t+\tau)+\beta M(\tau)\big)y\big(\omega_c t+\beta M(0)\big)dt\Big] \\ &= E\big[R_y\big(\omega_c\tau+\beta M(\tau)-\beta M(0)\big)\big], \end{aligned} \tag{2.24}$$

where $y(t)$ is assumed to be well-behaved so that the interchange of the expectation with the limit is allowed. From (2.17),

$$S_{y_m}(\omega) = \int_{-\infty}^{\infty} E\big[R_y\big(\omega_c\tau+\beta M(\tau)-\beta M(0)\big)\big]e^{-j\omega\tau}d\tau. \tag{2.25}$$

In the context of rate modulation, (2.25) can be interpreted in a meaningful way. The time-average autocorrelation function given in (2.24) can alternatively be arrived at by assuming that the modulating signal, $M(t)$, is independent of the position of $\mathbf{x}$ along its orbit. In this case, let θ be a random variable that is uniformly distributed on $[-T,T]$ and is independent of $M(t)$. First assume that $y(t)$ is periodic with period T. If $Y_m(t) = h\big(\mathbf{x}(t+\theta)\big) = y_m(t+\theta)$, then

$$R_{Y_m}(\tau) = \frac{1}{2T} \int_{-T}^{T} E[y(\omega_c(t+\tau+\theta)+\beta M(t+\tau+\theta))y(\omega_c(t+\theta)+\beta M(t+\theta))]d\theta. \tag{2.26}$$

For the general case in which $y(t)$ may not be periodic, the limit as the period of $y(t)$ goes to infinity is taken, in which case

$$R_{Y_m}(\tau) = \lim_{T\to\infty} \frac{1}{2T} \int_{-T}^{T} E[y(\omega_c(\tau+\theta)+\beta M(\tau))y(\omega_c(\theta)+\beta M(0))]d\theta, \tag{2.27}$$

which is the same as the time-average autocorrelation function given in (2.24). In other words, the power density spectrum of $y_m(t)$ given in (2.25) can be interpreted as

the expected power in $y_m(t)$ assuming that the position of $\mathbf{x}$ is randomly distributed along its orbit, independently of $M(t)$.

From (2.25), the relationship between the power density spectrum of $y_m(t)$ and the power density spectrum of $y(t)$ can be established. From the definition of the power density spectrum given in (2.17),

$$R_y(\tau) = \frac{1}{2\pi} \int_{-\infty}^{\infty} S_y(\lambda) e^{j\lambda\tau} d\lambda. \tag{2.28}$$

Substituting (2.28) into (2.25) results in

$$S_{y_m}(\omega) = \frac{1}{2\pi} \int_{-\infty}^{\infty} E\left[\int_{-\infty}^{\infty} S_y(\lambda) e^{j\lambda(\omega_c\tau + \beta M(\tau) - \beta M(0))} d\lambda \right] e^{-j\omega\tau} d\tau \tag{2.29}$$

$$= \frac{1}{2\pi} \int_{-\infty}^{\infty} S_y(\lambda) \int_{-\infty}^{\infty} E\left[e^{j\lambda\beta(M(\tau) - M(0))} \right] e^{-j(\omega - \omega_c\lambda)\tau} d\tau d\lambda \tag{2.30}$$

$$= \frac{1}{2\pi\omega_c} \int_{-\infty}^{\infty} S_y\left(\frac{\lambda}{\omega_c}\right) \int_{-\infty}^{\infty} E\left[e^{j\frac{\lambda\beta}{\omega_c}(M(\tau) - M(0))} \right] e^{-j(\omega - \lambda)\tau} d\tau d\lambda. \tag{2.31}$$

Defining the random variable α_τ to be $\alpha_\tau = M(\tau) - M(0)$, α_τ has a characteristic function given by

$$\phi(\omega, \tau) = E[e^{j\omega\alpha_\tau}]. \tag{2.32}$$

Substituting the characteristic equation of α_τ given in (2.32) into (2.31) gives

$$S_{y_m}(\omega) = \frac{1}{2\pi\omega_c} \int_{-\infty}^{\infty} S_y\left(\frac{\lambda}{\omega_c}\right) \int_{-\infty}^{\infty} \phi\left(\frac{\lambda\beta}{\omega_c}, \tau\right) e^{-j(\omega - \lambda)\tau} d\tau d\lambda. \tag{2.33}$$

Denoting the Fourier transform of $\phi(\lambda, \tau)$ as

$$\Phi(\lambda, \omega) = \int_{-\infty}^{\infty} \phi(\lambda, \tau) e^{-j\omega\tau} d\tau, \tag{2.34}$$

the expression in (2.33) becomes

$$S_{y_m}(\omega) = \frac{1}{2\pi\omega_c} \int_{-\infty}^{\infty} S_y\Big(\frac{\lambda}{\omega_c}\Big)\Phi\Big(\frac{\lambda\beta}{\omega_c}, \omega - \lambda\Big)d\lambda. \tag{2.35}$$

From (2.35), $S_{y_m}(\omega)$ and $S_y(\omega)$ are related through a linear integral transform where $\Phi\Big(\frac{\lambda\beta}{\omega_c}, \omega - \lambda\Big)$ is the transform kernel. Since the integral transform is linear, if the relationship between $S_{y_m}(\omega)$ and $S_y(\omega)$ is known for all $S_y(\omega) \in \mathcal{A}$, where $\mathcal{A}$ is some set of functions, then the relationship is known for all $S_y(\omega) \in \mathcal{B}$, where $\mathcal{B}$ is the set of all linear combinations of functions in $\mathcal{A}$. For many modulating signals, the power density spectrum corresponding to $R_{y_m}(\tau) = E[\cos\big(\omega_0\tau + \beta M(\tau) - \beta M(0)\big)]$ is known. For example, when $M(\tau) = \sin(\omega_m\tau + \theta)$, where θ is a random variable with a probability density function that is uniform on $[0, 2\pi]$, the power density spectrum of $y_m(t)$ is [11]

$$S_{y_m}(\omega) = \frac{1}{2}\sum_{k=-\infty}^{\infty} J_k^2(\beta)[\delta(\omega - \omega_c - k\omega_m) + \delta(\omega + \omega_c - k\omega_m)], \tag{2.36}$$

where $J_k(\cdot)$ is the k^{th} order Bessel function of the first kind. Comparing (2.36) with (2.35), the kernel of the integral transform is given by

$$\Phi\Big(\frac{\lambda\beta}{\omega_c}, \omega\Big) = \sum_{k=-\infty}^{\infty} J_k^2\Big(\frac{\lambda\beta}{\omega_c}\Big)\delta(\omega - k\omega_m). \tag{2.37}$$

From the linearity of the integral operator, $S_{y_m}(\omega)$ can be determined for any carrier wave, $y(t)$, that can be expressed as a linear combination of sinusoids.

Another example of a type of modulation for which $S_{y_m}(\omega)$ is known when $R_y(\tau) = \cos(\omega_0\tau)$ is the case in which $M(t)$ is a Gaussian random process with a power density spectrum given by

$$S_M(\omega) = \frac{2\pi\sigma^2}{\omega_m}\Pi\Big(\frac{\omega}{\omega_m}\Big), \tag{2.38}$$

where

$$\Pi(\omega) = \begin{cases} 1 & \omega \leq \frac{1}{2}, \\ 0 & \omega > \frac{1}{2}. \end{cases} \tag{2.39}$$

In this case, the power density spectrum of $y_m(t)$ is [13]

$$S_{y_m}(\omega) = \frac{1}{2}\sum_{k=0}^{\infty} \Pi\left(\frac{\beta\omega}{\omega_m}\right)^{(k)_*} [\delta(\omega - \omega_0) + \delta(\omega + \omega_0)], \tag{2.40}$$

where the notation $(k)_*$ denotes self-convolution k times, that is,

$$\begin{aligned} G(\omega)^{(0)_*} &= \delta(\omega) \\ G(\omega)^{(k)_*} &= G(\omega)^{(k-1)_*} * G(\omega). \end{aligned} \tag{2.41}$$

In this case,

$$\Phi\left(\frac{\lambda\beta}{\omega_c}, \omega\right) = \sum_{k=0}^{\infty} \Pi\left(\frac{\beta\lambda}{\omega_c\omega_m}\right)^{(k)_*}. \tag{2.42}$$

An explicit formula for each term in the right hand side of (2.42) is [12]

$$\Pi\left(\frac{\beta\omega}{\omega_c\omega_m}\right)^{(k)_*} = \sum_{n=0}^{k+1} \frac{(-1)^n}{k!}\binom{k+1}{n}\left(\frac{\beta\omega}{\omega_c\omega_m} + \frac{k+1}{2} - n\right)^k u\left(\frac{\beta\omega}{\omega_c\omega_m} + \frac{k+1}{2} - n\right), \tag{2.43}$$

where

$$u(\omega) = \begin{cases} 0 & \omega < 0, \\ 1 & \omega \geq 0. \end{cases} \tag{2.44}$$

Power Density Spectrum of a Modulated van der Pol Carrier The van der Pol oscillator is given by

$$\begin{aligned} \dot{x}_1 &= x_2, \\ \dot{x}_2 &= \lambda(1 - x_1^2)x_2 - x_1, \end{aligned} \tag{2.45}$$

where λ is a positive constant. An unmodulated carrier wave, such as $y(t) = x_1(t)$, is obtained by numerically integrating the van der Pol equations given in (2.45). A

plot of the unmodulated carrier wave and an estimate of its power density spectrum for $\lambda = 3$ is shown in Figure 2-3.

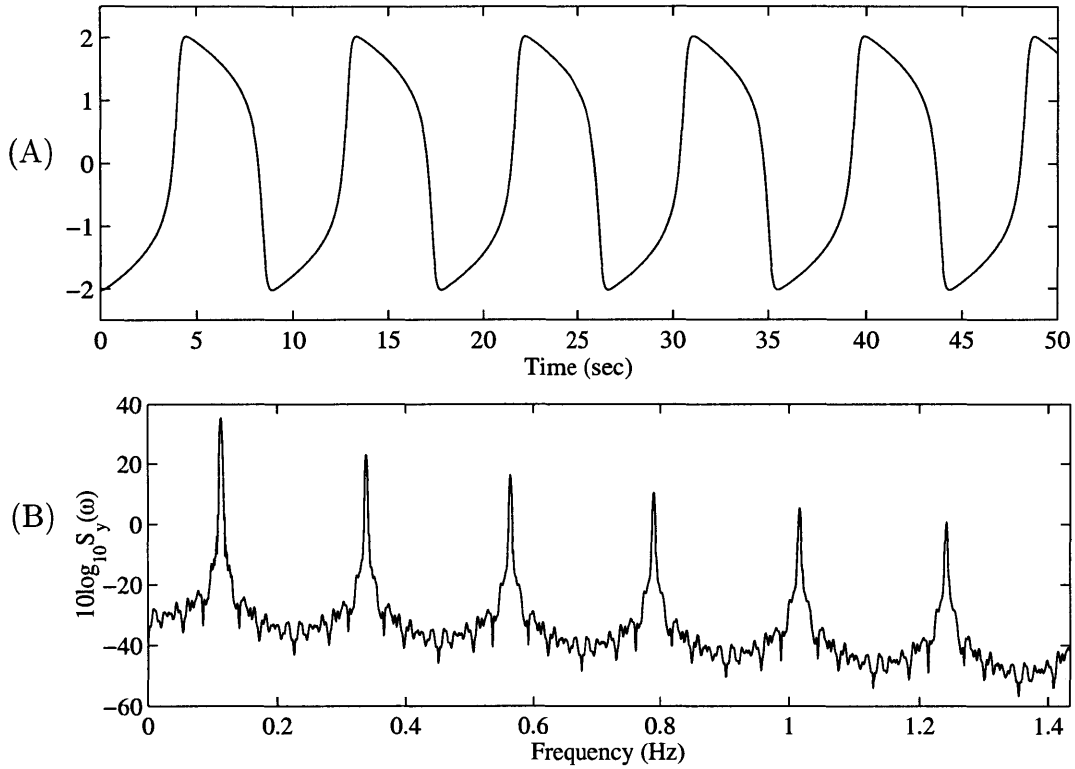

Figure 2-3: Unmodulated carrier wave (A) and its power density spectrum (B) for the van der Pol oscillator ($\lambda = 3$).

The modulated van der Pol equations are

$$\begin{aligned} \dot{x}_1 &= \big(\omega_c + \beta m(t)\big)x_2, \\ \dot{x}_2 &= \big(\omega_c + \beta m(t)\big)(\lambda(1 - x_1^2)x_2 - x_1), \\ y &= x_1, \end{aligned} \tag{2.46}$$

When $m(t) = \sin(\omega_m t + \theta)$, where θ is a random variable that is distributed uniformly on $[0, 2\pi]$, $M(t) = -\frac{1}{\omega_m}\cos(\omega_m t + \theta)$. The power density spectrum is, from (2.35) and (2.37),

$$S_{y_m}(\omega) = \frac{1}{2\pi\omega_c} \sum_{k=-\infty}^{\infty} \int_{-\infty}^{\infty} S_y\Big(\frac{\lambda}{\omega_c}\Big) J_k^2\Big(\frac{\lambda\beta}{\omega_m\omega_c}\Big)\delta(\omega - \lambda - k\omega_m)d\lambda. \tag{2.47}$$

Each term of the series in (2.47) can be generated by multiplying $S_y(\frac{\omega}{\omega_c})$ by $J_k^2(\frac{\beta\omega}{\omega_m\omega_c})$, and shifting the result by $k\omega_m$. An example of the estimated power density spectrum is shown in Figure 2-4.

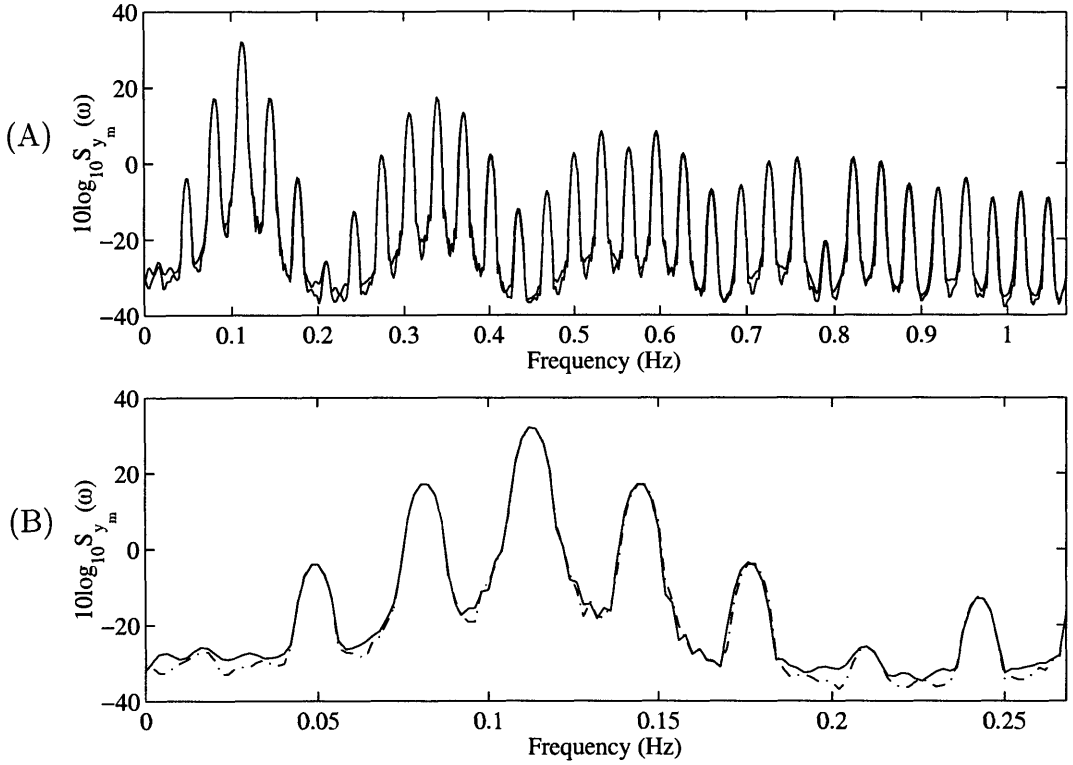

Figure 2-4: (A) Estimated power density spectrum of y_m for the van der Pol oscillator ($\omega_c = 1$, $\beta = 0.1$, $\omega_m = 0.2$), (B) Power density spectrum on an expanded scale - direct estimation (solid), estimation using (2.47) (dashed).

The advantage of using (2.47) over a direct simulation of (2.46) is that using (2.47) only requires the nominal system given in (2.45) to be numerically integrated once. Given the nominal carrier wave, computing the power density spectrum of the modulated carrier only involves scalar multiplications, shifts, and additions of the nominal power density spectrum.

Power Density Spectrum of a Modulated Lorenz Carrier The power density spectrum of a carrier wave generated from the Lorenz system, given in (2.12), can also be approached in the same manner. However, the power density spectrum of

the Lorenz system is closely approximated by a decaying exponential, as shown in Figure 2-5, and this can be exploited to derive a more direct representation for the power density spectrum when the modulation is sinusoidal. Returning to (2.29),

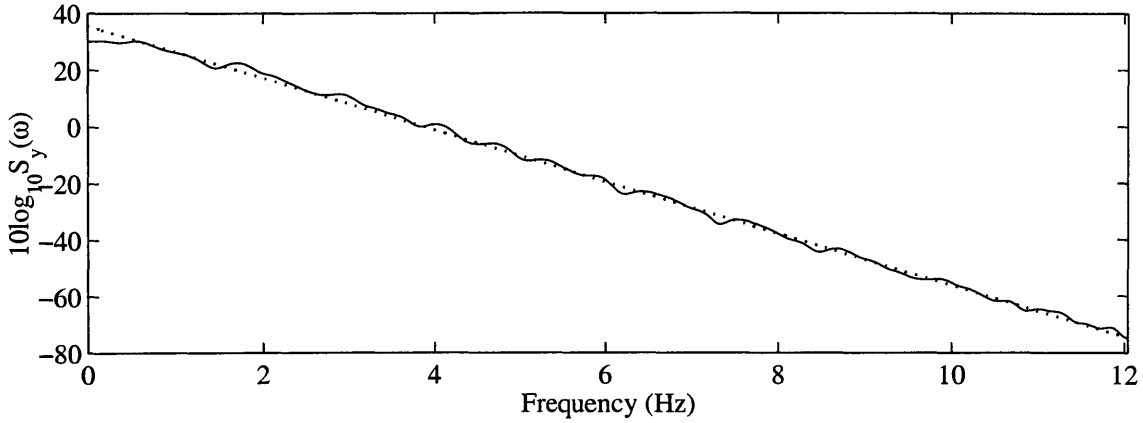

Figure 2-5: Estimated power density spectrum of the unmodulated Lorenz carrier wave (solid) and a decaying exponential approximation (dotted).

which is repeated in (2.48),

$$S_{y_m}(\omega) = \frac{1}{2\pi}\int_{-\infty}^{\infty} E\left[\int_{-\infty}^{\infty} S_y(\lambda)e^{j\lambda(\omega_c\tau+\beta M(\tau)-\beta M(0))}d\lambda\right]e^{-j\omega\tau}d\tau, \qquad (2.48)$$

and substituting the approximation $S_y(\omega) \approx 3569e^{-0.336|\omega|}$ gives

$$S_{y_m}(\omega) = \frac{1}{2\pi}\int_{-\infty}^{\infty} E\left[\int_{-\infty}^{\infty} 3569e^{-0.336|\lambda|}e^{j\lambda(\omega_c\tau+\beta M(\tau)-\beta M(0))}d\lambda\right]e^{-j\omega\tau}d\tau. \qquad (2.49)$$

If the modulating signal is $m(t) = \sin(\omega_m t + \theta)$, where θ is a random variable that is distributed uniformly on $[0, 2\pi]$, then $M(t) = -\frac{1}{\omega_m}\cos(\omega_m t + \theta)$ and (2.49) becomes

$$S_{y_m}(\omega) = \frac{1}{2\pi\omega_c}\int_{-\infty}^{\infty}\int_{-\infty}^{\infty} 3569e^{-0.336\left|\frac{\lambda}{\omega_c}\right|}e^{j\lambda\tau}\frac{1}{2\pi}\int_0^{2\pi} e^{j\frac{2\lambda\beta}{\omega_c\omega_m}\sin\left(\frac{\omega_m\tau}{2}\right)\cos(\theta)}d\theta d\lambda e^{-j\omega\tau}d\tau. \qquad (2.50)$$

The innermost integral in (2.50) is [1]

$$\frac{1}{2\pi}\int_0^{2\pi} e^{j2\frac{\lambda\beta}{\omega_c\omega_m}\sin\left(\frac{\omega_m\tau}{2}\right)\cos(\theta))}d\theta = J_0\Big(\frac{2\lambda\beta}{\omega_c\omega_m}\sin\big(\frac{\omega_m\tau}{2}\big)\Big), \tag{2.51}$$

where $J_0(\cdot)$ is the zero-order Bessel function of the first kind. Substituting (2.51) into (2.50) results in

$$S_{y_m}(\omega) = \frac{1}{2\pi\omega_c}\int_{-\infty}^{\infty}\int_{-\infty}^{\infty} 3569e^{-0.336\left|\frac{\lambda}{\omega_c}\right|}e^{-j(\omega-\lambda)\tau}J_0\Big(\frac{2\lambda\beta}{\omega_c\omega_m}\sin\big(\frac{\omega_m\tau}{2}\big)\Big)d\lambda d\tau \tag{2.52}$$

$$= \frac{1}{2\pi\omega_c}\int_{-\infty}^{\infty} e^{-j\omega\tau}\int_{-\infty}^{\infty} 3569e^{-0.336\left|\frac{\lambda}{\omega_c}\right|}e^{j\lambda\tau}J_0\Big(\frac{2\lambda\beta}{\omega_c\omega_m}\sin\big(\frac{\omega_m\tau}{2}\big)\Big)d\lambda d\tau \tag{2.53}$$

The innermost integral in (2.53) is [1]

$$\frac{1}{2\pi\omega_c}\int_{-\infty}^{\infty} 3569e^{-0.336\left|\frac{\lambda}{\omega_c}\right|}e^{j\lambda\tau}J_0\Big(\frac{2\lambda\beta}{\omega_c\omega_m}\sin\big(\frac{\omega_m\tau}{2}\big)\Big)d\lambda = \tag{2.54}$$

$$\frac{1}{\pi\omega_c}\Re e\left\{\int_0^{\infty} 3569e^{-0.336\left(\frac{\lambda}{\omega_c}\right)}e^{j\lambda\tau}J_0\Big(\frac{2\lambda\beta}{\omega_c\omega_m}\sin\big(\frac{\omega_m\tau}{2}\big)\Big)d\lambda\right\}$$

$$= \frac{1}{\pi\omega_c}\Re e\left\{\frac{3569}{\sqrt{\left(\frac{2\beta}{\omega_c\omega_m}\sin\left(\frac{\omega_m\tau}{2}\right)\right)^2+\left(\frac{0.336}{\omega_c}+j\tau\right)^2}}\right\} \tag{2.55}$$

where the fact that $J_0(\cdot)$ is an even function has been used. Substituting (2.55) into (2.53) results in

$$S_{y_m}(\omega) = \int_{-\infty}^{\infty}\frac{1}{\pi\omega_c}\Re e\left\{\frac{3569}{\sqrt{\left(\frac{2\beta}{\omega_c\omega_m}\sin\left(\frac{\omega_m\tau}{2}\right)\right)^2+\left(\frac{0.336}{\omega_c}+j\tau\right)^2}}\right\}e^{-j\omega\tau}d\tau. \tag{2.56}$$

In other words, the power density spectrum of the modulated Lorenz carrier wave is the Fourier transform of the function given in (2.55). To approximate $S_{y_m}(\omega)$, the function in (2.55) is sampled and its discrete-time Fourier transform is computed. An example of the predicted power density spectrum using this technique is shown

in Figure 2-6 along with the estimated power density spectrum obtained from the periodogram of a numerical simulation of the modulated Lorenz equations given in (2.13).

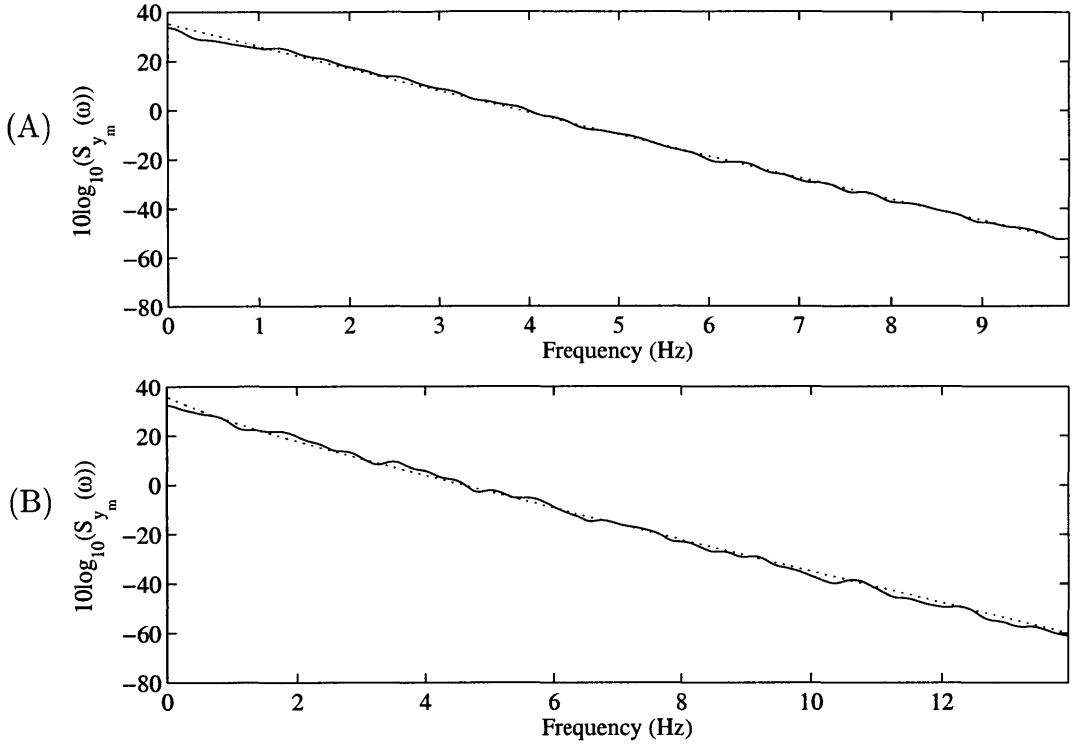

Figure 2-6: Predicted power density spectrum of the modulated Lorenz carrier wave – predicted from (2.56) (dotted) and estimated from periodogram (solid) for (A) $\beta = 0.1$, $\omega_m = 0.2$, and $\omega_c = 1$ and (B) $\beta = 0.5$, $\omega_m = 0.5$, and $\omega_c = 1$.

2.3 Bandwidth Expansion of Modulated Systems

As with FM signals, rate modulated signals are generally not band-limited. However, for many signals, most of the signal power is contained in a finite spectral range. The working definition that is adopted for bandwidth is the smallest spectral range that contains ninety-eight percent of the signal power. In this section, results from Section 2.2 are used to determine the bandwidth of the carrier waves generated by two rate-modulation systems that are used as examples throughout this thesis.

Bandwidth of a Modulated van der Pol Carrier The effective bandwidth of the modulated van der Pol Carrier is approximated by estimating the power density spectrum as described in Section 2.2 and then finding ω_{98} such that the spectral range $[0, \omega_{98}]$ contains ninety-eight percent of the average power. The results for $\lambda = 0.5$ and $\lambda = 3$ are shown in Table 2.1 and Table 2.2, respectively.

	ω_m				
β	0.1	0.2	0.3	0.4	0.5
0.1	1.4765	1.389	1.389	1.389	1.395
0.2	1.577	1.577	1.395	1.395	1.489
0.3	1.678	1.590	1.678	1.772	1.495
0.4	1.778	1.778	1.690	1.791	1.879
0.5	1.879	1.791	1.879	1.791	1.891

Table 2.1: Bandwidth (in rad/sec) of the modulated van der Pol carrier wave for $\lambda = 0.5$ ($\omega_c = 1$, unmodulated bandwidth = 1.389 (rad/sec)).

	ω_m				
β	0.1	0.2	0.3	0.4	0.5
0.1	2.331	2.331	2.425	2.143	2.136
0.2	2.526	2.532	2.438	2.532	2.626
0.3	2.639	2.727	2.727	2.538	2.633
0.4	2.827	2.740	2.733	2.752	2.633
0.5	2.928	2.934	3.022	2.934	2.645

Table 2.2: Bandwidth (in rad/sec) of the modulated van der Pol carrier wave for $\lambda = 3$ ($\omega_c = 1$, unmodulated bandwidth = 2.136 (rad/sec)).

Bandwidth of a Modulated Lorenz Carrier The width of the frequency range that contains ninety-eight percent of the signal power is summarized in Table 2.3. For the range of values in Table 2.3, the bandwidth of the modulated carrier is independent of ω_m.

	ω_m				
β	0.1	0.2	0.3	0.4	0.5
0.1	11.676	11.676	11.676	11.676	11.676
0.2	11.844	11.844	11.844	11.844	11.844
0.3	12.125	12.125	12.125	12.125	12.125
0.4	12.516	12.516	12.516	12.516	12.516
0.5	13.000	13.000	13.000	13.000	13.000

Table 2.3: Bandwidth (in rad/sec) of the modulated Lorenz carrier wave ($\omega_c = 1$, unmodulated bandwidth = 11.649 (rad/sec)).

Chapter 3

Demodulation

The previous chapter describes how an information signal can be modulated onto a carrier wave generated by a dynamical system. This chapter describes how the information signal can be recovered. The dynamical system used in the modulator is assumed to have a known exponentially convergent observer, which is described below. Using a novel perturbation technique, the observer is systematically modified so that it is capable of extracting the information signal from the modulated carrier wave. The end result is a systematic procedure for constructing demodulators when the observer assumption holds. These demodulators can be modified to enhance aspects of their performance. Three examples of such enhancements are presented which result in improved tracking capability, increased noise immunity, and a reduced number of nonlinearities present in the demodulator. The system that results from reducing the number of nonlinearities is shown to be equivalent to an alternative least-squares solution for demodulation.

3.1 Observers and Self-Synchronizing Systems

3.1.1 Observers

An observer is a system that reconstructs the full state of a dynamical system from the output of the dynamical system. For example, consider a dynamical system

$$\begin{aligned} \dot{\mathbf{x}} &= \mathbf{f}(\mathbf{x}), \\ y &= h(\mathbf{x}), \end{aligned} \tag{3.1}$$

where $\mathbf{x}$ and $\mathbf{f}(\cdot)$ are N-dimensional vectors and y is a scalar. An observer of this system is any system, $\hat{\mathbf{f}}(\cdot)$, such that if

$$\dot{\mathbf{z}} = \hat{\mathbf{f}}(\mathbf{z}, y), \tag{3.2}$$

then $\mathbf{z}$ converges to $\mathbf{x}$. It is a local observer if it converges only when $\mathbf{x}$ remains in a subset of the phase space, i.e. $\mathbf{x} \in D \subset \mathbb{R}^N$. Since the dynamical systems used for modulation remain on their periodic, aperiodic, or chaotic orbits, it is only necessary for the observers to be local observers, converging when $\mathbf{x}$ lies on the orbit. An exponentially convergent observer is an observer with the property that $\|\mathbf{z}-\mathbf{x}\| < e^{-\lambda t}$ for some $\lambda > 0$.

3.1.2 Self-Synchronizing Systems

Self-synchronizing systems have the property that when a state variable from one system drives a replica system, the replica state variables converge to the drive state variables. In other words, the replica system is an observer. An example of a self-synchronizing system is the chaotic Lorenz system described at the end of Section 2.2.

The equations for the Lorenz system are

$$\begin{aligned} \dot{x}_1 &= \sigma(x_2 - x_1), \\ \dot{x}_2 &= r x_1 - x_1 x_3 - x_2, \\ \dot{x}_3 &= x_1 x_2 - b x_3, \end{aligned} \tag{3.3}$$

where σ, r, and b are constant parameters. If a replica system is driven by x_1 in the following way,

$$\begin{aligned} \dot{z}_1 &= \sigma(z_2 - z_1), \\ \dot{z}_2 &= r z_1 - x_1 z_3 - z_2, \\ \dot{z}_3 &= x_1 z_2 - b z_3, \end{aligned} \tag{3.4}$$

then $\mathbf{z}$ converges to $\mathbf{x}$ exponentially. In general, self-synchronizing systems have the form

$$\begin{aligned} \text{Drive System:} &\begin{cases} \dot{\mathbf{x}} = \mathbf{f}(\mathbf{x}) \\ y = h(\mathbf{x}) \end{cases} \\ \text{Replica System:} &\begin{cases} \dot{\mathbf{z}} = \mathbf{f}(\mathbf{z}, y) \end{cases} \end{aligned} \tag{3.5}$$

3.1.3 Observers as Self-Synchronizing Replica Systems

Because the modulator remains on its orbit, the modulator dynamical system and the observer can be formulated as a drive/replica pair. Suppose the drive system is given by

$$\begin{aligned} \dot{\mathbf{x}} &= \mathbf{f}(\mathbf{x}), \\ y &= h(\mathbf{x}), \end{aligned} \tag{3.6}$$

where $\mathbf{x} \in D \subset \mathbb{R}^N$, and a local observer system given by

$$\dot{\mathbf{z}} = \hat{\mathbf{f}}(\mathbf{z}, y). \tag{3.7}$$

From the assumption that the observer is convergent for $\mathbf{x} \in D$, if the systems are perfectly synchronized at some time, i.e. $\mathbf{z}(t_0) = \mathbf{x}(t_0) \in D$, then they remained synchronized for $t > t_0$. For this to hold, it must be the case that

$$\mathbf{f}(\mathbf{x}) = \hat{\mathbf{f}}(\mathbf{x}, y), \qquad \text{for } \mathbf{x} \in D. \tag{3.8}$$

This means that the system in (3.6) can be replaced with

$$\begin{aligned} \dot{\mathbf{x}} &= \hat{\mathbf{f}}(\mathbf{x}, y) \\ y &= h(\mathbf{x}). \end{aligned} \tag{3.9}$$

Note that (3.9) and (3.7) are a drive/replica pair.

3.2 Demodulator Structure

The basic structure of a demodulator is shown in Figure 3-1. The rate-modulated observer is given by

$$\dot{\mathbf{z}} = (\omega_c + \beta\hat{m})\hat{\mathbf{f}}(\mathbf{z}, y), \tag{3.10}$$

where $\hat{m}$ is the rate estimate. The observer, $\hat{\mathbf{f}}(\cdot, \cdot)$ is assumed to be a known exponentially convergent local observer of the dynamical system used in the modulator. The rate estimator takes as its input the reconstructed state from the observer and the transmitted signal and tracks $m(t)$. The low-pass filter removes any spectral energy known not to be present in the original modulating signal, $m(t)$. This system can be

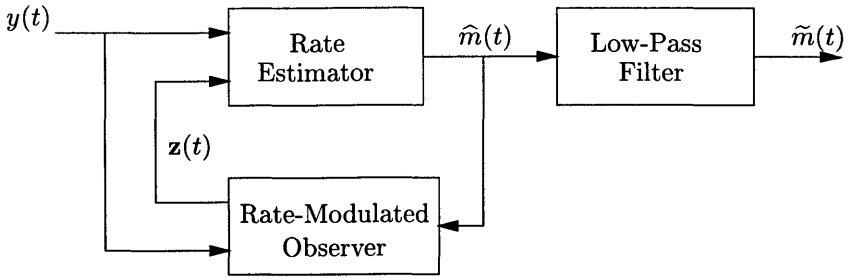

Figure 3-1: A block diagram of the basic demodulator structure. The signal $y(t)$ is the transmitted signal, $\hat{m}(t)$ is the estimate of the modulating signal, and $\mathbf{z}(t)$ is the estimate of state-variables of the transmitter system.

represented mathematically as

$$\begin{aligned}
\text{Modulator:} &\begin{cases} \dot{\mathbf{x}} = (\omega_c + \beta m)\mathbf{f}(\mathbf{x}), \\ y = h(\mathbf{x}), \end{cases} \\
\text{Demodulator:} &\begin{cases} \dot{\mathbf{z}} = (\omega_c + \beta \hat{m})\hat{\mathbf{f}}(\mathbf{z}, y), \\ \hat{m} = \mathcal{G}(\mathbf{z}, y), \\ \dot{\boldsymbol{\varsigma}} = A_p \boldsymbol{\varsigma} + B_p \hat{m}, \\ \tilde{m} = C_p \boldsymbol{\varsigma} + D_p \hat{m}, \end{cases}
\end{aligned} \tag{3.11}$$

where $\mathcal{G}$ is an operator that represents the rate estimator and A_p, B_p, C_p, and D_p represent the low-pass filter.

3.3 Demodulator Design

Assuming that the dynamical system used in the modulator has a known exponentially convergent local observer, the observer can be modified so that it is an exponentially convergent observer of the modulator when $m(t) = m_0$, where m_0 is an unknown constant. If the rate estimator converges to m_0, then the augmented observer is assumed to be able to track a time-varying $m(t)$ provided that $m(t)$ varies sufficiently slow.

The design of the rate estimator is based on a technique developed in Appendix A that is referred to as a backwards perturbation expansion. The essential step in this perturbation expansion is to express the modulator state, $\mathbf{x}$, as a perturbation expansion about the demodulator state, $\mathbf{z}$, in terms of the rate estimate error, $e_m = \hat{m} - m_0$. By expanding the modulator as a perturbation about the demodulator, the resulting expansion terms depend only on variables local to the demodulator. The perturbation variables can then be combined in such a way that they force the demodulator rate estimate error to zero. Summarizing the results obtained in Appendix A, if the dynamical system used in the modulator is of the form

$$\begin{aligned} \dot{\mathbf{x}} &= \mathbf{F}(\mathbf{x};\theta), \\ y &= h(\mathbf{x}), \end{aligned} \tag{3.12}$$

where θ is an unknown parameter and $\mathbf{x} \in D \subset \mathbb{R}^N$, and the known exponentially convergent observer is of the form

$$\dot{\mathbf{z}} = \hat{\mathbf{F}}(\mathbf{z}, y; \theta), \tag{3.13}$$

for $\mathbf{x} \in D$, then the system given by

$$\begin{aligned} \dot{\mathbf{z}} &= \hat{\mathbf{F}}(\mathbf{z}, y; \hat{\theta}), \\ \dot{\hat{\theta}} &= K(h(\mathbf{z}) - y)\boldsymbol{\xi}_1, \\ \dot{\boldsymbol{\xi}}_1 &= \Big(\frac{\partial \hat{\mathbf{F}}}{\partial \mathbf{z}}(\mathbf{z}, y; \hat{\theta}) + Kr(\mathbf{z}, \boldsymbol{\xi}_1)\Big)\boldsymbol{\xi}_1 - \frac{\partial \hat{\mathbf{F}}}{\partial \theta}(\mathbf{z}, y; \hat{\theta}), \end{aligned} \tag{3.14}$$

is an exponentially convergent observer of the system given in (3.12), where

$$r(\mathbf{z}, \boldsymbol{\xi}_1) = \Big(\frac{\partial h}{\partial \mathbf{z}}(\mathbf{z}) \cdot \boldsymbol{\xi}_1\Big) \cdot g\Big(\frac{\partial h}{\partial \mathbf{z}}(\mathbf{z}) \cdot \boldsymbol{\xi}_1\Big), \tag{3.15}$$

$\operatorname{sgn}(g(\alpha)) = \operatorname{sgn}(\alpha)$, and assuming that $h(\mathbf{x})$ is persistently exciting (see Appendix A).

For rate modulated systems,

$$\hat{\mathbf{F}}(\mathbf{z}, y; \hat{m}) = (\omega_c + \beta\hat{m})\hat{\mathbf{f}}(\mathbf{z}, y). \tag{3.16}$$

Substituting the form given in (3.16) into (3.14), the demodulator system, including the low-pass filter shown in Figure 3-1, is given by

$$\begin{aligned}
\dot{\mathbf{z}} &= (\omega_c + \beta\hat{m})\hat{\mathbf{f}}(\mathbf{z}, y) \\
\hat{y} &= h(\mathbf{z}) \\
\dot{\hat{m}} &= K(\hat{y} - y)g\Big(\frac{\partial h}{\partial \mathbf{z}}(\mathbf{z}) \cdot \boldsymbol{\xi}_1\Big) \\
\dot{\boldsymbol{\xi}}_1 &= (\omega_c + \beta\hat{m})\Big(\frac{\partial \hat{\mathbf{f}}}{\partial \mathbf{z}}(\mathbf{z}, y) + Kr(\mathbf{z}, \boldsymbol{\xi}_1)\Big)\boldsymbol{\xi}_1 - \beta\mathbf{f}(\mathbf{z}, y), \\
\dot{\boldsymbol{\varsigma}} &= A_p\boldsymbol{\varsigma} + B_p\hat{m}, \\
\tilde{m} &= C_p\boldsymbol{\varsigma} + D_p\hat{m},
\end{aligned} \tag{3.17}$$

where

$$r(\mathbf{z}, \boldsymbol{\xi}_1) = \Big(\frac{\partial h}{\partial \mathbf{z}}(\mathbf{z}) \cdot \boldsymbol{\xi}_1\Big) \cdot g\Big(\frac{\partial h}{\partial \mathbf{z}}(\mathbf{z}) \cdot \boldsymbol{\xi}_1\Big), \tag{3.18}$$

$0 < K < K_*$ for some K_*, $\text{sgn}(g(a)) = \text{sgn(a)}$, and A_p, B_p, C_p, and D_p correspond to the low-pass filter.

The determination of K_* requires, in general, the use of numerical techniques. The difficulty lies in the fact that the explicit determination of K_* requires knowledge of a Lyapunov function for the linear, time-varying system given by

$$\dot{\boldsymbol{\xi}}_1 = \frac{\partial \hat{\mathbf{f}}}{\partial \mathbf{x}}(\mathbf{x}, y)\boldsymbol{\xi}_1. \tag{3.19}$$

Lyapunov functions are usually difficult to determine. However, K_* can be estimated by numerically computing the Floquet exponents [9] or the Lyapunov exponents [14].

3.4 Examples of the Basic Demodulator

In this section, demodulation is demonstrated for two dynamical systems. The first is based on the van der Pol oscillator, which is a two-dimensional nonlinear system with a periodic attractor. The second system is the Lorenz system, which is a chaotic system with a strange attractor.

3.4.1 The van der Pol Oscillator

The differential equations corresponding to the van der Pol oscillator are

$$\begin{aligned} \dot{x}_1 &= x_2, \\ \dot{x}_2 &= \lambda(1 - x_1^2)x_2 - x_1, \end{aligned} \tag{3.20}$$

where $\lambda > 0$. An exponentially convergent observer of the van der Pol oscillator is

$$\begin{aligned} \dot{z}_1 &= z_2 + y - z_1, \\ \dot{z}_2 &= \lambda(1 - y^2)z_2 - y. \end{aligned} \tag{3.21}$$

Introducing modulation to (3.20) and following the formulation specified in (3.17), the complete modulation/demodulation system is given by

$$\underline{\text{Modulator}} \tag{3.22}$$

$$\begin{aligned}
\dot{x}_1 &= (\omega_c + \beta m)x_2, \\
\dot{x}_2 &= (\omega_c + \beta m)\big(\lambda(1 - x_1^2)x_2 - x_1\big), \\
y &= x_1,
\end{aligned}$$

$$\underline{\text{Demodulator}}$$

$$\begin{aligned}
\dot{z}_1 &= (\omega_c + \beta\hat{m})\big(z_2 + y - z_1\big), \\
\dot{z}_2 &= (\omega_c + \beta\hat{m})\big(\lambda(1 - y^2)z_2 - y\big), \\
\dot{\hat{m}} &= K(z_1 - y)\text{sgn}(\psi_1), \\
\begin{bmatrix} \dot{\psi}_1 \\ \dot{\psi}_2 \end{bmatrix} &= (\omega_c + \beta\hat{m})\left(\begin{bmatrix} -1 & 1 \\ 0 & \lambda(1 - y^2) \end{bmatrix} + \right. \\
&\qquad \left. + KI|\psi_1| \right) \begin{bmatrix} \psi_1 \\ \psi_2 \end{bmatrix} - \beta \begin{bmatrix} z_2 + y - z_1 \\ \lambda(1 - y^2)z_2 - y \end{bmatrix}, \\
\dot{\varsigma} &= A_p\varsigma + B_p\hat{m}, \\
\tilde{m} &= C_p\varsigma + D_p\hat{m},
\end{aligned}$$

where I is the 2×2 identity matrix. The convergence of $\hat{m}$ when $K = 1$, $\lambda = 1$, and $\beta = 1$ is shown in Figure 3-2. The convergence of the state variable z_2 to x_2 is shown in Figure 3-3.

3.4.2 The Lorenz System

Repeating (3.3), the Lorenz equations are

$$\begin{aligned}
\dot{x}_1 &= \sigma(x_2 - x_1), \\
\dot{x}_2 &= rx_1 - x_1x_3 - x_2, \\
\dot{x}_3 &= x_1x_2 - bx_3,
\end{aligned} \tag{3.23}$$

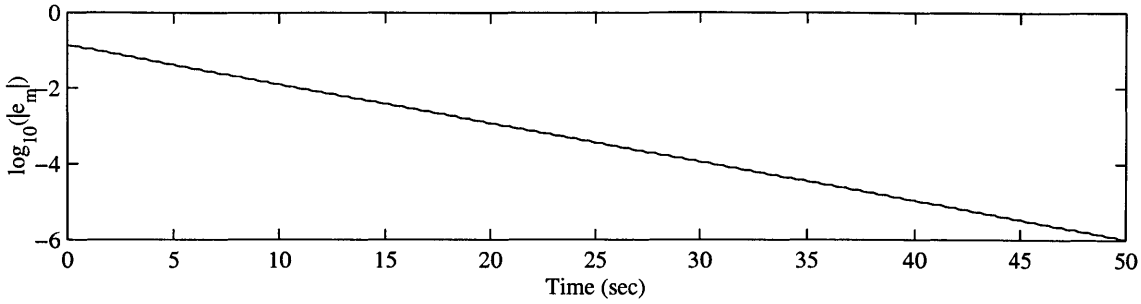

Figure 3-2: Convergence of the rate estimate for the van der Pol based system with $K = 1$ and $\beta = 1$.

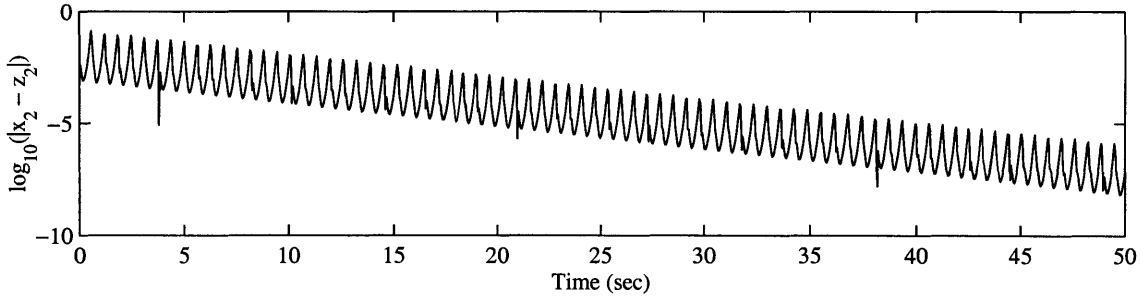

Figure 3-3: Convergence of the state estimate for the van der Pol based system with $K = 1$ and $\beta = 1$.

where, for example, $\sigma = 10$, $r = 25$, and $b = 8/3$. An exponentially convergent observer of this system is

$$\begin{aligned} \dot{z}_1 &= \sigma(z_2 - z_1), \\ \dot{z}_2 &= ry - yz_3 - z_2, \\ \dot{z}_3 &= yz_2 - bz_3, \end{aligned} \tag{3.24}$$

Adding the modulation to (3.3) and following the formulation specified in (3.17), the modulator and demodulator are given by

$$\underline{\text{Modulator}} \tag{3.25}$$

$$\begin{aligned}
\dot{x}_1 &= (\omega_c + \beta m)\sigma(x_2 - x_1), \\
\dot{x}_2 &= (\omega_c + \beta m)\big(rx_1 - x_1x_3 - x_2\big), \\
\dot{x}_3 &= (\omega_c + \beta m)\big(x_1x_2 - bx_3\big), \\
y &= x_1,
\end{aligned}$$

$$\underline{\text{Demodulator}} \tag{3.26}$$

$$\begin{aligned}
\dot{z}_1 &= (\omega_c + \beta \hat{m})\sigma(z_2 - z_1), \\
\dot{z}_2 &= (\omega_c + \beta \hat{m})\big(ry - yz_3 - z_2\big), \\
\dot{z}_3 &= (\omega_c + \beta \hat{m})\big(yz_2 - bz_3\big), \\
\dot{\hat{m}} &= K(z_1 - y)\text{sgn}(\psi_1), \\
\begin{bmatrix} \dot{\psi}_1 \\ \dot{\psi}_2 \\ \dot{\psi}_3 \end{bmatrix} &= (\omega_c + \beta \hat{m})\left(\begin{bmatrix} \sigma & \sigma & 0 \\ 0 & -1 & -y \\ 0 & y & -b \end{bmatrix} + KI|\psi_1| \right) \begin{bmatrix} \psi_1 \\ \psi_2 \\ \psi_3 \end{bmatrix} - \beta \begin{bmatrix} \sigma(z_2 - z_1) \\ ry - yz_3 - z_2 \\ yz_2 - bz_3 \end{bmatrix}, \\
\dot{\varsigma} &= A_p\varsigma + B_p\hat{m}, \\
\tilde{m} &= C_p\varsigma + D_p\hat{m},
\end{aligned}$$

where I is the 3×3 identity matrix. The convergence of $\hat{m}$ when $K = 0.02$ and $\beta = 1$ is shown in Figure 3-4. The convergence of the state variable z_2 to x_2 and z_3 to x_3 is shown in Figure 3-5.

3.5 Demodulator Enhancements

In this section, modifications are made to the demodulator to improve its performance in various ways. First, a low-pass filter is added between the rate estimator

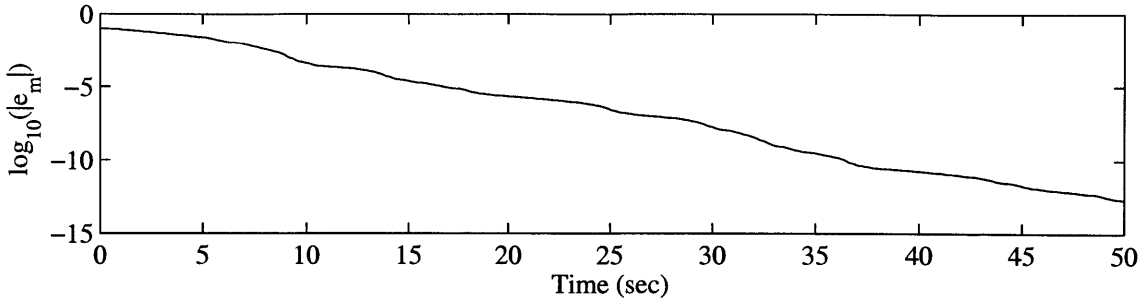

Figure 3-4: Convergence of the rate estimate for the Lorenz based system with $K = 0.02$ and $\beta = 1$.

and the observer to remove spectral energy in $\hat{m}(t)$ that is outside the bandwidth of $m(t)$. Second, K is increased beyond the value for which the perturbation expansion analysis guarantees stability. Although stability is no longer guaranteed, numerical simulations suggest that the demodulator remains stable over a range of $K > K_*$. A larger value for K allows $\hat{m}(t)$ to track faster signals. Finally, many of the nonlinearities in the demodulator are removed by approximating the rate estimator with a linear system. The system that results from the approximation is equivalent to a least-squares approach to designing a demodulator.

3.5.1 Filtering

To remove spectral energy in $\hat{m}(t)$ that is outside the bandwidth of $m(t)$, a filter is added to the feedback loop as shown in Figure 3-6. The filtering operation, denoted as $\langle\cdot\rangle$, is given by

$$\langle\hat{m}(t)\rangle = \int_0^t \psi(t,\tau)\hat{m}(\tau)d\tau, \tag{3.27}$$

where $\psi(t,\tau)$ is the kernel. If the support of this kernel is sufficiently small compared to the rate at which m and $\hat{m}$ vary, then

$$\begin{aligned}\langle\dot{\hat{m}}\rangle &= -K\Big\langle\Big(\frac{\partial h}{\partial \mathbf{z}}(\mathbf{z})\cdot\boldsymbol{\xi}_1\Big)\cdot g\Big(\frac{\partial h}{\partial \mathbf{z}}(\mathbf{z})\cdot\boldsymbol{\xi}_1\Big)(\hat{m}-m)\Big\rangle \\ &\approx -K\Big\langle\Big(\frac{\partial h}{\partial \mathbf{z}}(\mathbf{z})\cdot\boldsymbol{\xi}_1\Big)\cdot g\Big(\frac{\partial h}{\partial \mathbf{z}}(\mathbf{z})\cdot\boldsymbol{\xi}_1\Big)\Big\rangle(\hat{m}-m).\end{aligned} \tag{3.28}$$

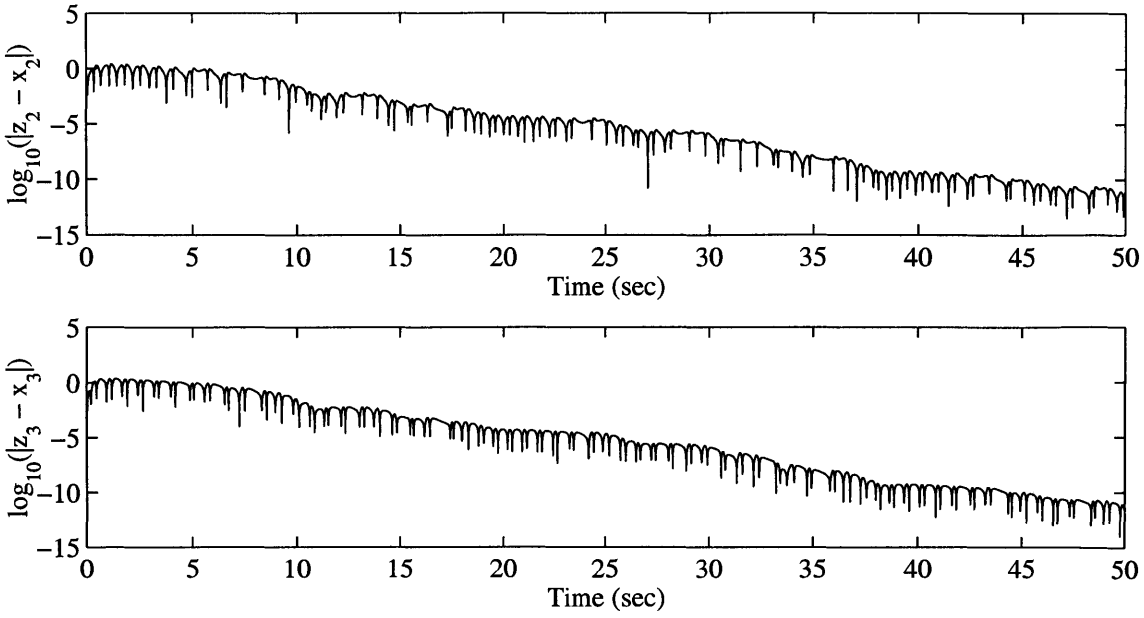

Figure 3-5: Convergence of z_2 to x_2 and z_3 to x_3 for the Lorenz based system with $K = 0.02$ and $\beta = 1$.

Effectively, the filter smooths the time-varying coefficient $\left(\frac{\partial h}{\partial \mathbf{z}}(\mathbf{z}) \cdot \boldsymbol{\xi}_1\right) \cdot g\left(\frac{\partial h}{\partial \mathbf{z}}(\mathbf{z}) \cdot \boldsymbol{\xi}_1\right)$.

3.5.2 Increasing the Convergence Rate

In Section 3.3, the gain parameter K had to be smaller than some K_* to guarantee that the perturbation expansion was bounded. For $K < K_*$, the rate estimate converged exponentially and monotonically. Choosing K slightly larger than K_* affects the system in two ways. First, since K scales the derivative of $\hat{m}$, increasing K increases the rate at which $\hat{m}$ can vary, allowing $\hat{m}$ to track signals that vary more rapidly. Second, the perturbation term may not remain bounded. Returning to the equation for the perturbation variable,

$$\dot{\boldsymbol{\xi}}_1 = (\omega_c + \beta\hat{m})\left(\frac{\partial \hat{\mathbf{f}}}{\partial \mathbf{z}}(\mathbf{z}, y) + Kr(\mathbf{z}, \boldsymbol{\xi}_1)\right)\boldsymbol{\xi}_1 - \beta\mathbf{f}(\mathbf{z}, y), \tag{3.29}$$

where

$$r(\mathbf{z}, \boldsymbol{\xi}_1) = \left(\frac{\partial h}{\partial \mathbf{z}}(\mathbf{z}) \cdot \boldsymbol{\xi}_1\right) \cdot g\left(\frac{\partial h}{\partial \mathbf{z}}(\mathbf{z}) \cdot \boldsymbol{\xi}_1\right). \tag{3.30}$$

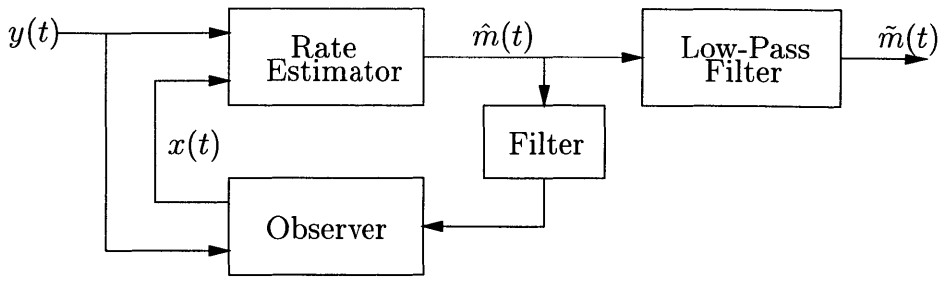

Figure 3-6: Demodulator with a filter in feedback path.

If K is set to zero in (3.29), then, from the analysis in Appendix A, $\boldsymbol{\xi}_1$ is bounded. Of course, the dynamics of the system are now changed and convergence is no longer guaranteed. Numerical experimentation suggests, however, that the system remains stable for a range of $K > K_*$.

As an example, consider the Lorenz based modulation/demodulation system given in (3.25) and (3.26) with $K > K_*$. The term $KIr(\mathbf{z}, \boldsymbol{\psi})$ is dropped from (3.29) and the demodulator equations become

$$\begin{aligned}
\dot{z}_1 &= (\omega_c + \beta\hat{m})\sigma(z_2 - z_1), \\
\dot{z}_2 &= (\omega_c + \beta\hat{m})\big(ry - yz_3 - z_2\big), \\
\dot{z}_3 &= (\omega_c + \beta\hat{m})\big(yz_2 - bz_3\big), \\
\dot{\hat{m}} &= K(z_1 - y)\mathrm{sgn}(\psi_1), \\
\begin{bmatrix} \dot{\psi}_1 \\ \dot{\psi}_2 \\ \dot{\psi}_3 \end{bmatrix} &= (\omega_c + \beta\hat{m}) \begin{bmatrix} \sigma & \sigma & 0 \\ 0 & -1 & -y \\ 0 & y & -b \end{bmatrix} \begin{bmatrix} \psi_1 \\ \psi_2 \\ \psi_3 \end{bmatrix} - \beta \begin{bmatrix} \sigma(z_2 - z_1) \\ ry - yz_3 - z_2 \\ yz_2 - bz_3 \end{bmatrix}.
\end{aligned} \tag{3.31}$$

The convergence of $\hat{m}$ for $K = 0.1$ and for $K = 0.02$ is compared in Figure 3-7.

An example of demodulation is shown in Figure 3-8. The parameters in this example are $\omega_c = 5$, $K = 0.6$, $\beta = 3$, and the modulating signal is a zero-mean Gaussian noise process band-limited to 0.4 Hz with a standard deviation of 0.5.

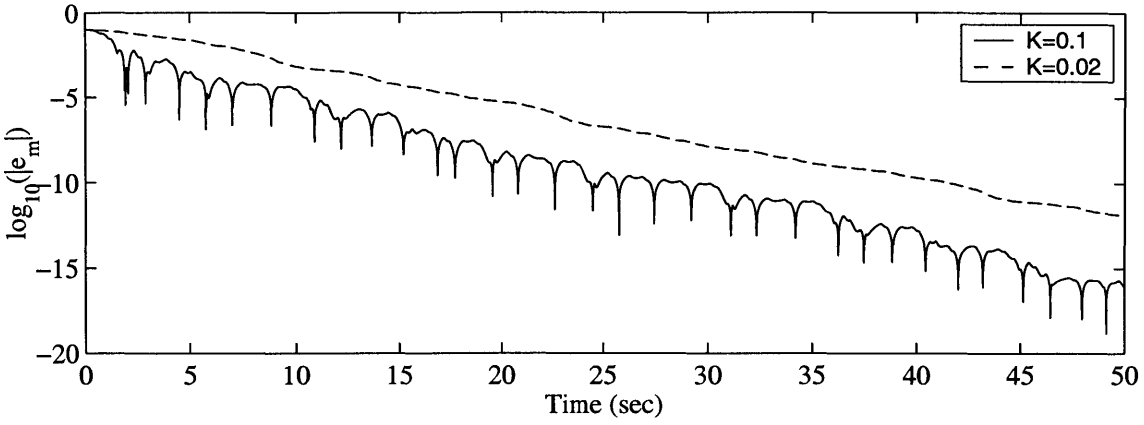

Figure 3-7: A comparison of the convergence of $\hat{m}$ when $K = 0.1$ and $K = 0.02$.

3.5.3 Reduction of the Number of Nonlinearities

The demodulators discussed so far have significant additional nonlinearities added beyond those already present in the dynamical system. These additional nonlinearities appear in the equation for $\boldsymbol{\xi}_1$, since as given in (3.17),

$$\dot{\boldsymbol{\xi}}_1 = (\omega_c + \beta\hat{m})\Big(\frac{\partial \hat{\mathbf{f}}}{\partial \mathbf{z}}(\mathbf{z}, y) + Kr(\mathbf{z}, \boldsymbol{\xi}_1)\Big)\boldsymbol{\xi}_1 - \beta\hat{\mathbf{f}}(\mathbf{z}, y), \tag{3.32}$$

where

$$r(\mathbf{z}, \boldsymbol{\xi}_1) = \Big(\frac{\partial h}{\partial \mathbf{z}}(\mathbf{z}) \cdot \boldsymbol{\xi}_1\Big) \cdot g\Big(\frac{\partial h}{\partial \mathbf{z}}(\mathbf{z}) \cdot \boldsymbol{\xi}_1\Big), \tag{3.33}$$

$0 < K < K_*$ for some K_*, and $\text{sgn}(g(a)) = \text{sgn(a)}$. Even when $K > K_*$ and $Kr(\mathbf{z}, \boldsymbol{\xi}_1)$ is removed, a nonlinear equation remains.

The last term, $\beta\hat{\mathbf{f}}(\mathbf{z}, y)$, also appears in the observer portion of the demodulator. Since $\hat{\mathbf{f}}(\mathbf{z}, y)$ is required by the observer, removing it from the rate estimator does not reduce the total number of nonlinearities present in the demodulator. This term is left as it is. The first term, $(\omega_c + \beta\hat{m})\frac{\partial \hat{\mathbf{f}}}{\partial \mathbf{z}}\boldsymbol{\xi}_1$, is generally nonlinear and does not appear elsewhere in the system. Approximating this term with a linear, time-invariant (LTI) system simplifies the hardware implementation of the demodulator.

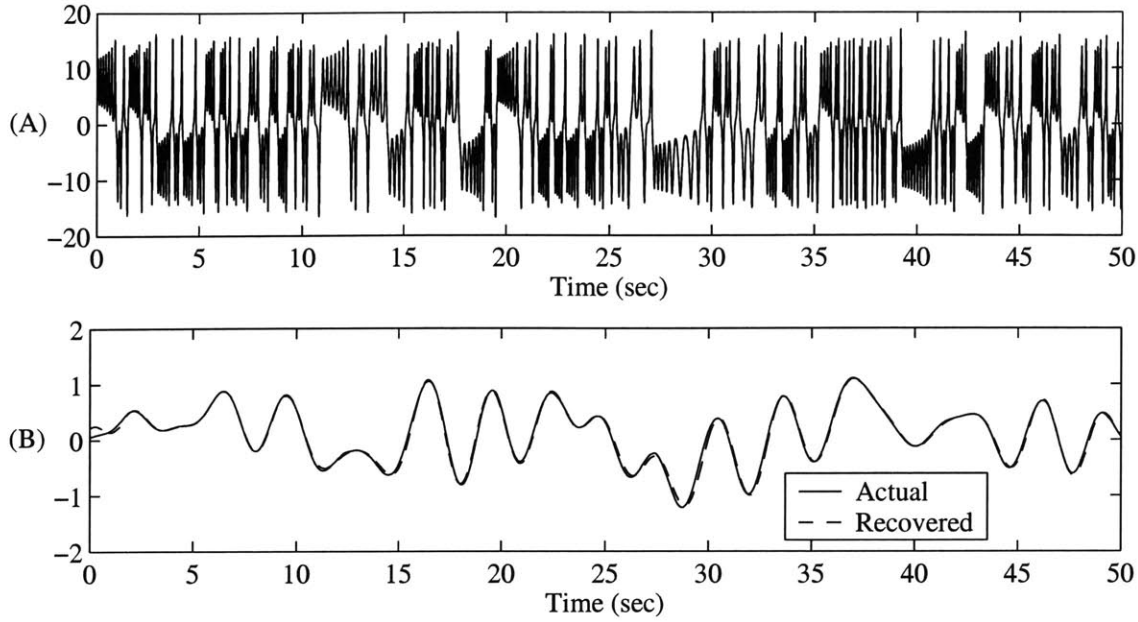

Figure 3-8: An example of demodulation. (A) The transmitted signal, $y(t)$. (B) The recovered signal (dashed), the actual modulating signal (solid).

First, if $\omega_c \gg \beta\hat{m}$ then[1]

$$\dot{\boldsymbol{\xi}}_1 \approx \omega_c \frac{\partial \hat{\mathbf{f}}}{\partial \mathbf{z}}(\mathbf{z}, y)\boldsymbol{\xi}_1 - \beta\hat{\mathbf{f}}(\mathbf{z}, y). \tag{3.34}$$

The time-varying gain matrix, $\frac{\partial \hat{\mathbf{f}}}{\partial \mathbf{z}}(\mathbf{z}, y)$, is generally nonlinear. However, the differential equation in (3.34) is linear with respect to $\boldsymbol{\xi}_1$ and is a time-varying linear filter with $-\beta\hat{\mathbf{f}}(\mathbf{z}, y)$ as its input. Using the notation $\langle\cdot\rangle$ to denote the filtering operation,

$$\boldsymbol{\xi}_1 = -\beta\langle\hat{\mathbf{f}}(\mathbf{z}, y)\rangle. \tag{3.35}$$

Replacing this linear time-varying filter with a linear time-invariant filter makes the equation for $\boldsymbol{\xi}_1$ consists of only linear components and $\hat{\mathbf{f}}(\mathbf{x}, y)$, the latter of which is already present in the demodulator.

The difference between the derivatives of $\hat{y}$ and y can be approximated in a manner

[1]Typically, ω_c is orders of magnitude greater than $\max_t(\beta\hat{m})$. For example, in FM radio broadcasts, ω_c is on the order of 10^7 times greater.

similar to $\hat{y} - y$,

$$\begin{aligned}\dot{\hat{y}} - \dot{y} = (\omega_c + \beta\hat{m})\frac{\partial h}{\partial \mathbf{z}}(\mathbf{z})\hat{\mathbf{f}}(\mathbf{z}, y) - \\ - (\omega_c + \beta(\hat{m} - e_m))\frac{\partial h}{\partial \mathbf{z}}(\mathbf{z} + \xi_1 e_m + \cdots)\hat{\mathbf{f}}(\mathbf{z} + \xi_1 e_m + \cdots, y) \\ \approx e_m \beta \frac{\partial h}{\partial \mathbf{z}}(\mathbf{z})\hat{\mathbf{f}}(\mathbf{z}, y).\end{aligned} \tag{3.36}$$

Filtering $\dot{\hat{y}} - \dot{y}$ with the same filter that appears in (3.35) results in

$$\langle \dot{\hat{y}} - \dot{y} \rangle \approx \beta \Big\langle \frac{\partial h}{\partial \mathbf{z}}(\mathbf{z})\hat{\mathbf{f}}(\mathbf{z}, y) \Big\rangle e_m, \tag{3.37}$$

assuming that e_m varies slowly with respect to the time constant of the filter so that e_m can be moved outside of the filtering operation. Combining (3.35) and (3.37), the rate estimator equation becomes

$$\dot{\hat{m}} = -K\beta \langle \dot{\hat{y}} - \dot{y} \rangle \langle \hat{\mathbf{f}}(\mathbf{z}, y) \rangle \tag{3.38}$$

$$\approx -K\beta \langle \hat{\mathbf{f}}(\mathbf{z}, y) \rangle^2 (\hat{m} - m), \tag{3.39}$$

where $h(\mathbf{z})$ is assumed to be a linear function of $\mathbf{z}$. Without this assumption, (3.35) should be changed to

$$\boldsymbol{\xi}_1 = -\beta \Big\langle \frac{\partial h}{\partial \mathbf{z}}(\mathbf{z})\hat{\mathbf{f}}(\mathbf{z}, y) \Big\rangle, \tag{3.40}$$

in which case the rate estimator equation becomes

$$\begin{aligned}\dot{\hat{m}} &= K\beta \langle \dot{\hat{y}} - \dot{y} \rangle \Big\langle \frac{\partial h}{\partial \mathbf{z}}(\mathbf{z})\hat{\mathbf{f}}(\mathbf{z}, y) \Big\rangle \\ &\approx -K\beta \Big\langle \frac{\partial h}{\partial \mathbf{z}}(\mathbf{z})\hat{\mathbf{f}}(\mathbf{z}, y) \Big\rangle^2 (\hat{m} - m).\end{aligned} \tag{3.41}$$

In both cases, the rate estimator equation has the form

$$\dot{\hat{m}} \approx -a(t)(\hat{m} - m), \tag{3.42}$$

where $a(t)$ is positive semi-definite, which suggests $\hat{m}$ converges to m.

An example of a system using this type of linearized demodulator is given in Chapter 5, where the system is constructed in hardware.

3.6 Gradient Descent Demodulators

In Section 3.5.3, the number of nonlinearities that appear in the demodulator are reduced by replacing the time-varying filter that appears in the rate estimator with an LTI filter. The resulting rate estimator is a special case of the type of rate estimator obtained from a gradient descent approach to designing the demodulator.

Starting with the structure shown in Figure 3-1, the rate estimator component of the demodulator is designed so that the rate estimate, $\hat{m}$, descends along the gradient of some distance measure between $\langle \dot{\hat{y}} \rangle$ and $\langle \dot{y} \rangle$. Specifically,

$$\dot{\hat{m}} = -K \frac{\partial d\big(\langle \dot{y} \rangle, \langle \dot{\hat{y}} \rangle\big)}{\partial \hat{m}}, \tag{3.43}$$

where $d(\cdot, \cdot)$ is a distance function and $\langle \cdot \rangle$ is an averaging operation given by

$$\langle \dot{y} \rangle = \int_0^t \psi(t, \tau) \dot{y}(\tau) d\tau \tag{3.44}$$

$$= y(t)\psi(t, t) - y(0)\psi(t, 0) - \int_0^t \frac{\partial \psi(t, \tau)}{\partial \tau} y(\tau) d\tau, \tag{3.45}$$

where $\psi(t, \tau)$ is the averaging kernel.

When the distance function is chosen to be the square of the distance between $\langle \dot{\hat{y}} \rangle$ and $\langle \dot{y} \rangle$, that is,

$$d(\langle \dot{\hat{y}} \rangle, \langle \dot{y} \rangle) = \big(\langle \dot{\hat{y}} \rangle - \langle \dot{y} \rangle\big)^2, \tag{3.46}$$

the corresponding least-squares rate estimator equation becomes

$$\begin{aligned}\dot{\hat{m}} &= -K\big(\langle\dot{\hat{y}}\rangle - \langle\dot{y}\rangle\big)\Big(\frac{\partial}{\partial\hat{m}}\big(\langle\dot{\hat{y}}\rangle - \langle\dot{y}\rangle\big)\Big) \\ &= -K\langle\dot{\hat{y}} - \dot{y}\rangle\Big\langle\frac{\partial}{\partial\hat{m}}\Big(\frac{\partial h(\mathbf{z})}{\partial\mathbf{z}}\frac{\partial\mathbf{z}}{\partial t}\Big)\Big\rangle \\ &= -K\beta\langle\dot{\hat{y}} - \dot{y}\rangle\Big\langle\frac{\partial h(\mathbf{z})}{\partial\mathbf{z}}\hat{\mathbf{f}}(\mathbf{z}, y)\Big\rangle.\end{aligned} \tag{3.47}$$

The rate estimator equation given in (3.47) is the same as that given in (3.41) for the linearized rate estimator.

Chapter 4

Demodulation in the Presence of Additive Noise

FM systems trade-off between noise immunity and bandwidth. The rate modulated systems developed in this thesis behave in a similar manner, that is, increasing β increases the bandwidth of the transmitted signal and increases the signal-to-noise ratio (SNR) at the output of the demodulator. In this chapter, a general approach is described and demonstrated to approximate the effects that additive white noise has on the performance of the demodulator in the high input SNR case.

In the previous chapters, the modulators and demodulators have been expressed as ordinary differential equations. When noise is added to these systems, they must be expressed as stochastic differential equations. This chapter begins with a brief introduction to stochastic differential equations and the relevant results from the Itô calculus, which describes how to manipulate and analyze stochastic differential equations. Using the rules of the Itô calculus, a set of ordinary differential equations are derived that govern the time evolution of the moments. When the system is nonlinear, low order moment equations depend on higher order moments, leading to an infinite hierarchy of equations. A technique called quasi-moment neglect closure (QMNC) is used to truncate these equations. The end result is a finite set of ordinary differential equations that approximate the behavior of the low order moments. From the moments, the time-varying probability distributions of the demodulator state

variables are approximated along with the SNR at the output of the demodulator.

Three different demodulators are analyzed in this chapter. The first system is based on a stiff harmonic oscillator, which is a system that has a circular orbit and is compatible with FM signals. It performs similar to the phase-locked loop (PLL)[1] with respect to the SNR at the output of the demodulator. The last two examples are based on the van der Pol oscillator and the Lorenz system. All three systems exhibit a bandwidth/noise-immunity trade-off.

4.1 Dynamical Systems and Stochastic Processes

A stochastic differential equation (SDE) [2, 4, 5] has the form

$$d\mathbf{x} = \mathbf{f}(\mathbf{x}, t)dt + \mathbf{g}(\mathbf{x}, t)dW(t), \tag{4.1}$$

where $dW(t)$ is defined as the derivative of a white noise process. That is, $dW(t) = \eta(t)dt$, where $\eta(t)$ is a white noise process. The notation for an SDE is different than the notation for an ordinary differential equation to emphasize the fact that the white noise process is not Riemann-Lebesgue integrable. Because white noise is not Riemann-Lebesgue integrable, the integral equation corresponding to (4.1) must be interpreted carefully. The most common interpretation results in the Itô calculus [4]. The Itô calculus is a special set of rules for manipulating SDEs. Two rules from the Itô calculus are used in this chapter.

Change of Variables Formula: Given an arbitrary SDE,

$$d\mathbf{x} = \mathbf{f}(\mathbf{x}, t)dt + \mathbf{g}(\mathbf{x}, t)dW(t), \tag{4.2}$$

[1]The phase-locked loop is analyzed in Appendix B.

let $h(\mathbf{x})$ be a scalar function of $\mathbf{x}$. Then $h(\mathbf{x})$ satisfies the stochastic differential equation given by

$$dz = \nabla h(\mathbf{x})\big(\mathbf{f}(\mathbf{x},t)dt + \mathbf{g}(\mathbf{x},t)dW(t)\big) + \frac{1}{2}\mathrm{tr}\big(\mathbf{g}(\mathbf{x},t)Q(t)\mathbf{g}^T(\mathbf{x},t)J_h(\mathbf{x})\big)dt, \qquad (4.3)$$

where $\nabla h(\mathbf{x})$ is the gradient of $h(\mathbf{x})$, $J_h(\mathbf{x})$ is the Jacobian matrix of $h(\mathbf{x})$, and $Q(t) = E[dW(t)dW(t)^T]$.

Mean Value Formula: Given a continuous, non-anticipatory function, $\mathbf{g}(\cdot,\cdot)$,

$$E[\int_{t_0}^{t} \mathbf{g}(\mathbf{x}(\tau),\tau)dW(\tau)] = 0. \qquad (4.4)$$

4.2 Moment Evolution

When a dynamical system is driven by additive white noise, the states become random variables, each with its own probability density function (pdf). These pdfs can be obtained exactly by solving what is known as the Fokker-Planck equation [4]. The Fokker-Planck equation is a parabolic partial differential equation with non-constant coefficients. It can be solved explicitly in only a few special cases. However, the closeness of the rate estimate, $\widehat{m}$, and the true rate, m, is of interest and can often be determined by approximating the first few moments of $\widehat{m}$. Also, from these first few moments, the pdfs of the state-variables can be approximated.

An ordinary differential equation that governs the evolution of the moments is obtained from Itô's change of variables formula. Given an arbitrary SDE,

$$d\mathbf{x} = \mathbf{f}(\mathbf{x},t)dt + \mathbf{g}(\mathbf{x},t)dW(t), \qquad (4.5)$$

let $h(\mathbf{x})$ be a polynomial function of the state-variables, for example, $h(\mathbf{x}) = x_1^2$ or $h(\mathbf{x}) = x_1x_2$. Applying Itô's change of variables formula given in (4.3), and taking

the expectation of (4.5) gives

$$E[dh(\mathbf{x})] = E[\nabla h(\mathbf{x})\mathbf{f}(\mathbf{x},t)dt] + E[\nabla h(\mathbf{x})\mathbf{g}(\mathbf{x},t)dW(t)]+ \\ + E[\frac{1}{2}\mathrm{tr}\big(\mathbf{g}(\mathbf{x},t)Q(t)\mathbf{g}^T(\mathbf{x},t)J_h(\mathbf{x})\big)dt]. \quad (4.6)$$

Since expectation and differentiation are both linear operators, they commute, giving

$$dE[h(\mathbf{x})] = E[\nabla h(\mathbf{x})\mathbf{f}(\mathbf{x},t)]dt + E[\nabla h(\mathbf{x})\mathbf{g}(\mathbf{x},t)d(t)]+ \\ + \frac{1}{2}E[\mathrm{tr}\big(\mathbf{g}(\mathbf{x},t)Q(t)\mathbf{g}^T(\mathbf{x},t)J_h(\mathbf{x})\big)]dt. \quad (4.7)$$

From the mean value formula given in (4.4), the second term is zero, which leaves

$$dE[h(\mathbf{x})] = E[\nabla h(\mathbf{x})\mathbf{f}(\mathbf{x},t)]dt + \frac{1}{2}E[\mathrm{tr}\big(\mathbf{g}(\mathbf{x},t)Q(t)\mathbf{g}^T(\mathbf{x},t)J_h(\mathbf{x})\big)]dt. \quad (4.8)$$

Since $dW(t)$ does not appear in (4.8), it is an ordinary differential equation and can be expressed in the usual deterministic form as

$$\frac{dE[h(\mathbf{x})]}{dt} = E[\nabla h(\mathbf{x})\mathbf{f}(\mathbf{x},t)] + \frac{1}{2}E[\mathrm{tr}\big(\mathbf{g}(\mathbf{x},t)Q(t)\mathbf{g}^T(\mathbf{x},t)J_h(\mathbf{x})\big)]. \quad (4.9)$$

By choosing $h(\mathbf{x})$ appropriately, the equation of motion for any moment from (4.9) can be derived. For example, substituting $h(\mathbf{x}) = x_1^3$ into (4.9) gives the equation of motion for the third moment of the state variable x_1.

Two difficulties arise when $\mathbf{f}(\mathbf{x},t)$ is nonlinear. First, a nonlinear $\mathbf{f}(\mathbf{x},t)$ makes $E[h(\mathbf{x})\mathbf{f}(\mathbf{x},t)]$ a function of higher order moments. For example, consider the scalar SDE,

$$dx = -x^3dt + dW(t). \quad (4.10)$$

From (4.9), the equation of motion for the first moment is

$$\frac{dE[x]}{dt} = -E[x^3], \quad (4.11)$$

which contains the third order moment, $E[x^3]$. Similarly, the differential equation for the third order moment contains the fifth order moment, and so on. In general, if the system is nonlinear, the differential equation for any moment depends on at least one higher order moment. If this hierarchy of moment equations is truncated, then there are more unknowns than equations and no solution. The second difficulty caused by a nonlinear $\mathbf{f}(\mathbf{x}, y)$ has to do with computing the expectations. The differential equations for the moments are are exact when the expectations are taken with respect to the true pdfs of the state variables. However, the true distributions are not known when the system is nonlinear[2]. To work around these two difficulties, a technique known as quasi-moment neglect closure is used.

4.3 Quasi-Moment Neglect Closure

As described in the preceding section, a nonlinear SDE results in a hierarchy of moment equations in which the lower order equations depend on the higher order equations. This hierarchy of equations can be closed by a technique called the quasi-moment neglect closure (QMNC) technique [8]. QMNC truncates the hierarchy by approximating the pdfs of the state variables as an Edgeworth series truncated to order N. This series is given by

$$p(\mathbf{x};t) = \Big(1 + \sum_{s=3}^{N} b(k_1, k_2, \ldots, k_n; t) \frac{\partial^{k_1}}{\partial x_1^{k_1}} \cdots \frac{\partial^{k_n}}{\partial x_n^{k_n}}\Big) p_G(\mathbf{x};t), \tag{4.12}$$

where $p(\mathbf{x};t)$ is the non-stationary, multivariate pdf of the state variables, $p_G(\mathbf{x};t)$ is a multivariate non-stationary Gaussian pdf, and the coefficients $b(k_1, k_2, \ldots, k_n; t)$ are called the quasi-moments. To show how approximating the pdfs of the state variables as an Edgeworth series truncated to order N closes the moment equations, the relationship between the moments and quasi-moments is derived. This relationship is derived by using the cumulants as an intermediate relationship between the moments

[2]When the equations are linear and the white noise is Gaussian, it can be shown that the resulting pdfs are all Gaussian.

and quasi-moments.

The relationship between the moments and the cumulants is established using the characteristic function, which is defined as

$$\Theta(\boldsymbol{\omega};t) = \int_{-\infty}^{\infty}\int_{-\infty}^{\infty}\cdots\int_{-\infty}^{\infty} e^{j\boldsymbol{\omega}^T\mathbf{x}}p(\mathbf{x};t)d\mathbf{x}, \tag{4.13}$$

where $p(\mathbf{x};t)$ is the time-varying pdf of the state-space solution. The moments can be computed from (4.13), and they are given by

$$E_{\mathbf{x}(t)}[x_1^{k_1}x_2^{k_2}\cdots x_n^{k_n};t] = (-j)^s\Big(\frac{\partial^s\Theta(\boldsymbol{\omega};t)}{\partial\omega_1^{k_1}\partial\omega_2^{k_2}\cdots\partial\omega_n^{k_n}}\Big)\Big|_{\boldsymbol{\omega}=0}, \tag{4.14}$$

where $s = \sum_{i=1}^n k_i$ is the order of the moment and $k_i \geq 0$ is an integer. To simplify subsequent expressions, the moments are denoted as

$$m_{k_1k_2\cdots k_n}(t) = E_{\mathbf{x}(t)}[x_1^{k_1}x_2^{k_2}\cdots x_n^{k_n};t]. \tag{4.15}$$

Using (4.14), the Taylor series expansion of $\Theta(\boldsymbol{\omega};t)$ is

$$\Theta(\boldsymbol{\omega};t) = 1 + \sum_{s=1}^{\infty}\frac{j^s}{s!}\sum_{\{k_1+\cdots+k_N=s\}} m_{k_1k_2\cdots k_n}(t)\omega_1^{k_1}\cdots\omega_n^{k_n}, \tag{4.16}$$

where the notation $\sum_{\{k_1+\cdots+k_n=s\}}$ means the summation over all $k_i \geq 0$ such that $\sum_{i=1}^n k_i = s$, where each k_i is an integer.

The cumulants are defined as the partial derivatives of the natural logarithm of the characteristic function evaluated at $\omega = 0$. Specifically,

$$\kappa_{k_1k_2\cdots k_n}(t) = (-j)^s\Big(\frac{\partial^s\ln\Theta(\boldsymbol{\omega};t)}{\partial\omega_1^{k_1}\partial\omega_2^{k_2}\cdots\partial\omega_n^{k_n}}\Big)\Big|_{\boldsymbol{\omega}=0}, \tag{4.17}$$

where $s = \sum_{i=1}^n k_i$. Using the cumulants, the Taylor series of $\ln\Theta(\boldsymbol{\omega};t)$ is

$$\Theta(\boldsymbol{\omega};t) = \exp\Big(\sum_{s=1}^{\infty}\frac{j^s}{s!}\sum_{\{k_1+\cdots+k_n=s\}}\kappa_{k_1k_2\cdots k_n}(t)\omega_1^{k_1}\cdots\omega_n^{k_n}\Big). \tag{4.18}$$

Substituting (4.18) into (4.14) gives the moments as functions of the cumulants. For example, the first moment in terms of the cumulants for a one dimensional system is

$$\begin{aligned} m_1(t) &= (-j)\Big(\frac{\partial \Theta(\omega_1;t)}{\partial \omega_1}\Big)\Big|_{\omega_1=0} \\ &= (-j)\frac{\partial}{\partial \omega_1}\big(je^{\kappa_1(t)\omega_1}\big)\Big|_{\omega_1=0} \\ &= \kappa_1(t). \end{aligned} \tag{4.19}$$

Higher order moments are derived in a similar manner and expressions for the first seven are given in Table 4.1. In Table 4.1, all the moments and cumulants are functions of time. The first N moments are in terms of the first N cumulants and this

$$\begin{aligned} m_1 &= k_1 \\ m_2 &= k_1^2 + k_2 \\ m_3 &= k_1^3 + 3\,k_1k_2 + k_3 \\ m_4 &= k_1^4 + 6\,k_1^2k_2 + 4\,k_1k_3 + 3\,k_2^2 + k_4 \\ m_5 &= k_1^5 + 10\,k_1^3k_2 + 10\,k_1^2k_3 + 15\,k_1k_2^2 + 5\,k_1k_4 + 10\,k_2k_3 + k_5 \\ m_6 &= k_1^6 + 15\,k_1^4k_2 + 20\,k_1^3k_3 + 45\,k_1^2k_2^2 + 15\,k_1^2k_4 + 60\,k_1k_2k_3 \\ &\quad + 15\,k_2^3 + 6\,k_1k_5 + 15\,k_2k_4 + 10\,k_3^2 + k_6 \\ m_7 &= k_1^7 + 21\,k_1^5k_2 + 35\,k_1^4k_3 + 105\,k_1^3k_2^2 + 35\,k_1^3k_4 \\ &\quad + 210\,k_1^2k_2k_3 + 105\,k_1k_2^3 + 21\,k_1^2k_5 + 105\,k_1k_2k_4 + 70\,k_1k_3^2 \\ &\quad + 105\,k_2^2k_3 + 7\,k_1k_6 + 21\,k_2k_5 + 35\,k_3k_4 + k_7 \end{aligned}$$

Table 4.1: Moments as functions of cumulants up to seventh order for a one-dimensional system.

relationship can be inverted to get the first N cumulants as functions of the first N moments. The resulting relationships are shown in Table 4.2.

The cumulants have been expressed as functions of the moments and the moments have been expressed as functions of the cumulants. Once similar relationships between

$$
\begin{aligned}
\kappa_1 &= m_1 \\
\kappa_2 &= m_2 - m_1^2 \\
\kappa_3 &= m_3 + 2\,m_1^3 - 3\,m_1 m_2 \\
\kappa_4 &= m_4 - 6\,m_1^4 + 12\,m_1^2 m_2 - 3\,m_2^2 - 4\,m_1 m_3 \\
\kappa_5 &= m_5 + 24\,m_1^5 - 60\,m_1^3 m_2 + 30\,m_1 m_2^2 + 20\,m_1^2 m_3 - 10\,m_2 m_3 - 5\,m_1 m_4 \\
\kappa_6 &= 360\,m_1^4 m_2 - 120\,m_1^6 - 6\,m_1 m_5 - 10\,m_3^2 - 15\,m_2 m_4 + 30\,m_1^2 m_4 \\
&\quad + 120\,m_1 m_2 m_3 - 120\,m_1^3 m_3 - 270\,m_1^2 m_2^2 + 30\,m_2^3 + m_6 \\
\kappa_7 &= -2520\,m_1^5 m_2 + 2520\,m_1^3 m_2^2 + 840\,m_1^4 m_3 + 720\,m_1^7 - 7\,m_1 m_6 \\
&\quad - 35\,m_3 m_4 + 140\,m_1 m_3^2 + 42\,m_1^2 m_5 - 21\,m_2 m_5 + 210\,m_2^2 m_3 \\
&\quad - 1260\,m_1^2 m_2 m_3 + 210\,m_1 m_2 m_4 - 630\,m_1 m_2^3 - 210\,m_1^3 m_4 + m_7
\end{aligned}
$$

Table 4.2: Cumulants as functions of moments up to seventh order for a one-dimensional system.

the quasi-moments and cumulants are derived, direct quasi-moment–moment relationships can be established. Substituting the Edgeworth expansion given in (4.12) into the characteristic function given in (4.13) results in

$$\Theta(\boldsymbol{\omega};t) = \Theta_G(\boldsymbol{\omega};t)\Big(1 + \sum_{s=3}^{\infty} \frac{j^s}{s!} b_{k_1 k_2 \cdots k_n}(t)\omega_1^{k_1}\omega_2^{k_2}\cdots\omega_n^{k_n}\Big), \tag{4.20}$$

where $\Theta_G(\boldsymbol{\omega};t)$ is the characteristic function of a multivariate Gaussian and $b_{k_1 k_2 \cdots k_n}(t)$ are the quasi-moments. The moment-generating function expressed in terms of cumulants in (4.18) can be rewritten as

$$
\begin{aligned}
\Theta(\omega;t) &= \exp\Big(\sum_{s=1}^{2} \frac{j^s}{s!} \sum_{\{k_1+\cdots+k_n=s\}} \kappa_{k_1 k_2 \cdots k_n}(t)\omega_1^{k_1}\cdots\omega_n^{k_n}\Big) \\
&\quad \times \exp\Big(\sum_{s=3}^{\infty} \frac{j^s}{s!} \sum_{\{k_1+\cdots+k_n=s\}} \kappa_{k_1 k_2 \cdots k_n}(t)\omega_1^{k_1}\cdots\omega_n^{k_n}\Big) \\
&= \Theta_G(\omega;t)\exp\Big(\sum_{s=3}^{\infty} \frac{j^s}{s!} \sum_{\{k_1+\cdots+k_n=s\}} \kappa_{k_1 k_2 \cdots k_n}(t)\omega_1^{k_1}\cdots\omega_n^{k_n}\Big).
\end{aligned} \tag{4.21}
$$

From (4.21) and (4.20), the quasi-moments and the cumulants are related through

$$\exp\Big(\sum_{s=3}^{\infty}\frac{j^s}{s!}\sum_{k_1+\cdots+k_N=s}\kappa(x_1^{k_1}x_2^{k_2}\cdots x_N^{k_N};t)\omega_1^{k_1}\cdots\omega_N^{k_N}\Big)= 1+\sum_{s=3}^{\infty}\frac{j^s}{s!}b(x_1^{k_1},\ldots,x_N^{k_N};t)\omega_1^{k_1}\cdots\omega_N^{k_N}. \quad (4.22)$$

Comparing the above expression to (4.16) and (4.18), the relationship between the quasi-moments and the cumulants is similar to that of the moments and the cumulants. In fact, the cumulant–quasi-moment relationships can be obtained directly from the moment-cumulant relationships. Combining (4.16) and (4.18) gives the relationship between the moments and cumulants used to derive Table 4.1 and Table 4.2. Specifically,

$$1+\sum_{s=1}^{\infty}\frac{j^s}{s!}\sum_{\{k_1+\cdots+k_N=s\}}m_{k_1k_2\cdots k_n}(t)\omega_1^{k_1}\cdots\omega_n^{k_n}= \exp\Big(\sum_{s=1}^{\infty}\frac{j^s}{s!}\sum_{\{k_1+\cdots+k_n=s\}}\kappa_{k_1k_2\cdots k_n}(t)\omega_1^{k_1}\cdots\omega_n^{k_n}\Big). \quad (4.23)$$

Comparing (4.22) with (4.23), the relationship between the quasi-moments and the cumulants is identical to the relationship between the moments and cumulants if the first and second order moments and cumulants in (4.23) are set to zero. Therefore, the quasi-moment–cumulant relationships can be obtained directly from Table 4.1 and Table 4.2 and are given in Table 4.3 and Table 4.4.

$\kappa_3 = b_3$	$\kappa_4 = b_4$
$\kappa_5 = b_5$	$\kappa_6 = -10\,b_3^2 + b_6$
$\kappa_7 = -35\,b_3b_4 + b_7$	

Table 4.3: Cumulants as functions of quasi-moments for up to seventh order.

Substituting the cumulant–quasi-moment relationships in Table 4.3 into the moment–

$b_3 = k_3$	$b_4 = k_4$
$b_5 = k_5$	$b_6 = 10\,k_3^2 + k_6$
$b_7 = 35\,k_3k_4 + k_7$	

Table 4.4: Quasi-moments as functions of cumulants for up to seventh order.

cumulant relationships in Table 4.1 gives the moments in terms of the quasi-moments, which are given in Table 4.5. Substituting the cumulant–moment relationships in

$$
\begin{aligned}
m_3 &= m_1^3 + 3\,m_1m_2 + b_3 \\
m_4 &= m_1^4 + 6\,m_1^2m_2 + 4\,m_1b_3 + 3\,m_2^2 + b_4 \\
m_5 &= m_1^5 + 10\,m_1^3m_2 + 10\,m_1^2b_3 + 15\,m_1m_2^2 + 5\,m_1b_4 + 10\,m_2b_3 + b_5 \\
m_6 &= m_1^6 + 15\,m_1^4m_2 + 20\,m_1^3b_3 + 45\,m_1^2m_2^2 + 15\,m_1^2b_4 \\
&\quad +60\,m_1m_2b_3 + 15\,m_2^3 + 6\,m_1b_5 + 15\,m_2b_4 + b_6 \\
m_7 &= m_1^7 + 21\,m_1^5m_2 + 35\,m_1^4b_3 + 105\,m_1^3m_2^2 + 35\,m_1^3b_4 \\
&\quad +210\,m_1^2m_2b_3 + 105\,m_1m_2^3 + 21\,m_1^2b_5 + 105\,m_1m_2b_4 + 70\,m_1b_3^2 \\
&\quad +105\,m_2^2b_3 + 7\,m_1\left(b_6 - 10\,{b_3}^2\right) + 21\,m_2b_5 + b_7
\end{aligned}
$$

Table 4.5: Moments as functions of quasi-moments up to seventh order for a one-dimensional system.

Table 4.2 into the quasi-moment–cumulant relationships in Table 4.4 gives the quasi-moments in terms of the moments, which are given in Table 4.6. To write a moment above order N in terms of moments at or below order N, all quasi-moments in Table 4.5 that are above order N are set to zero and the quasi-moment–moment expressions from Table 4.6 are substituted for the remaining moments. For example, m_5 can be determined in terms of m_1, m_2, and m_3 for a third order closure. From Table 4.5,

$$m_5 = m_1^5 + 10\,m_1^3m_2 + 10\,m_1^2b_3 + 15\,m_1m_2^2 + 5\,m_1b_4 + 10\,m_2b_3 + b_5. \tag{4.24}$$

$$
\begin{aligned}
b_3 &= m_3 + 2\,m_1^3 - 3\,m_1 m_2 \\
b_4 &= m_4 - 6\,m_1^4 + 12\,m_1^2 m_2 - 3\,m_2^2 - 4\,m_1 m_3 \\
b_5 &= m_5 + 24\,m_1^5 - 60\,m_1^3 m_2 + 30\,m_1 m_2^2 + 20\,m_1^2 m_3 - 10\,m_2 m_3 - 5\,m_1 m_4 \\
b_6 &= m_6 + 240\,m_1^4 m_2 - 180\,m_1^2 m_2^2 - 80\,m_1^3 m_3 + 30\,m_1^2 m_4 \\
&\quad -15\,m_2 m_4 + 30\,m_2^3 - 6\,m_1 m_5 - 80\,m_1^6 + 60\,m_1 m_2 m_3 \\
b_7 &= m_7 + 300\,m_1^7 - 1050\,m_1^5 m_2 + 1050\,m_1^3 m_2^2 + 350\,m_1^4 m_3 \\
&\quad -315\,m_1 m_2^3 - 140\,m_1^3 m_4 + 105\,m_2^2 m_3 \\
&\quad +42\,m_1^2 m_5 - 21\,m_2 m_5 - 7\,m_1 m_6 - 420\,m_1^2 m_2 m_3 + 105\,m_1 m_2 m_4
\end{aligned}
$$

Table 4.6: Quasi-moments as functions of moments for up to seventh order for a one-dimensional system.

Setting b_4 and b_5 to zero in (4.24) gives

$$m_5 = m_1^5 + 10\,m_1^3 m_2 + 10\,m_1^2 b_3 + 15\,m_1 m_2^2 + 10\,m_2 b_3. \tag{4.25}$$

From Table 4.6,

$$b_3 = m_3 + 2\,m_1^3 - 3\,m_1 m_2, \tag{4.26}$$

and substituting (4.26) into (4.25) gives

$$
\begin{aligned}
m_5 = m_1^5 + 10\,m_1^3 m_2 + 10\,m_1^2(m_3 + 2\,m_1^3 - 3\,m_1 m_2) + 15\,m_1 m_2^2 + 10\,m_2(m_3 \\
+ 2\,m_1^3 - 3\,m_1 m_2).
\end{aligned} \tag{4.27}
$$

In summary, the assumption that the pdfs of the state variables can be approximated as an Edgeworth series truncated to the N^{th} order makes the moments above order N functions of the moments at or below order N and closes the differential moment equations at order N. A detailed example of applying this technique to the second-order phase-locked loop, a two-dimensional system, is given in Appendix B.

4.4 The Channel and Demodulator as Stochastic Differential Equations

When the modulated signal, $y_m(t)$, is corrupted with additive white noise, the demodulator is preceded with a filter that filters out any spectral energy that is outside the bandwidth of $y_m(t)$. Assuming that the pre-filter passes the modulated signal, $y_m(t)$, without significantly altering it, the noise model shown in Figure 4-1 is used. The pre-filter written as an SDE is

$$\begin{aligned} d\vartheta &= A\vartheta dt + BdW(t) \\ \nu &= C\vartheta, \end{aligned} \tag{4.28}$$

where A, B, and C are the matrices and vectors associated with the state-space representation of the filter. In general, the state-space form of a filter has an additional parameter, D, and the output of the filter is $\nu = C\vartheta + DdW(t)$. However, a filter that has $D = 0$ must always be chosen. Otherwise, the demodulator equation for $\mathbf{z}$ becomes

$$\dot{\mathbf{z}} = (\omega_c + \beta\hat{m})\hat{\mathbf{f}}(\mathbf{z}, y + C\vartheta + DdW(t)). \tag{4.29}$$

If $\hat{\mathbf{f}}(\cdot,\cdot)$ is nonlinear with respect to its second argument, the noise process appears nonlinearly in the demodulator, and the demodulator does not have the form of an

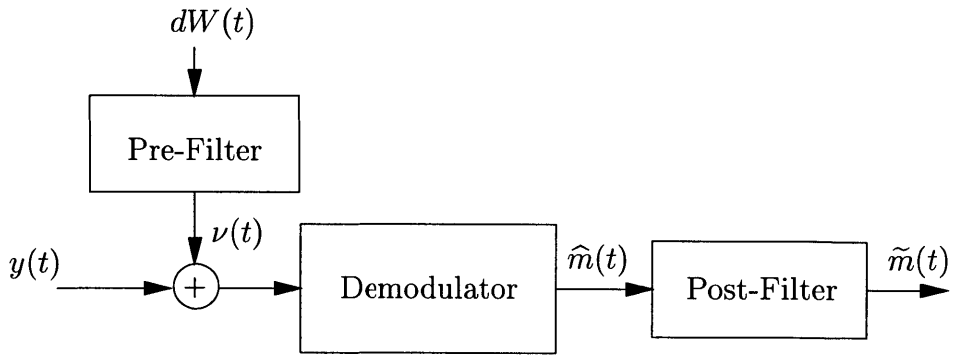

Figure 4-1: Demodulator noise model.

SDE as described in Section 4.1.

The SDE for the complete demodulator, including the pre- and post-filters, is

$$\begin{aligned}
d\mathbf{z} &= (\omega_c + \beta\hat{m})\hat{\mathbf{f}}(\mathbf{z}, y+\nu)dt, \\
d\hat{m} &= -K\Big(h(\mathbf{z}) - y + \nu\Big) \cdot g\Big(\frac{\partial h}{\partial \mathbf{z}}(\mathbf{z}) \cdot \boldsymbol{\xi}_1\Big)dt, \\
d\boldsymbol{\xi}_1 &= \Big((\omega_c + \beta\hat{m})\frac{\partial \hat{\mathbf{f}}}{\partial \mathbf{z}}(\mathbf{z}, y+\nu) + IKr(\mathbf{z}, \boldsymbol{\xi}_1)\Big)\boldsymbol{\xi}_1 dt - \beta\hat{\mathbf{f}}(\mathbf{z}, y+\nu)dt, \\
d\boldsymbol{\vartheta} &= A\boldsymbol{\vartheta}dt + BdW(t), \\
\nu &= C\boldsymbol{\vartheta}, \\
d\boldsymbol{\varsigma} &= A_p\boldsymbol{\varsigma}dt + B_p\hat{m}dt, \\
\tilde{m} &= C_p\boldsymbol{\varsigma} + D_p\hat{m},
\end{aligned} \tag{4.30}$$

where A, B, and C correspond to the pre-filter filter and A_p, B_p, C_p, and D_p correspond to the post-filter.

4.5 Examples

In this section, the QMNC technique is applied to three examples[3]. The first example is based on a system referred to as the stiff harmonic oscillator. The stiff harmonic oscillator has sinusoidal solutions, and therefore can be used to generate FM signals. The associated demodulator can therefore be used to demodulate FM signals. This is an example of how different demodulators can be used for the same carrier wave as described in Section 3.1.3. The second example is based on the van der Pol oscillator and the last example is based on the chaotic Lorenz system, both of which have already been used as examples in Chapter 3.

[3]In addition to the examples in this section, a detailed example of applying the QMNC technique to the phase-locked loop is given Appendix B.

4.5.1 The Stiff Harmonic Oscillator

The stiff harmonic oscillator has a circular limit cycle like a harmonic oscillator, but it has an added nonlinearity to make the limit cycle globally attracting. The differential equations describing the oscillator are

$$\begin{aligned} \dot{x}_1 &= K_S\Big(1 - \sqrt{x_1^2 + x_2^2}\Big)x_1 - x_2, \\ \dot{x}_2 &= K_S\Big(1 - \sqrt{x_1^2 + x_2^2}\Big)x_2 + x_1, \end{aligned} \tag{4.31}$$

where K_S is the "stiffness" constant that determines how quickly the system converges to its stable limit cycle. Figure 4-2 shows the effect that K_S has on the rate at which the system approaches its limit cycle[4].

The Modulator: Introducing the modulation as described in Chapter 2, the modulator is given by

$$\begin{aligned} \dot{x}_1 &= \big(\omega_c + \beta m(t)\big)\left(K_S\Big(1 - \sqrt{x_1^2 + x_2^2}\Big)x_1 - x_2\right), \\ \dot{x}_2 &= \big(\omega_c + \beta m(t)\big)\left(K_S\Big(1 - \sqrt{x_1^2 + x_2^2}\Big)x_2 + x_1\right). \end{aligned} \tag{4.32}$$

Since the modulator operates on the unit circle, $x_1^2 + x_2^2 = 1$ and (4.32) can be simplified to

$$\begin{aligned} \dot{x}_1 &= -\big(\omega_c + \beta m(t)\big)x_2, \\ \dot{x}_2 &= \big(\omega_c + \beta m(t)\big)x_1. \end{aligned} \tag{4.33}$$

The system in (4.33) is a rate modulated harmonic oscillator.

[4]The term "stiff" comes from the fact that for large values of K_S, the convergence to the limit cycle is much faster than the oscillatory rate. Dynamical systems that evolve on two different time scales are called "stiff".

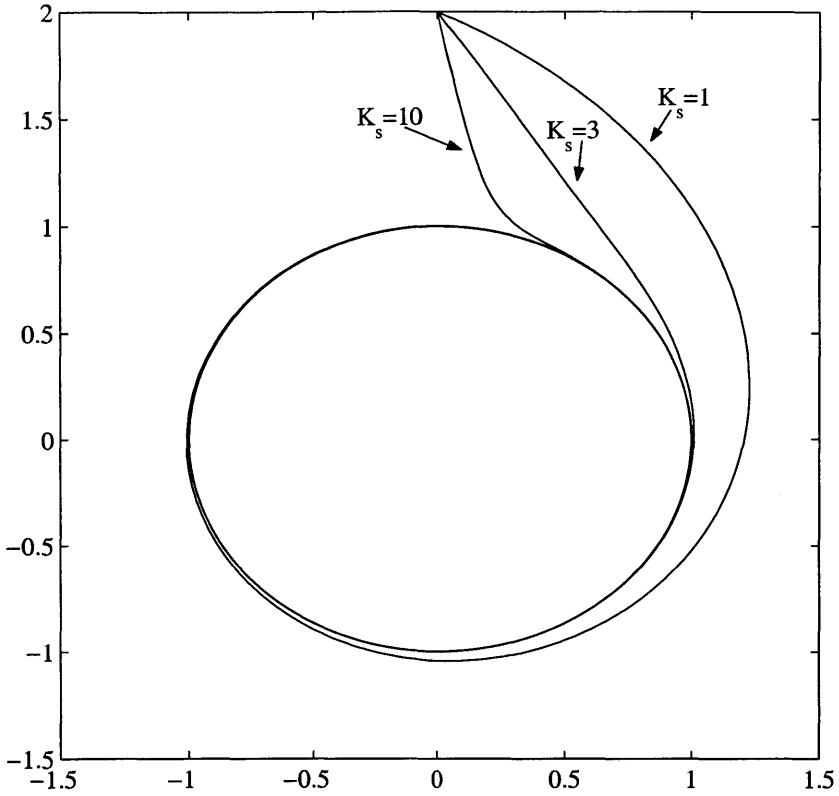

Figure 4-2: The effect of K_S on the rate of convergence of the stiff harmonic oscillator.

The Channel and Pre-Filter: The transmitted signal is $y = x_2$. The channel is an additive white Gaussian noise channel and the pre-filter is given by

$$\begin{aligned} d\boldsymbol{\vartheta} &= A\boldsymbol{\vartheta}dt + BdW(t) \\ \nu &= C\boldsymbol{\vartheta}, \end{aligned} \tag{4.34}$$

where A, B, and C correspond to a bandpass filter with a bandwidth of B_W centered at ω_c. The noise process, $dW(t)$, is a Gaussian white noise process. B_W is chosen to be equal to the bandwidth of the transmitted signal as obtained from Carson's rule, which is $B_W = 2\omega_m(\frac{\beta}{\omega_m} + 1)$ when $m(t) = \sin(\omega_m t)$.

The Demodulator: An exponentially convergent observer for the stiff harmonic oscillator is

$$\begin{aligned}\dot{z}_1 &= K_S\Big(1-\sqrt{z_1^2+z_2^2}\Big)z_1 - z_2,\\ \dot{z}_2 &= K_S\Big(1-\sqrt{z_1^2+z_2^2}\Big)z_2 + z_1 + K_1(y-z_2),\end{aligned} \tag{4.35}$$

where $y = x_2$. Choosing $g(\psi_2) = \psi_2$ and following the demodulator design procedure of Section 3.5.2, the demodulator equations are

$$\begin{aligned}\dot{z}_1 &= (\omega_c + \beta\hat{m})\left(K_S\Big(1-\sqrt{z_1^2+z_2^2}\Big)z_1 - z_2\right),\\ \dot{z}_2 &= (\omega_c + \beta\hat{m})\left(K_S\Big(1-\sqrt{z_1^2+z_2^2}\Big)z_2 + z_1 + K_1(y+\nu-z_2)\right),\\ \dot{\hat{m}} &= KK_S\frac{\omega_c}{\beta}(z_2-(y+\nu))\psi_2,\\ \begin{bmatrix}\dot{\psi}_1\\ \dot{\psi}_2\end{bmatrix} &= (\omega_c+\beta\hat{m})K_S\begin{bmatrix}1-\frac{2z_1^2+z_2^2}{\sqrt{z_1^2+z_2^2}} & -\frac{z_1z_2}{\sqrt{z_1^2+z_2^2}}-\frac{1}{K_S}\\ -\frac{z_1z_2}{\sqrt{z_1^2+z_2^2}}+\frac{1}{K_S} & 1-\frac{z_1^2+2z_2^2}{\sqrt{z_1^2+z_2^2}}-\frac{K_1}{K_S}\end{bmatrix}\begin{bmatrix}\psi_1\\ \psi_2\end{bmatrix} -\\ &\qquad \omega_c\begin{bmatrix}K_S\Big(1-\sqrt{z_1^2+z_2^2}\Big)z_1 - z_2\\ K_S\Big(1-\sqrt{z_1^2+z_2^2}\Big)z_2 + z_1 + K_1(y+\nu-z_2)\end{bmatrix},\end{aligned} \tag{4.36}$$

where the equations for $\boldsymbol{\psi}$ and $\hat{m}$ have been rescaled so that the rate of convergence of the rate estimator is approximately independent of ω_c, β, and K_S. The estimate, $\hat{m}(t)$, is subsequently filtered with a low-pass filter that has the same bandwidth as $m(t)$,

$$\begin{aligned}\dot{\boldsymbol{\varsigma}} &= A_p\boldsymbol{\varsigma} + B_p\hat{m}\\ \tilde{m} &= C_p\boldsymbol{\varsigma} + d_p\hat{m}.\end{aligned} \tag{4.37}$$

Error Dynamics: The performance of the demodulator is quantified through the statistics of the error between the modulator state variables and the demodulator state variables. To write the error equations, two states that correspond to the demodulator

states ψ_1 and ψ_2 are added to the modulator to obtain a one to one correspondence between the modulator and demodulator state variables.. The additional modulator states are

$$\begin{bmatrix}\dot{\zeta}_1\\ \dot{\zeta}_2\end{bmatrix} = (\omega_c+\beta m)K_S \begin{bmatrix} 1-\frac{2x_1^2+x_2^2}{\sqrt{x_1^2+x_2^2}} & -\frac{x_1x_2}{\sqrt{x_1^2+x_2^2}}-\frac{1}{K_S} \\ -\frac{x_1x_2}{\sqrt{x_1^2+x_2^2}}+\frac{1}{K_S} & 1-\frac{x_1^2+2x_2^2}{\sqrt{x_1^2+x_2^2}}-\frac{K_1}{K_S}\end{bmatrix}\begin{bmatrix}\zeta_1\\ \zeta_2\end{bmatrix} - \omega_c \begin{bmatrix} K_S\left(1-\sqrt{x_1^2+x_2^2}\right)x_1 - x_2 \\ K_S\left(1-\sqrt{x_1^2+x_2^2}\right)x_2 + x_1\end{bmatrix}. \tag{4.38}$$

Since the demodulator operates on the unit circle, $x_1^2+x_2^2=1$ and (4.38) can be simplified to

$$\begin{bmatrix}\dot{\zeta}_1\\ \dot{\zeta}_2\end{bmatrix} = (\omega_c+\beta m)K_S \begin{bmatrix} -x_1^2 & -x_1x_2-\frac{1}{K_S} \\ -x_1x_2+\frac{1}{K_S} & -x_2^2\end{bmatrix}\begin{bmatrix}\zeta_1\\ \zeta_2\end{bmatrix} - \omega_c K_S \begin{bmatrix}-x_2\\ x_1\end{bmatrix}. \tag{4.39}$$

Defining $\mathbf{e_z} = \mathbf{z}-\mathbf{x}$, $\mathbf{e}_{\boldsymbol{\psi}} = \boldsymbol{\psi}-\boldsymbol{\zeta}$, and $e_m = \hat{m}-m$, the error equations are

$$\begin{aligned}
\dot{\mathbf{e}}_{\mathbf{z}} &= \big(\omega_c+\beta(m+e_m)\big)\big(\mathbf{f}(\mathbf{x}+\mathbf{e_z},y)-\mathbf{f}(\mathbf{x},y)\big)+\beta e_m\mathbf{f}(\mathbf{x},y),\\
\dot{e}_m &= KK_S\frac{\omega_c}{\beta}e_{z_1}(\zeta_1+e_{\psi_1}),\\
\dot{\mathbf{e}}_{\boldsymbol{\psi}} &= \big(\omega_c+\beta(m+e_m)\big)\frac{\partial \mathbf{f}}{\partial \mathbf{x}}(\mathbf{x}+\mathbf{e_z},y)\mathbf{e}_{\boldsymbol{\psi}}-\omega_c\mathbf{f}(\mathbf{x}+\mathbf{e_z},y).
\end{aligned} \tag{4.40}$$

Applying Quasi-moment Neglect Closure: The quasi-moment neglect closure technique allows only polynomial nonlinearities. Any nonlinearities that are not polynomials are approximated through a multivariate Taylor series expansion. Two subexpressions appear in (4.36) that are not polynomials in the error variables, specifically

$$\begin{aligned}
s_1(\mathbf{z}) &= \sqrt{z_1^2+z_2^2} = \sqrt{(x_1+e_{z_1})^2+(x_2+e_{z_2})^2},\\
s_2(\mathbf{z}) &= \frac{1}{\sqrt{z_1^2+z_2^2}} = \frac{1}{\sqrt{(x_1+e_{z_1})^2+(x_2+e_{z_2})^2}}.
\end{aligned} \tag{4.41}$$

The subexpressions in (4.41) are approximated with a second order Taylor series expansion with respect to e_{z_1} and e_{z_2}.

The Moment Equations: The equations for $\mathbf{e_z}$, e_m, and $\mathbf{e}_\psi$ consist of five equations. The pre-filter is a tenth order band-pass filter and the post-filter is fifth order low-pass filter. Including the filters, the system has a total of twenty states. Closing the moment equations at second order requires all the first and second order moments. The second order moments correspond to a symmetric twenty by twenty covariance matrix, making a total of $N(N+1)/2 = 210$ second order moments. The first-order moments must also be computed, bringing the total up to 230. Finally, the modulator states $\mathbf{x}$ and ζ add another four states, making a total of 234 differential moment equations. The moment equations were derived using Maple, a symbolic math processing software package. The resulting differential equations for the moments were numerically integrated in Matlab.

Results: The output SNR of the demodulator is defined to be

$$\mathrm{SNR}_{\mathrm{out}} = 10\log_{10}\left(\frac{\overline{m^2}}{\overline{(\hat{m}-m)^2}}\right)\ (\mathrm{dB}), \tag{4.42}$$

where $\overline{m^2}$ is the average power in m. Figure 4-3 shows the demodulator output SNR versus the baseband output SNR for $\beta = 2$, 5, and 10. The baseband output SNR is

$$\mathrm{SNR}_{\mathrm{b}} = 10\log_{10}\left(\frac{\pi\omega_m}{N_0}\right)\ (\mathrm{dB}), \tag{4.43}$$

where ω_m is the bandwidth of the information signal, $m(t)$, and N_0 is the level of the power density spectrum of the white noise. $\mathrm{SNR}_{\mathrm{b}}$ corresponds to the output SNR achieved if the information signal, $m(t)$, is sent directly through the additive white noise channel and subsequently filtered with a low-pass filter with a cut-off frequency of ω_m. Therefore, plotting $\mathrm{SNR}_{\mathrm{out}}$ as a function of $\mathrm{SNR}_{\mathrm{b}}$ shows how rate modulation compares to using no modulation. From the plot, increasing β increases the noise immunity. In Table 4.7, the SNR at the output of the stiff harmonic demodulator is compared to the SNR at the output of the second-order PLL analyzed in Appendix B.

A comparison between the time-averaged pdfs obtained from the QMNC tech-

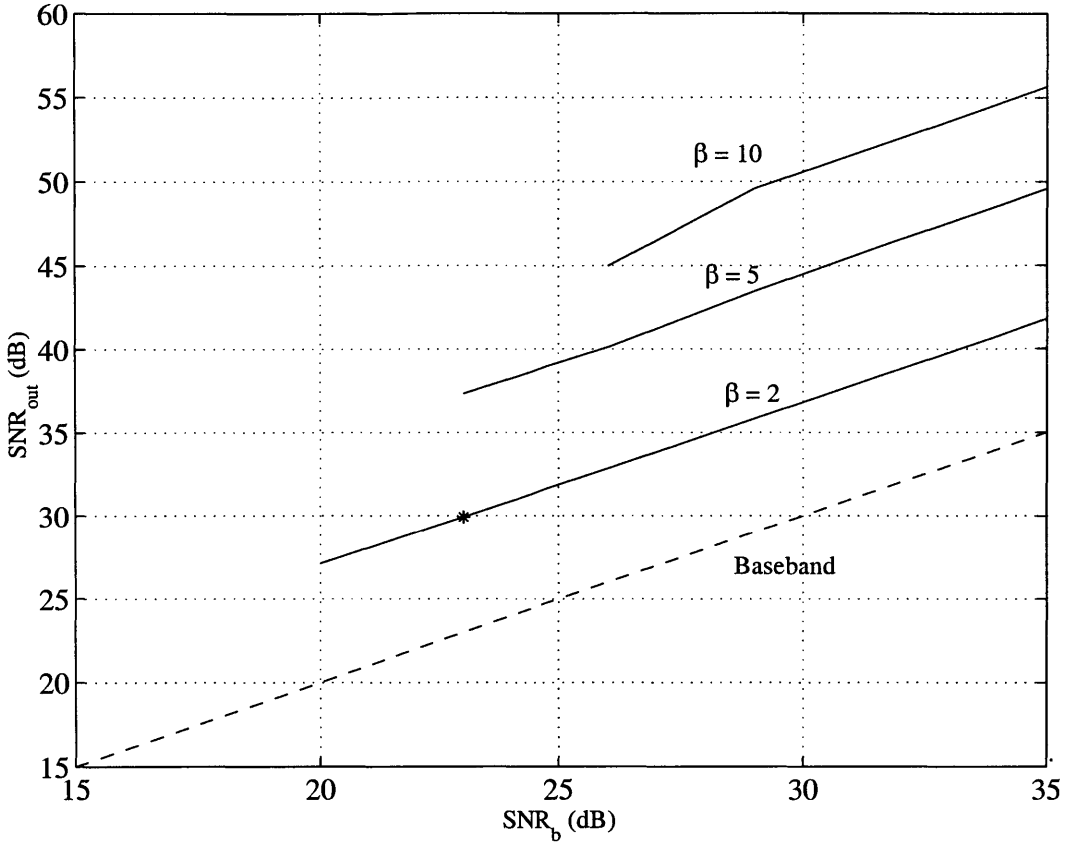

Figure 4-3: SNR_{out} vs. SNR_b for $\beta = 2, 5$, and 10 for the stiff harmonic oscillator. The pdfs associated with the point marked with a '$*$' are shown in Figure 4-4.

	β					
	2		5		10	
SNR_b	SHO	PLL	SHO	PLL	SHO	PLL
35	41.80	43.92	49.58	51.60	55.66	57.90
32	38.80	40.92	46.57	48.88	52.59	54.90
29	35.82	37.91	43.46	45.87	49.58	51.89
26	32.84	34.89	40.12	42.84	44.98	48.87
23	29.91	31.84	37.33	39.80	—	45.82
20	27.12	28.75	—	36.71	—	42.73

Table 4.7: A performance comparison between the stiff harmonic oscillator and the PLL.

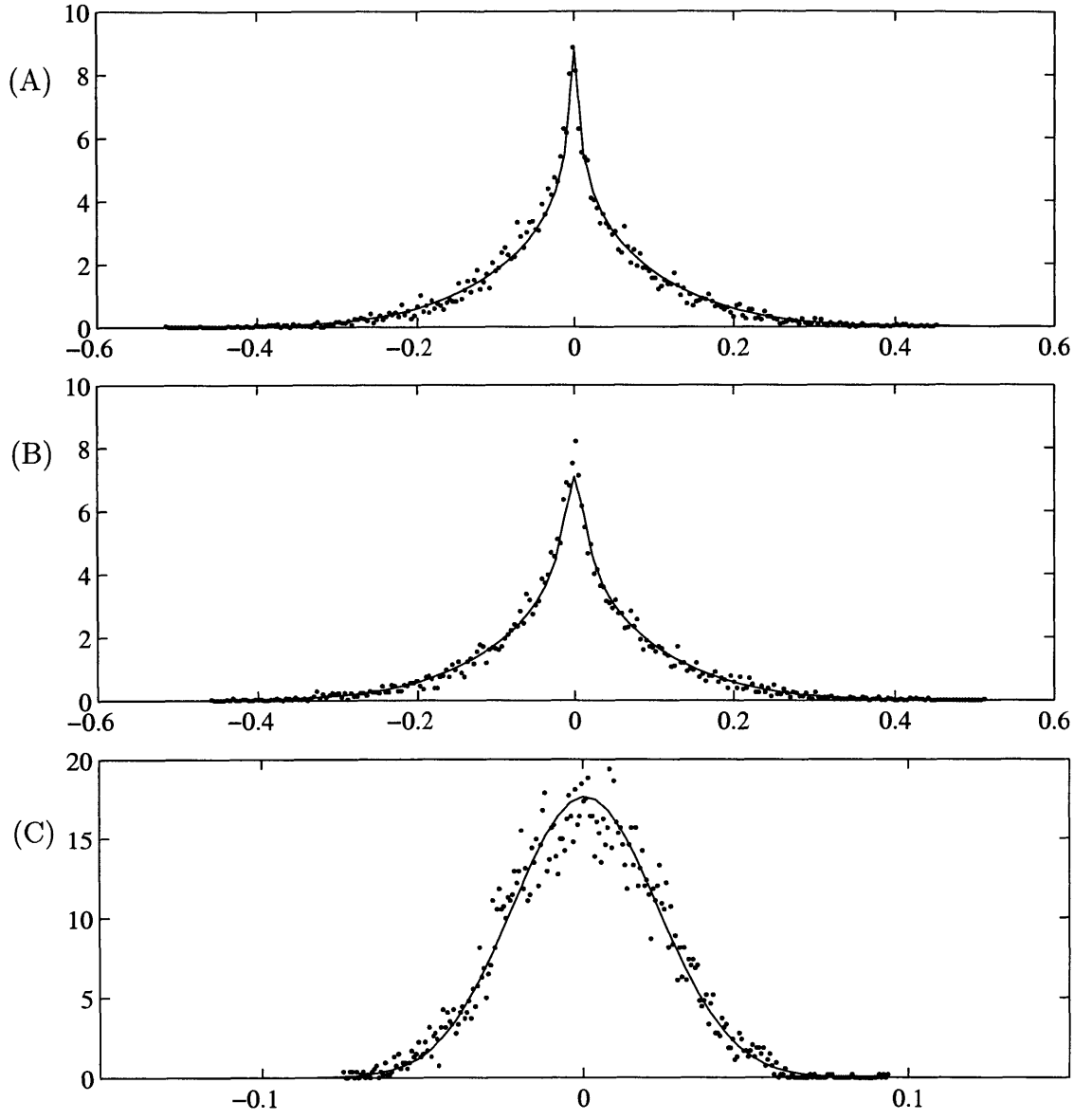

Figure 4-4: A comparison of the pdfs of the stiff harmonic oscillator obtained from the QMNC technique (solid line) and a direct simulation (dots), (A) $p(e_{z_1})$, (B) $p(e_{z_2})$, and (C), $p(\tilde{m})$.

nique and the time-averaged pdfs obtained from a direct simulation of the stochastic differential equations is shown in Figure 4-4 for $\beta = 2$ and $\text{SNR}_\text{b} = 23$ (dB), which corresponds to the data point marked with an asterisk in Figure 4-3. The mean of e_m predicted by the QMNC technique is 6.77×10^{-4} and the mean of e_m estimated from the direct simulation is 6.76×10^{-4}. The average SNR at the output of the demodulator predicted by the QMNC technique is 29.91 dB and the estimated average SNR at the output of the demodulator is 29.66 dB.

The stiffness parameter, K_stiff, also affects the SNR at the output of the demodulator. In Figure 4-5, SNR_out is shown as a function of K_stiff for $K_\text{stiff} = 0.2$, 0.5, 1, 2, and 5, $\beta = 2$, and $\text{SNR}_\text{b} = 35$ (dB).

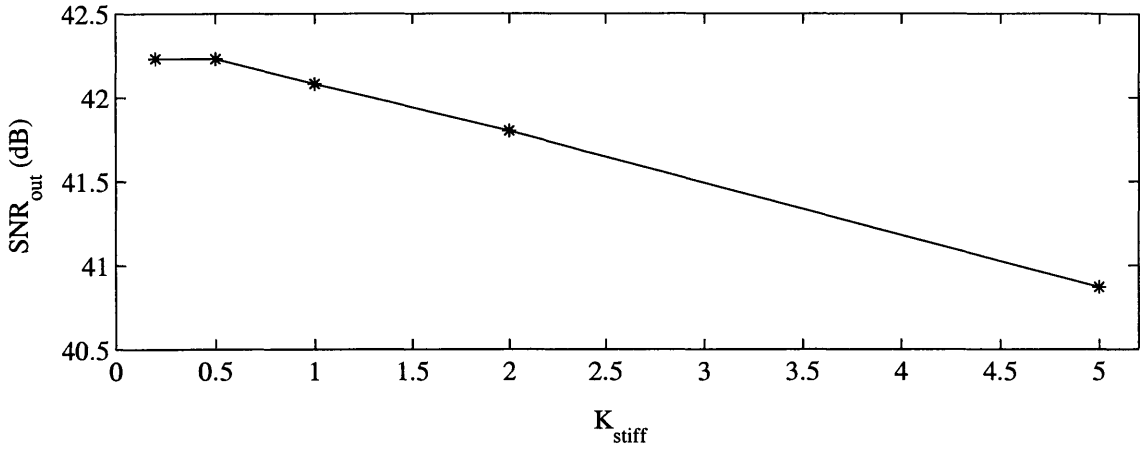

Figure 4-5: The effect of the stiffness parameter on the output SNR, $\beta = 2$, and $\text{SNR}_\text{b} = 35$ (dB).

Threshold: Just as with the PLL analyzed in Appendix B, the moment equations have been closed at second order, which means that the demodulator state variables are assumed to be Gaussian. The match between the pdfs predicted by the QMNC technique and the pdfs estimated from a direct simulation of the nonlinear system shown in Figure 4-4 indicates that for sufficiently high input SNRs, this assumption is valid. However, as with the PLL, the stiff harmonic oscillator system exhibits a threshold effect as SNR_b decreases and the second order QMNC fails to capture this phenomenon. Instead, the QMNC moment equations become unstable.

4.5.2 The van der Pol Oscillator

The differential equations describing the behavior of the van der Pol oscillator are

$$\begin{aligned} \dot{x}_1 &= x_2, \\ \dot{x}_2 &= \lambda(1 - x_1^2)x_2 - x_1, \end{aligned} \tag{4.44}$$

where λ is a positive constant.

The Modulator: Introducing modulation as described in Chapter 2, the modulator is given by

$$\begin{aligned} \dot{x}_1 &= (\omega_c + \beta m)x_2, \\ \dot{x}_2 &= (\omega_c + \beta m)\big(\lambda(1 - x_1^2)x_2 - x_1\big). \end{aligned} \tag{4.45}$$

The Channel and Pre-Filter: The transmitted signal is $y = x_1$. the channel is an additive white noise channel and the pre-filter is given by

$$\begin{aligned} d\boldsymbol{\vartheta} &= A\boldsymbol{\vartheta}dt + BdW(t), \\ \nu &= C\boldsymbol{\vartheta}, \end{aligned} \tag{4.46}$$

where A, B, and C correspond to a bandpass filter with a bandwidth of B_W centered at ω_c. The noise process, $dW(t)$, is a Gaussian white noise process. B_W is chosen to be equal to the bandwidth of the transmitted signal as described in Section 2.3.

The Demodulator: An exponentially convergent observer for the van der Pol oscillator is

$$\begin{aligned} \dot{z}_1 &= z_2 + K_1(y - z_1), \\ \dot{z}_2 &= \lambda(1 - z_1^2)z_2 - z_1, \end{aligned} \tag{4.47}$$

where K_1 is a positive constant. Choosing $g(\psi_1) = \psi_1$ and following the demodulator design procedure of Section 3.5.2, the demodulator equations are, after rescaling[5],

$$\begin{aligned}
\dot{z}_1 &= (\omega_c + \beta\hat{m})\big(z_2 + K_1(y + \nu - z_1)\big), \\
\dot{z}_2 &= (\omega_c + \beta\hat{m})\big(\lambda(1 - z_1^2)z_2 - z_1\big), \\
\dot{\hat{m}} &= K\frac{\omega_c}{\beta}\big(z_1 - (y + \nu)\big)\psi_1, \\
\begin{bmatrix}\dot{\psi}_1 \\ \dot{\psi}_2\end{bmatrix} &= (\omega_c + \beta\hat{m})\begin{bmatrix}-K_1 & 1 \\ -2\lambda z_1 z_2 - 1 & \lambda(1 - z_1^2)\end{bmatrix}\begin{bmatrix}\psi_1 \\ \psi_2\end{bmatrix} - \omega_c\begin{bmatrix}z_2 + K_1(y + \nu - z_1) \\ \lambda(1 - z_1^2)z_2 - z_1\end{bmatrix}.
\end{aligned} \tag{4.48}$$

The estimate, $\hat{m}$, is subsequently filtered with a low-pass filter that has the same bandwidth as $m(t)$,

$$\begin{aligned}
\dot{\boldsymbol{\varsigma}} &= A_p\boldsymbol{\varsigma} + B_p\hat{m}, \\
\tilde{m} &= C_p\boldsymbol{\varsigma} + d_p\hat{m}.
\end{aligned} \tag{4.49}$$

Error Dynamics: To get a one to one correspondence between the state variables of the modulator and the state variables of the demodulator, the modulator is augmented so that it has state variables corresponding to the demodulator state variables ψ_1 and ψ_2. The additional modulator state variables are

$$\begin{bmatrix}\dot{\zeta}_1 \\ \dot{\zeta}_2\end{bmatrix} = (\omega_c + \beta m)\begin{bmatrix}-K_1 & 1 \\ -2\lambda x_1 x_2 - 1 & \lambda(1 - x_1^2)\end{bmatrix}\begin{bmatrix}\zeta_1 \\ \zeta_2\end{bmatrix} - \omega_c\begin{bmatrix}x_2 \\ \lambda(1 - x_1^2)x_2 - x_1\end{bmatrix} \tag{4.50}$$

Defining $\mathbf{e_z} = \mathbf{z} - \mathbf{x}$, $e_{\boldsymbol{\psi}} = \boldsymbol{\psi} - \boldsymbol{\zeta}$, and $e_m = \hat{m} - m$, the error equations are

$$\begin{aligned}
\dot{\mathbf{e}}_\mathbf{z} &= \big(\omega_c + \beta(m + e_m)\big)\big(\hat{\mathbf{f}}(\mathbf{x} + \mathbf{e_z}, y) - \hat{\mathbf{f}}(\mathbf{x}, y)\big) + \beta e_m\hat{\mathbf{f}}(\mathbf{x}, y), \\
\dot{e}_m &= K\frac{\omega_c}{\beta}(\zeta_1 + e_{\psi_1}), \\
\dot{\mathbf{e}}_{\boldsymbol{\psi}} &= \big(\omega_c + \beta(m + e_m)\big)\frac{\partial\hat{\mathbf{f}}}{\partial\mathbf{x}}(\mathbf{x} + \mathbf{e_z}, y)\mathbf{e}_{\boldsymbol{\psi}} - \omega_c\hat{\mathbf{f}}(\mathbf{x} + \mathbf{e_z}, y).
\end{aligned} \tag{4.51}$$

[5]The equations for $\hat{m}$ and $\boldsymbol{\psi}$ are rescaled so that the rate of convergence of the rate estimator is independent of ω_c and β.

Applying Quasi-Moment Neglect Closure: All nonlinearities that appear in the error equations are polynomials and the quasi-moment neglect closure technique can be applied directly to the error equations.

The Moment Equations: The equations for $\mathbf{e_z}$, e_m, and $\mathbf{e}_\psi$ consist of a total of five equations. The pre-filter is a fifth order low-pass filter and the post-filter is a third-order low-pass filter. Including the filters, the system has a total of thirteen states. Closing the moment equations at second order requires all the first and second order moments. The second order moments correspond to a symmetric thirteen by thirteen covariance matrix, making a total of $N(N+1)/2 = 91$ second order moments. Including the first-order moments brings the total to 104 moment equations. Finally, the modulator states $\mathbf{x}$ and $\boldsymbol{\zeta}$ must be included, bringing the total number of equations to 108. The moment equations were derived using Maple and the resulting differential equations were numerically integrated in Matlab.

Results: The output SNR of the demodulator is defined to be

$$\mathrm{SNR}_{\mathrm{out}} = 10\log_{10}\left(\frac{\overline{m^2}}{\overline{(\hat{m}-m)^2}}\right)\ (\mathrm{dB}), \tag{4.52}$$

where $\overline{m^2}$ is the average power in m. Figure 4-6 shows the demodulator output SNR versus the baseband output SNR for $\beta = 0.2$, 0.5, and 0.7. The baseband output SNR is

$$\mathrm{SNR}_{\mathrm{b}} = 10\log_{10}\left(\frac{\pi\omega_m}{N_0}\right)\ (\mathrm{dB}), \tag{4.53}$$

where ω_m is the bandwidth of the information signal, $m(t)$, and N_0 is the level of the power density spectrum of the white noise. $\mathrm{SNR}_{\mathrm{b}}$ corresponds to the output SNR achieved if the information signal, $m(t)$, is sent directly through the additive white noise channel and subsequently filtered with a low-pass filter with a cut-off frequency of ω_m. Therefore, plotting $\mathrm{SNR}_{\mathrm{out}}$ as a function of $\mathrm{SNR}_{\mathrm{b}}$ shows how rate modulation compares to using no modulation. From the plot, increasing β increases the noise immunity.

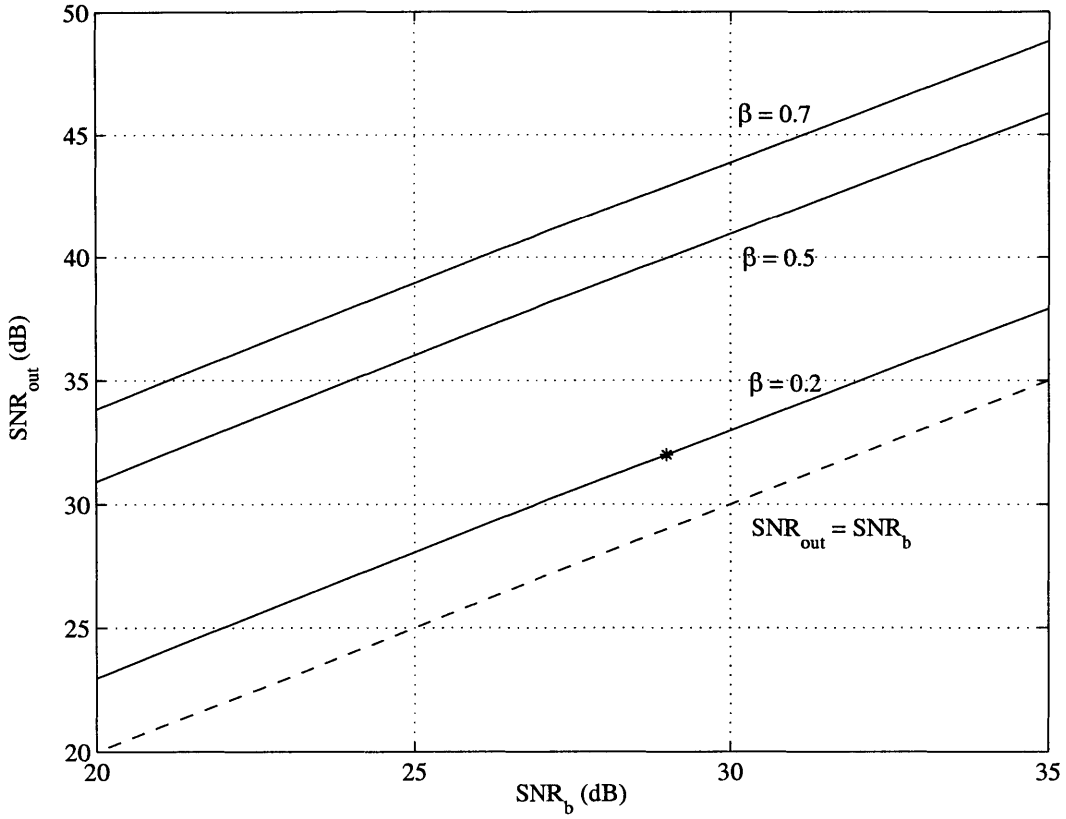

Figure 4-6: SNR_{out} vs. SNR_b for $\beta = 0.2$, 0.5, and 0.7 for the van der Pol oscillator. The pdfs associated with the point marked with a '$*$' are shown in Figure 4-7.

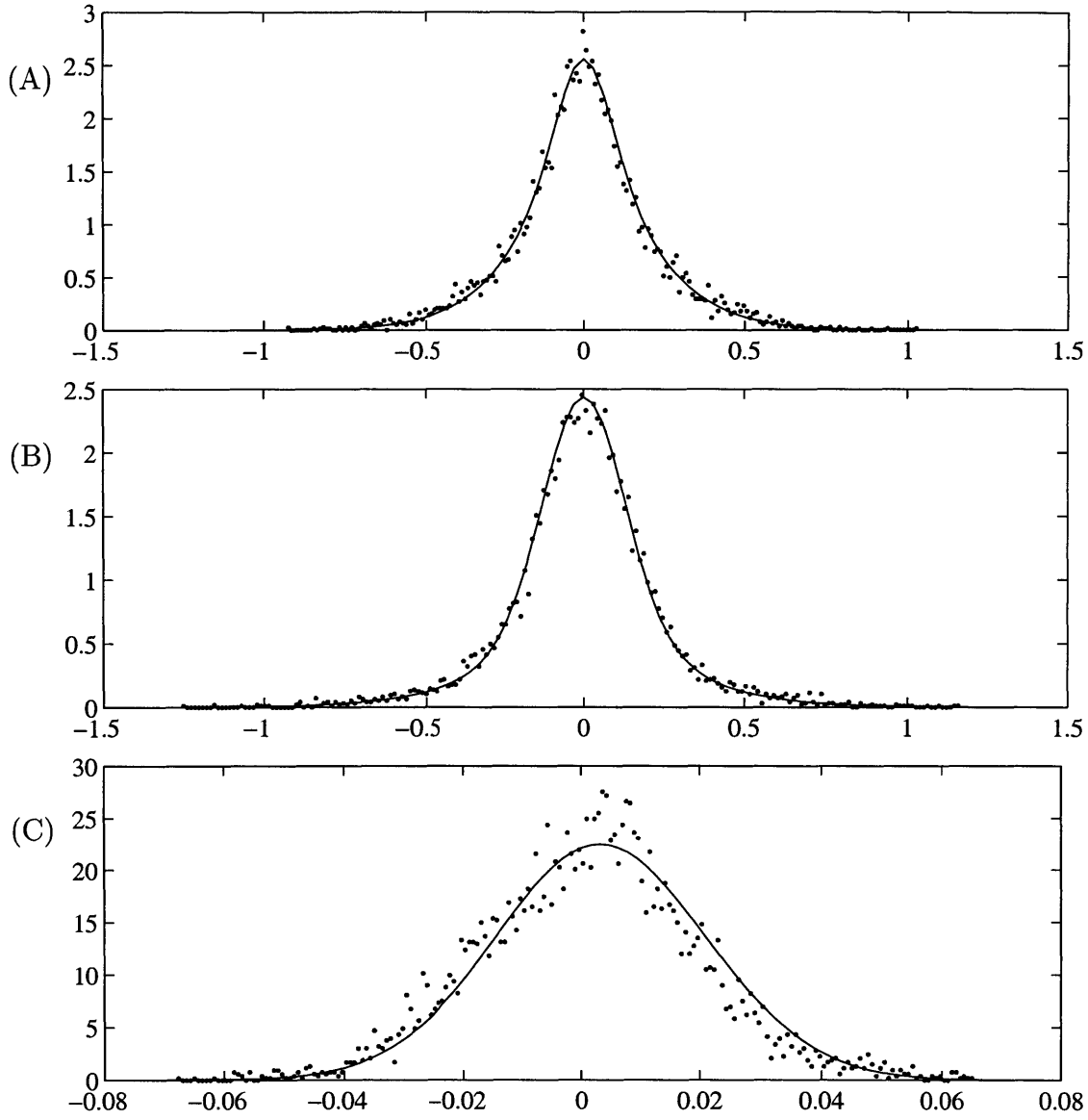

Figure 4-7: A comparison of the pdfs of the van der Pol system obtained from the QMNC technique (solid line) and a direct simulation (dots), (A) $p(e_{z_1})$, (B) $p(e_{z_2})$, and (C), $p(\tilde{m})$.

A comparison between the time-averaged pdfs obtained from the QMNC technique and the time-averaged pdfs obtained from a direct simulation of the stochastic differential equations is shown in Figure 4-7 for $\beta = 0.2$ and $\mathrm{SNR_b} = 29$ (dB), which corresponds to the data point marked with an asterisk in Figure 4-6. The mean of e_m predicted by the QMNC technique is 3.25×10^{-3} and the mean of e_m estimated from the direct simulation is 1.30×10^{-3}. The average SNR at the output of the demodulator predicted by the QMNC technique is 32.00 dB and the estimated average SNR at the output of the demodulator is 31.79 dB.

4.5.3 The Lorenz System

The Lorenz system, which is given by

$$\begin{aligned} \dot{x}_1 &= \sigma(x_2 - x_1), \\ \dot{x}_2 &= r x_1 - x_1 x_3 - x_2, \\ \dot{x}_3 &= x_1 x_2 - b x_3, \end{aligned} \tag{4.54}$$

is a chaotic system for appropriate choices of the constants σ, r, and b.

The Modulator: Introducing modulation as described in Chapter 2, the modulator is given by

$$\begin{aligned} \dot{x}_1 &= (\omega_c + \beta m)\sigma(x_2 - x_1), \\ \dot{x}_2 &= (\omega_c + \beta m)\big(r x_1 - x_1 x_3 - x_2\big), \\ \dot{x}_3 &= (\omega_c + \beta m)\big(x_1 x_2 - b x_3\big). \end{aligned} \tag{4.55}$$

The Channel and Pre-Filter: The transmitted signal is $y = x_1$. The channel is an additive white noise channel and the pre-filter is given by

$$\begin{aligned} d\boldsymbol{\vartheta} &= A\boldsymbol{\vartheta} dt + B dW(t), \\ \nu &= C\boldsymbol{\vartheta}, \end{aligned} \tag{4.56}$$

where A, B, and C correspond to a bandpass filter with a bandwidth of B_W centered at ω_c. The noise process, $dW(t)$, is a Gaussian white noise process. B_W is chosen to be equal to the bandwidth of the transmitted signal as described in Section 2.3.

The Demodulator: An exponentially convergent observer for the Lorenz system is

$$\begin{aligned} \dot{z}_1 &= \sigma(z_2 - z_1), \\ \dot{z}_2 &= ry - yz_3 - z_2, \\ \dot{z}_3 &= yz_2 - bz_3. \end{aligned} \tag{4.57}$$

Choosing $g(\psi_1) = \psi_1$ and following the demodulator design procedure of Section 3.5.2, the demodulator equations are, after rescaling[6],

$$\begin{aligned} \dot{z}_1 &= (\omega_c + \beta\hat{m})\sigma(z_2 - z_1), \\ \dot{z}_2 &= (\omega_c + \beta\hat{m})\big(r(y+\nu) - (y+\nu)z_3 - z_2\big), \\ \dot{z}_3 &= (\omega_c + \beta\hat{m})\big((y+\nu)z_2 - bz_3\big), \\ \dot{\hat{m}} &= K\frac{\omega_c}{\beta}(z_1 - (y+\nu))\psi_1, \\ \begin{bmatrix} \dot{\psi}_1 \\ \dot{\psi}_2 \\ \dot{\psi}_3 \end{bmatrix} &= (\omega + \beta\hat{m}) \begin{bmatrix} -\sigma & \sigma & 0 \\ 0 & -1 & -(y+\nu) \\ 0 & y+\nu & -b \end{bmatrix} \begin{bmatrix} \psi_1 \\ \psi_2 \\ \psi_3 \end{bmatrix} - \omega_c \begin{bmatrix} \sigma(z_2 - z_1) \\ r(y+\nu) - (y+\nu)z_3 - z_2 \\ (y+\nu)z_2 - bz_3 \end{bmatrix}. \end{aligned} \tag{4.58}$$

The estimate, $\hat{m}$, is subsequently filtered with a low-pass filter that has the same bandwidth as $m(t)$,

$$\begin{aligned} \dot{\boldsymbol{\varsigma}} &= A_p\boldsymbol{\varsigma} + B_p\hat{m}, \\ \tilde{m} &= C_p\boldsymbol{\varsigma} + d_p\hat{m}. \end{aligned} \tag{4.59}$$

[6]The equations for $\hat{m}$ and $\boldsymbol{\psi}$ are rescaled so that the rate of convergence of $\hat{m}$ is independent of ω_c and β.

Error Dynamics: The probability density functions are computed for the error between the state variables of the modulator and the state variables of the demodulator. To get a one to one correspondence between the state variables of the modulator and the state variables of the demodulator, the modulator is augmented so that it has state variables corresponding the demodulator state variables ψ_1 and ψ_2. The additional modulator state variables are

$$\begin{bmatrix} \dot{\zeta}_1 \\ \dot{\zeta}_2 \\ \dot{\zeta}_3 \end{bmatrix} = (\omega + \beta\hat{m}) \begin{bmatrix} -\sigma & \sigma & 0 \\ 0 & -1 & -x_1 \\ 0 & x_1 & -b \end{bmatrix} \begin{bmatrix} \zeta_1 \\ \zeta_2 \\ \zeta_3 \end{bmatrix} - \omega_c \begin{bmatrix} \sigma(x_2 - x_1) \\ rx_1 - x_1x_3 - x_2 \\ x_1x_2 - bx_3 \end{bmatrix}. \tag{4.60}$$

Applying Quasi-Moment Neglect Closure: The equations for the demodulator are in polynomial form, so the quasi-moment neglect technique can be applied directly to the error equations.

The Moment Equations: The equations for $\mathbf{e_z}$, e_m, and $\mathbf{e_\psi}$ consist of seven equations. The pre-filter is a fifth-order low-pass filter and the post-filter is a third-order low-pass filter. Including the filters, the system has a total of fifteen states. Closing the moment equations at second order requires all of the first and second order moments. The second order moments correspond to a symmetric fifteen by fifteen matrix, making a total of $N(N+1)/2 = 120$ second order moments. The first-order moments must also be computed, bring the total to 135. Finally, the modulator states $\mathbf{x}$, and $\boldsymbol{\zeta}$ add another six equations, bringing the total to 141. The moment equations were generated using Maple and were numerically integrated using Matlab.

Results: The SNR at the input to the demodulator is defined as

$$\mathrm{SNR_{in}} = 10\log_{10}\left(\frac{\overline{y^2}}{\overline{\nu^2}}\right). \tag{4.61}$$

The SNR at the output of the demodulator is defined as

$$\mathrm{SNR}_{\mathrm{out}} = 10 \log_{10} \left(\frac{\overline{m^2}}{\overline{(m - \hat{m})^2}} \right). \tag{4.62}$$

Figure 4-8 shows a plot of the output SNR as a function of the input SNR for $\beta =$ 0.2, 0.5, and 0.7. Similar to the previous modulation/demodulation systems, there is a trade-off between noise-immunity and bandwidth

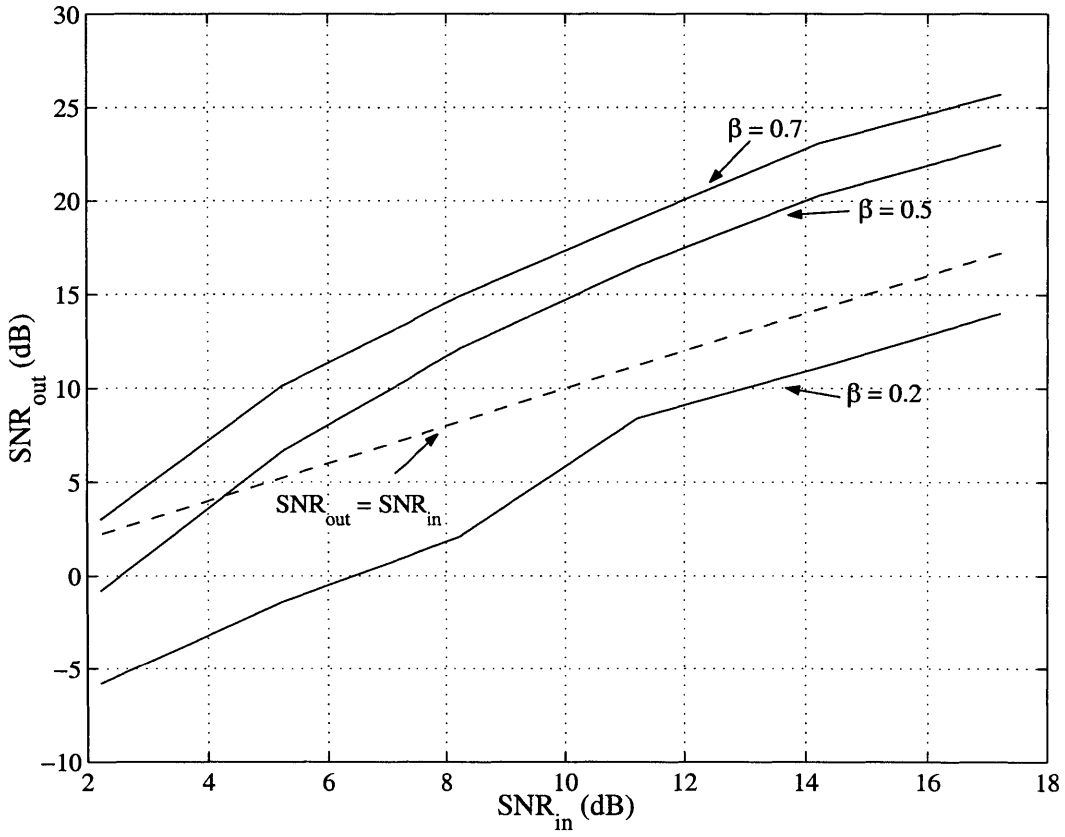

Figure 4-8: $\mathrm{SNR}_{\mathrm{out}}$ vs. $\mathrm{SNR}_{\mathrm{in}}$ for the Lorenz based system for $\beta = 0.2$, 0.5, and 0.7.

Figure 4-9 compares the probability density functions approximated using the QMNC technique and the probability density function estimated by a direct simulation of the SDE.

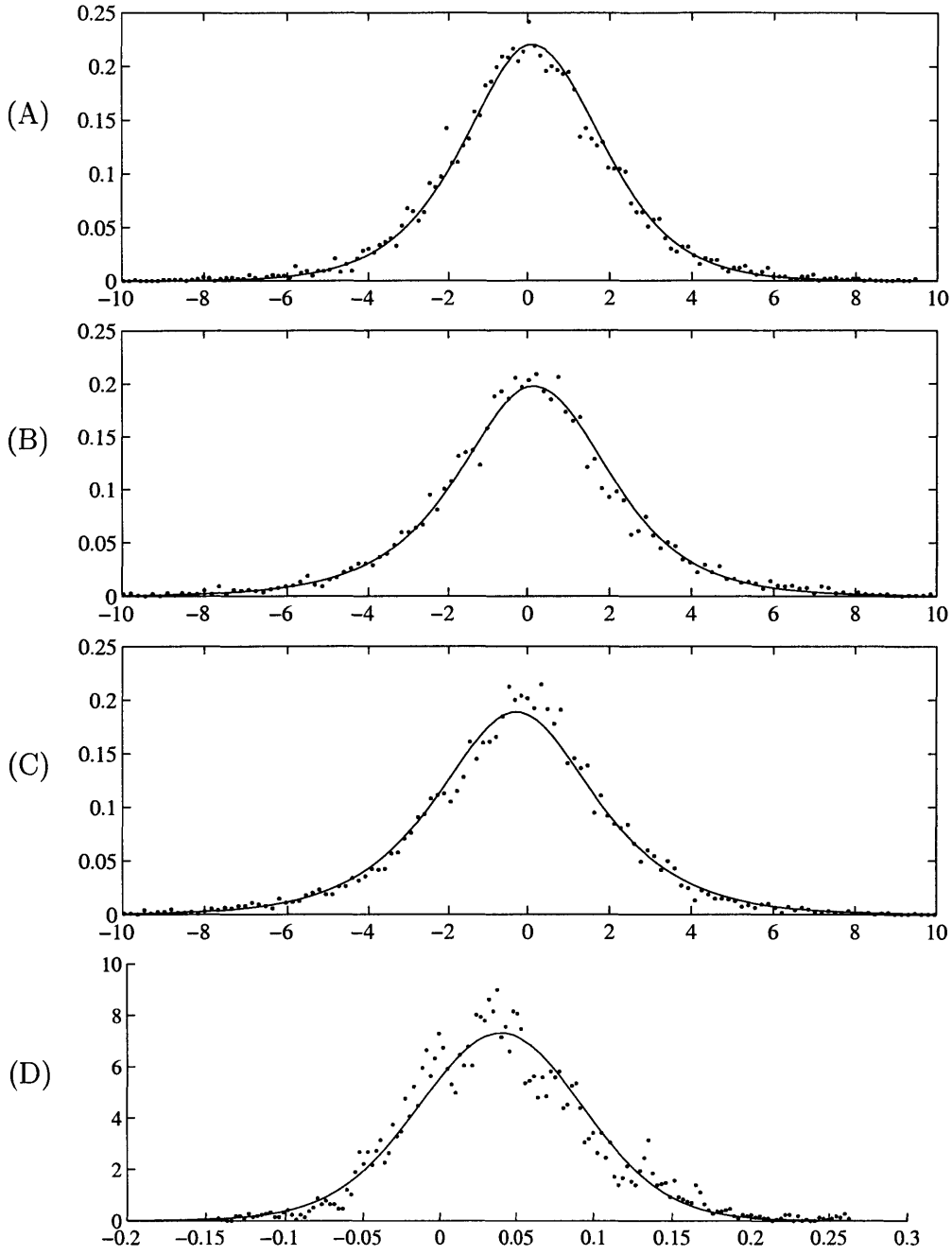

Figure 4-9: A comparison of the pdfs (QMNC - solid, SDE - dotted) for the Lorenz system for $\mathrm{SNR_{in}} = 15$ dB, $\omega_m = 0.2$ (rad/sec), $\beta = 0.5$, $\omega_c = 1$ (rad/sec), (A) $p(z_1 - x_1)$, (B) $p(z_2 - x_2)$, (C) $p(z_3 - x_3)$, and (D) $p(\widetilde{m})$.

Chapter 5

Design and Construction of Lorenz Based Modulator and Demodulator Circuits

In this chapter, the design and construction of a prototype of a complete modulation/demodulation system based on the chaotic Lorenz system is described. The circuits are constructed with analog components, the nonlinear terms being implemented with analog multipliers. The other components used to build the circuits are operational amplifiers, resistors, and capacitors.

Section 5.1 describes the Lorenz-based modulator and demodulator circuits. Section 5.2 summarizes some basic issues that were considered regarding the layout of the components. Section 5.3 provides examples of the performance of the system.

5.1 Modulator and Demodulator Circuits

5.1.1 Rescaled Lorenz Equations

The operational amplifiers and the analog multipliers used have an input/output range of ± 12 volts. The circuit is designed such that the state variables correspond to voltage levels in the circuit and the Lorenz equations must be rescaled so that all

voltage levels remain within the operating range of the components. The rescaled variables are $X_1 = \frac{1}{2}x_1$, $X_2 = \frac{1}{2}x_2$, and $X_3 = \frac{2}{9}x_3$. The rescaled Lorenz equations implemented in the circuit are

$$\begin{aligned} \dot{X}_1 &= \sigma(X_2 - X_1), \\ \dot{X}_2 &= rX_1 - \frac{9}{2}X_1X_3 - X_2, \\ \dot{X}_3 &= \frac{8}{9}X_1X_2 - bX_3, \end{aligned} \tag{5.1}$$

where σ, r, and b are 10, 25, and $\frac{8}{3}$, respectively. As shown in Figure 5-1, X_1, X_2, and X_3 remain within ± 12.

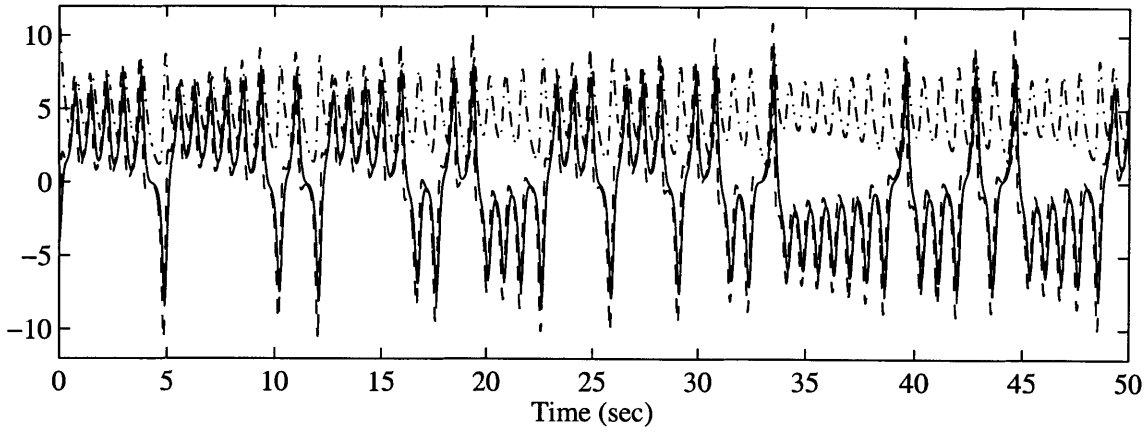

Figure 5-1: Rescaled Lorenz variables from simulation, X_1 (solid), X_2 (dash), and X_3 (dash-dot).

5.1.2 Modulator Circuit

Introducing modulation into the rescaled Lorenz equations, as described in Chapter 2, the modulator equations become

$$\begin{aligned}
\dot{X}_1 &= \big(\omega_c + \beta m(t)\big)\Big(\sigma(X_2 - X_1)\Big), \\
\dot{X}_2 &= \big(\omega_c + \beta m(t)\big)\Big(rX_1 - \frac{9}{2}X_1X_3 - X_2\Big), \\
\dot{X}_3 &= \big(\omega_c + \beta m(t)\big)\Big(\frac{8}{9}X_1X_2 - bX_3\Big), \\
y &= X_1,
\end{aligned} \tag{5.2}$$

The analog circuit implementation of (5.2) is shown in Figure 5-2 The operational amplifiers perform the operations of addition, subtraction, multiplication by a constant, and integration. The nonlinear terms, such as X_1X_3, are implemented with analog multipliers[1]. The set of equations that describe the behavior of the modulator circuit are

$$\dot{V}_1 = \frac{1}{C_{101}}\Big(\frac{1}{R_{114}} + \frac{m(t)}{10R_{115}}\Big)\Big(\frac{R_{102}}{R_{101}}V_2 - \Big(\frac{R_{104}}{R_{103}+R_{104}}\Big)\Big(1 + \frac{R_{102}}{R_{101}}\Big)V_1\Big)$$

$$\dot{V}_2 = \frac{1}{C_{102}}\Big(\frac{1}{R_{116}} + \frac{m(t)}{10R_{117}}\Big)\frac{R_{121}}{R_{120}}\Big\{\Big(\frac{R_{109}}{R_{108}+R_{109}}\Big)\Big(1 + \frac{R_{106}}{R_{105}} + \frac{R_{106}}{R_{107}}\Big)V_1 - \frac{R_{106}}{10R_{107}}V_1V_3 - \frac{R_{106}}{R_{105}}V_2\Big\}$$

$$\dot{V}_3 = \frac{1}{C_{103}}\Big(\frac{1}{R_{118}} + \frac{m(t)}{10R_{119}}\Big)\Big\{\Big(\frac{R_{113}}{R_{112}+R_{113}}\Big)\Big(1 + \frac{R_{111}}{R_{110}}\Big)V_3 - \frac{R_{111}}{10R_{110}}V_1V_2\Big\}.$$

[1]The multiplier circuits have as their output the product of the inputs divided by ten, which is the reason some terms in the circuit equations are divided by ten.

5.1.3 Demodulator Circuit

The Lorenz system has the following observer when $y(t) = X_1(t)$,

$$\begin{aligned} \hat{F}_1 &= \sigma(\hat{X}_2 - y) \\ \dot{\hat{X}}_2 &= ry - \frac{9}{2}y\hat{X}_3 - \hat{X}_2 \\ \dot{\hat{X}}_3 &= \frac{8}{9}y\hat{X}_2 - b\hat{X}_3, \end{aligned} \tag{5.3}$$

where X_1 is not generated, since only $\hat{F}_1 = \sigma(\hat{X}_2 - y)$ is needed.

Following the linearization procedure described in Section 3.5.3 and using a first-order low-pass filter that has cut-off frequency of ω_L, the rate estimation equations are

$$\begin{aligned} \dot{\hat{m}} &= -K\big((\omega_c + \beta\hat{m})r_1 - (y - r_2)\big)r_1, \\ \dot{r}_1 &= -\omega_L(r_1 - \hat{F}_1), \\ \dot{r}_2 &= -\omega_L(r_2 - y). \end{aligned} \tag{5.4}$$

Analog circuit implementations of (5.3) and (5.4) are shown in Figure 5-3 and Figure 5-4, respectively. The equations that describe the behavior of the demodulator circuit are

$$\begin{aligned} \hat{F}_1 &= \frac{R_{202}}{R_{201}}\hat{V}_2 - \frac{R_{204}}{R_{203}+R_{204}}\Big(1 + \frac{R_{202}}{R_{201}}\Big)y \\ \dot{\hat{V}}_2 &= \frac{1}{C_{201}}\Big(\frac{1}{R_{214}} + \frac{\hat{m}(t)}{10R_{215}}\Big)\frac{R_{219}}{R_{218}}\Big\{ - \frac{R_{206}}{10R_{207}}yV_3 - \frac{R_{206}}{R_{205}}V_2 + \\ &\qquad + \Big(\frac{R_{209}}{R_{208}+R_{209}}\Big)\Big(1 + \frac{R_{206}}{R_{205}} + \frac{R_{206}}{R_{207}}\Big)y\Big\} \\ \dot{\hat{V}}_3 &= \frac{1}{C_{202}}\Big(\frac{1}{R_{216}} + \frac{\hat{m}(t)}{10R_{217}}\Big)\Big\{\Big(\frac{R_{213}}{R_{212}+R_{213}}\Big)\Big(1 + \frac{R_{211}}{R_{210}}\Big)V_3 - \\ &\qquad - \frac{R_{211}}{10R_{210}}yV_2\Big\}, \end{aligned} \tag{5.5}$$

where $y = V_1$.

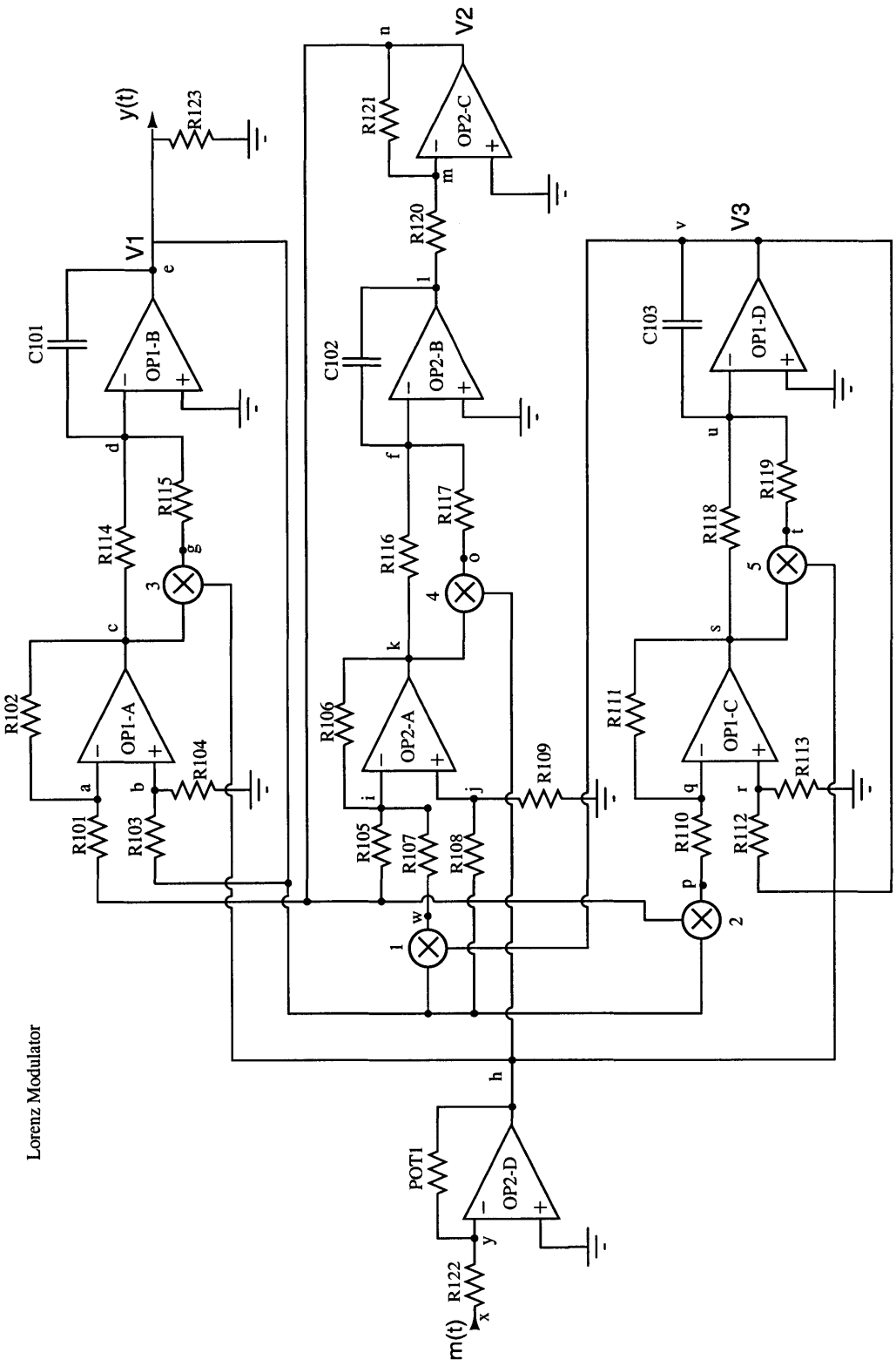

Figure 5-2: Circuit diagram for the Lorenz-based modulator.

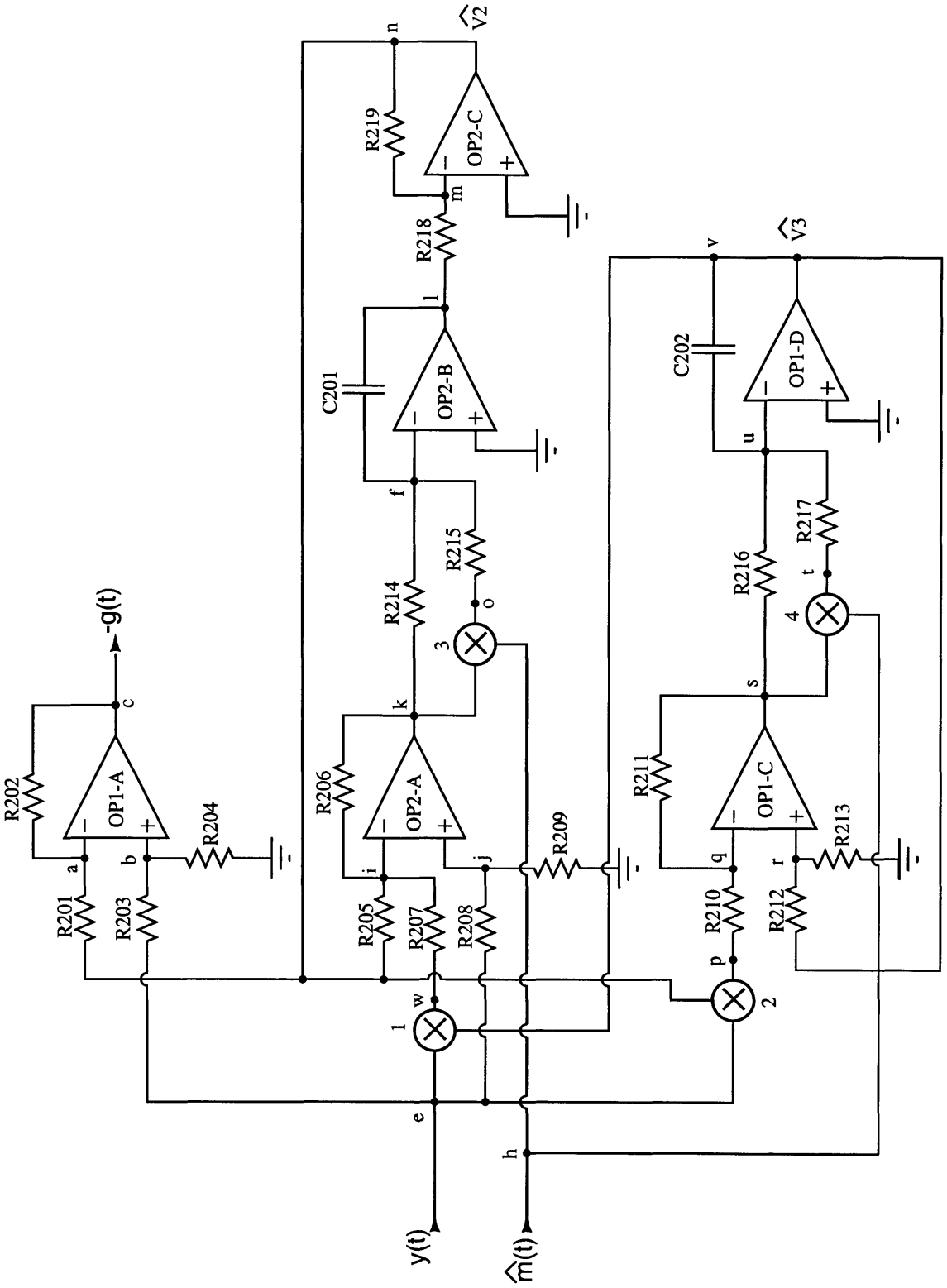

Figure 5-3: Circuit diagram for the Lorenz-based demodulator – observer component.

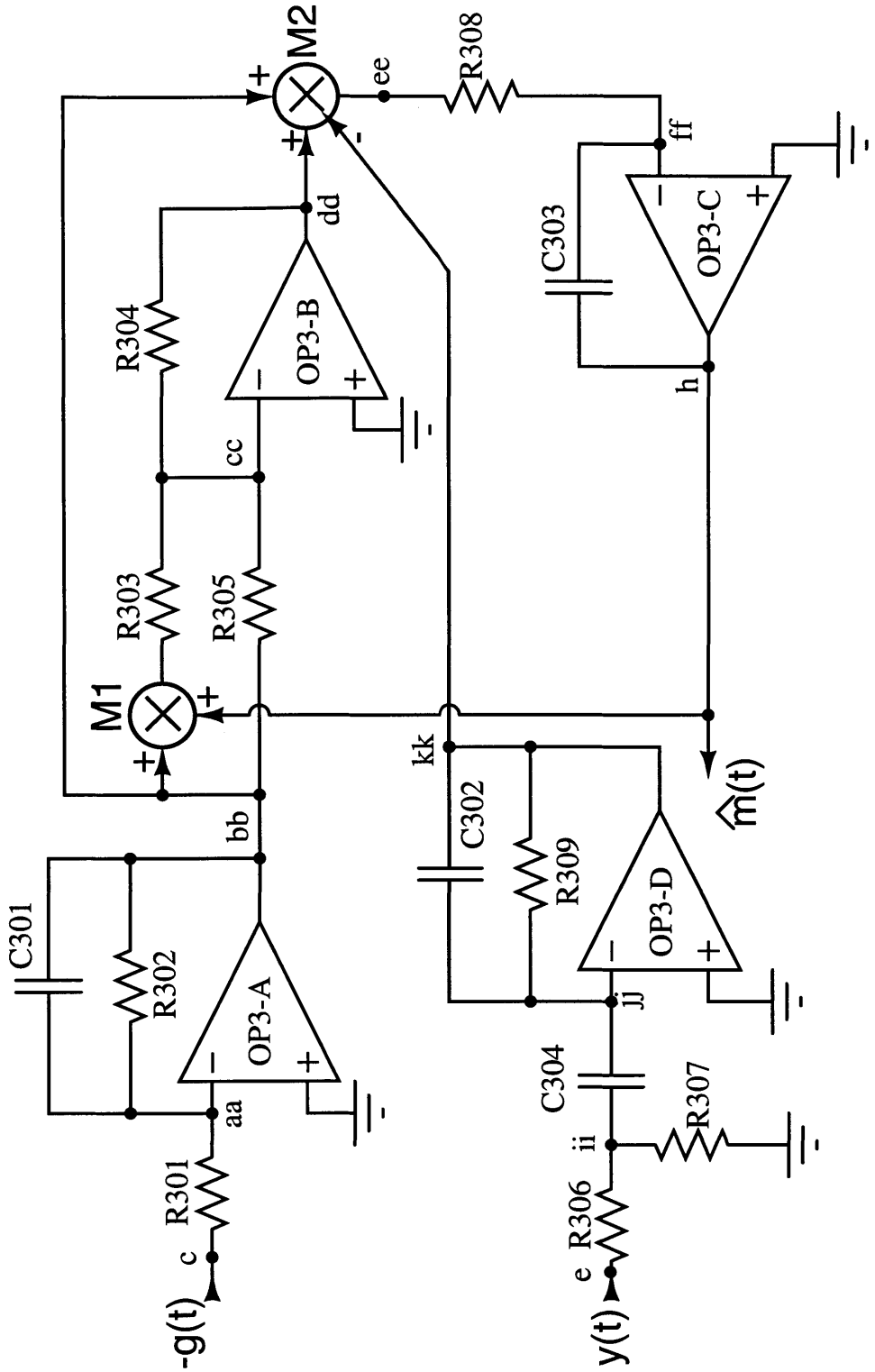

Figure 5-4: Circuit diagram for the Lorenz-based demodulator – rate-estimator component.

The equations describing the rate estimator behavior are

$$\begin{aligned}
\dot{\hat{m}} &= -\frac{1}{100C_{303}}\left\{\frac{1}{R_{309}}\left(\frac{R_{304}}{R_{305}}+\frac{R_{304}}{10R_{303}}\hat{m}\right)r_1^2-\frac{1}{R_{308}}(y-r_2)r_1\right\},\\
\dot{r}_1 &= \frac{1}{C_{302}R_{309}}(r_1-\hat{F}_1),\\
\dot{r}_2 &= \frac{1}{C_{301}R_{302}}(r_2-y).
\end{aligned} \tag{5.6}$$

Component values are listed in Table 5.1. The resistors are the surface mount type and have a 1% tolerance. The capacitors are axial lead polypropylene capacitors with a 2.5% tolerance. The operational amplifier used is the OP467 by Analog Devices. The analog multiplier used is the AD734 by Analog Devices. The choice of component values makes $\omega_c \approx 196,000$, $\beta \approx 36,700$, and $\omega_L \approx 1,960,000$.

Component	Value	Component	Value	Component	Value
R101	2kΩ	R102	2kΩ	R103	2kΩ
R104	2kΩ	R105	68.1kΩ	R106	4.75kΩ
R107	1.54kΩ	R108	4.75kΩ	R109	3.32kΩ
R110	1.21kΩ	R111	1.54kΩ	R112	10kΩ
R113	2kΩ	R114	2.32kΩ	R115	1.24kΩ
R116	1.74kΩ	R117	887Ω	R118	3.57kΩ
R119	1.78kΩ	R120	1kΩ	R121	2kΩ
R201	2kΩ	R202	2kΩ	R203	2kΩ
R204	2kΩ	R205	68.1kΩ	R206	4.75kΩ
R207	1.54kΩ	R208	4.75kΩ	R209	2.49kΩ
R210	1.21kΩ	R211	1.54kΩ	R212	10kΩ
R213	2kΩ	R214	1.74kΩ	R215	887Ω
R216	3.57kΩ	R217	1.78kΩ	R218	1kΩ
R219	2kΩ				
R301	2.32kΩ	R302	2.32kΩ	R303	4.99kΩ
R304	10kΩ	R305	10kΩ	R306	2kΩ
R307	2kΩ	R308	1kΩ	R309	2.32kΩ
C101	220pF	C102	220pF	C103	220pF
C201	220pF	C202	220pF		
C301	220pF	C302	220pF	C303	10nF

Table 5.1: Passive component values.

5.2 Design Considerations

Analog circuits, especially those that have power in the radio frequency (RF) range, must be designed carefully to avoid electro-magnetic interference, both internally and externally generated. In this section, some of the design issues encountered in building the prototype are discussed.

5.2.1 Fabrication

The circuit boards used were double-sided boards made by chemically etching the circuit trace pattern. The circuit layouts for both sides of the modulator board and the demodulator board are shown in Figure 5-5 and Figure 5-6, respectively. Two-sided boards pose some problems because ground planes, power planes, and several traces have to be broken to route the connections. Many traces had to be jumped by breaking the trace on the board and reconnecting it using wire. Also, the ground planes, which are the large black spaces in Figure 5-5 and Figure 5-6, had to be broken up so that traces could be routed. These ground planes were then reconnected with wire.

5.2.2 Circuit Layout

In laying out the circuit, the following considerations were important:

High frequency signals: Signal traces that are carrying the derivative signals $\dot{V}_1$, $\dot{V}_2$, $\dot{V}_3$, $\dot{\hat{V}}_2$, and $\dot{\hat{V}}_3$ were routed first. They were made as short as possible and shielded by ground traces if possible. Also, if possible, two derivative traces were not routed next to each other or next any IC pins that are sensitive to these signals.

Ground returns: All signals have a return path to ground that terminates near the signal source. This is particularly important for high frequency signals. If there is no direct signal return, high frequency signals will couple electro-magnetically.

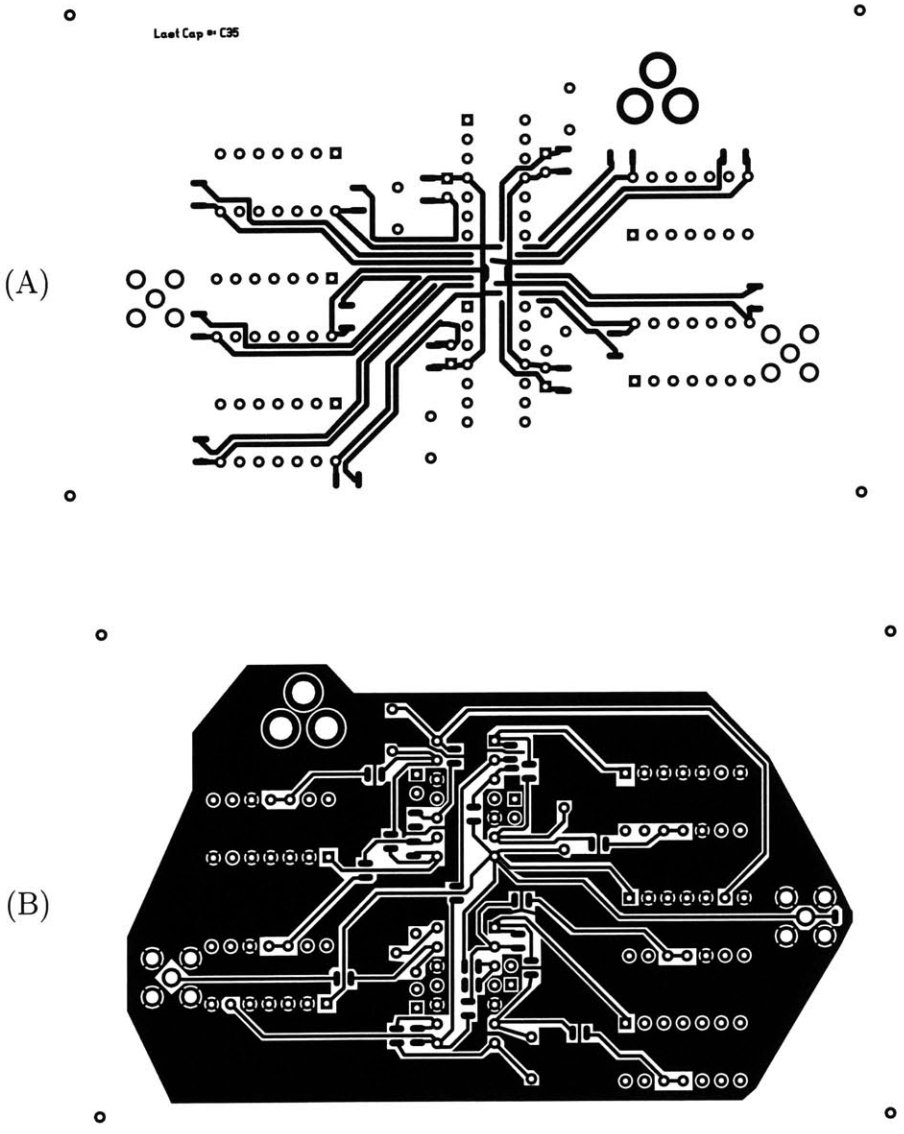

Figure 5-5: Etch patterns for the component-side (A) and solder-side (B) of the modulator circuit (actual size).

(A)

(B)

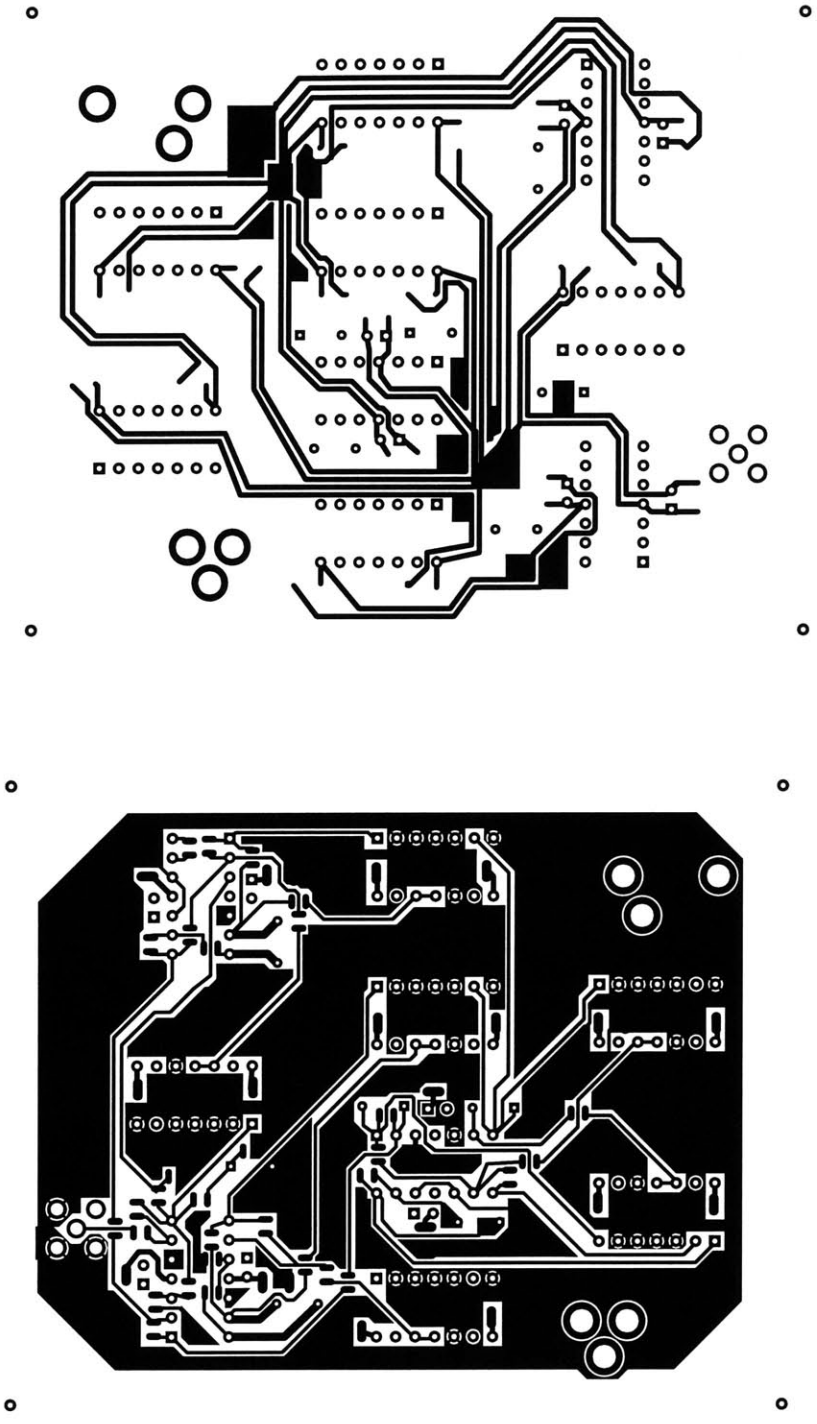

Figure 5-6: Etch patterns for the component-side (A) and solder-side (B) of the demodulator circuit (actual size).

Ground plane: All open space in the circuit was covered with ground planes. The ground planes were connected together at one central location to avoid ground loops.

Power supply decoupling: Bypass capacitors were placed between power and ground near every IC.

5.3 Demodulation Examples

In this section, the performance of the circuit is demonstrated by showing examples of demodulation. The first modulating signal used is a pure sine wave with a frequency of 1kHz. The second modulating signal used is a speech signal.

Figure 5-7 compares the demodulated sine wave with the modulating sine wave.

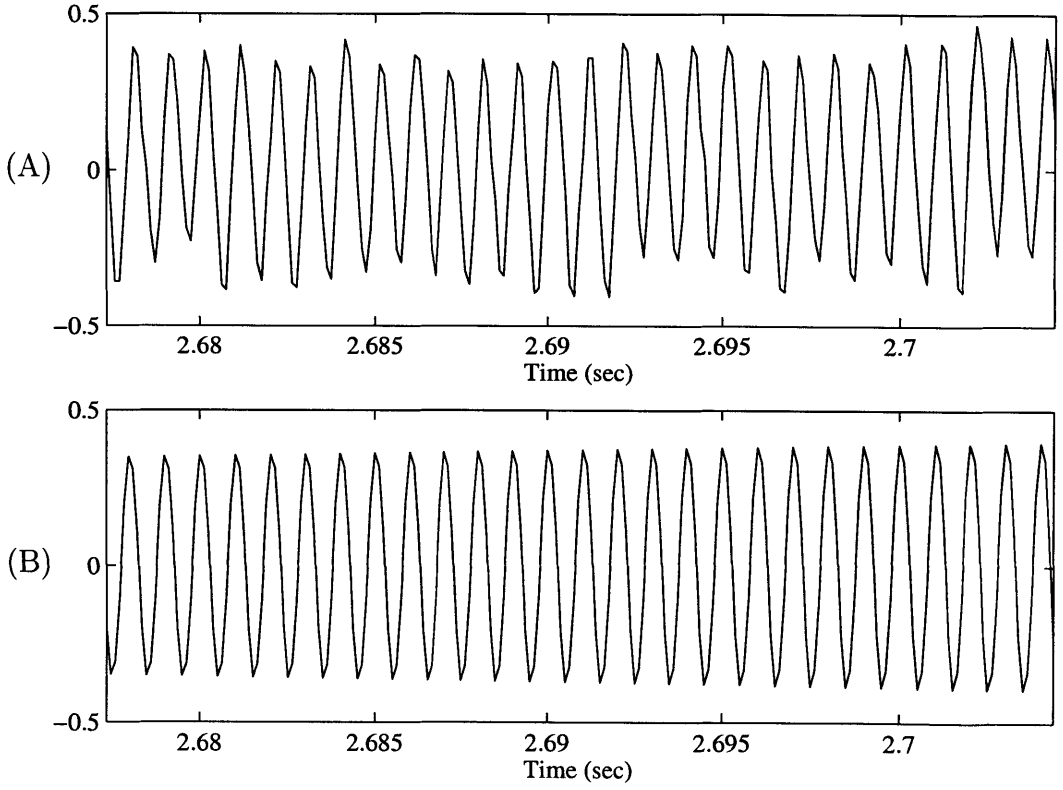

Figure 5-7: (A) The demodulated 1kHz sine wave and (B) the 1kHz sine wave.

In Figure 5-8, the result of modulating and then demodulating a speech waveform

and the original speech waveform of an utterance of the word "this" are shown.

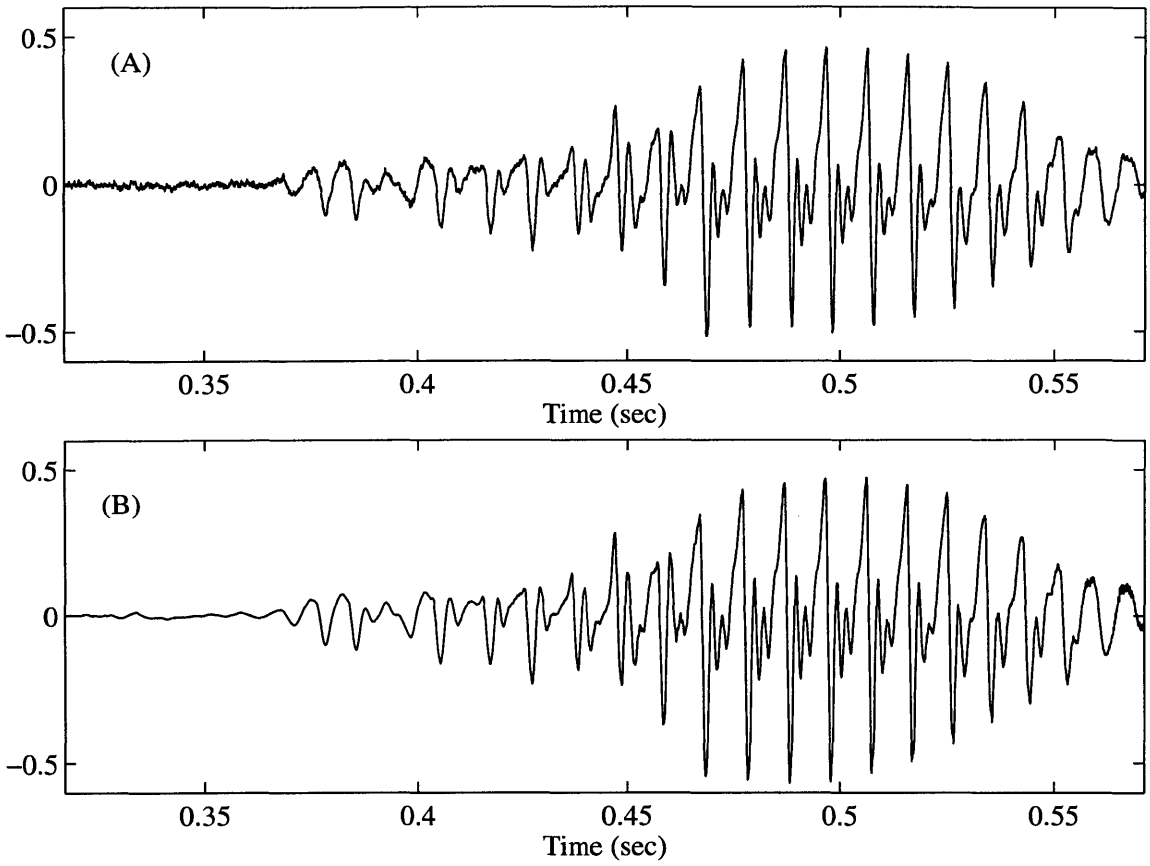

Figure 5-8: (A) The demodulated speech waveform and (B) the original speech waveform.

Chapter 6

Summary and Conclusions

In this thesis, a generalization of frequency modulation (FM) was developed that was referred to as rate modulation. A rate modulator consists of a dynamical system whose rate of evolution is modulated by a continuous-time information signal. The carrier wave is a linear or nonlinear scalar function of the state variables of the modulated dynamical system. Our approach to designing a corresponding rate demodulator assumed that the dynamical system used in the modulator has a known exponentially convergent observer. The demodulator was constructed by systematically modifying the observer in a manner based on a new perturbation technique developed in this thesis.

Chapter 2 began with a reinterpretation of FM from a dynamical systems perspective, which led to the more general notion of rate modulation. The remainder of the chapter focused on the effect that modulation has on the bandwidth of the modulated carrier wave. In particular, the power density spectrum of the modulated carrier wave was related to the unmodulated carrier wave through a linear integral transform. Because the relationship is linear and the effect of certain types of modulation is known when the carrier wave is sinusoidal, explicit representations were found for the kernel of the integral transform. Knowledge of the kernel allowed the power density spectrum of the modulated carrier to be determined from the power density spectrum of the unmodulated carrier wave. The special case of the Lorenz system was also examined. The power density spectrum of the first state variable of

the Lorenz system can be approximated with a decaying exponential. Because of this special structure of the power density spectrum, an explicit formula was obtained for the autocorrelation function of the modulated carrier wave, from which the power density spectrum was determined.

In Chapter 3, the design of demodulators was described. To design the demodulators, a new perturbation technique that was developed in this thesis was used that is referred to as a backwards perturbation expansion. In the perturbation technique, the modulator state variables are expanded about the demodulator state variables in terms of the rate estimate error. This produces expansion terms that depend only on signals that are local to the demodulator. These expansion variables can then be combined in such a way that the demodulator converges exponentially to the state and rate of the modulator. The demodulators obtained from the perturbation technique were then modified to enhance aspects of their performance. First, a filter was added in the feedback path of the rate estimate to smooth the rate estimate. Second, it was empirically shown that the rate estimator could be modified so that the demodulator can track signals that vary more rapidly. Finally, the rate estimator was simplified by approximating the nonlinear, time-varying components with linear, time-invariant components. The chapter concluded by showing how the resulting demodulator is equivalent to a least-squares approach to demodulation.

In Chapter 4, the probability density functions of the state variables of the demodulator were approximated when the carrier wave was corrupted with additive white Gaussian noise. When a dynamical system is driven by white noise, it becomes a stochastic differential equation and cannot be analyzed with the usual rules of calculus. In the beginning of the chapter, results from the theory of stochastic differential equations were briefly overviewed along with the related Itô calculus that is drawn upon throughout the remainder of the chapter. Itô's change of variables formula was then used to generate the differential equations that describe the evolution of the time-varying moments of the state-variables. For nonlinear systems, low-order moment equations depend on higher-order moments, leading to an infinite hierarchy of equations. This set of equations was closed by the quasi-moment neglect

closure technique. Essentially, this technique is based on approximating the probability distribution of the state variables as a truncated Edgeworth series. Truncating the Edgeworth series at order N closes the moment equations at order N, and the moment equations can then be solved. In the examples, the Edgeworth series was truncated at second order, which means that the distribution of the state variables was assumed to be Gaussian. As the input SNR is increased, the effects of the nonlinearities becomes more significant and the Gaussian approximation is no longer valid. In this case, the moment equations became unstable. Therefore, the QMNC technique can only be used when the input SNR is sufficiently high.

Finally, in Chapter 5, a circuit implementation of a Lorenz based modulator and demodulator systems was presented. The prototype circuit was described and an example of demodulation of a sine wave speech waveform was included.

6.1 Suggestions for Further Research

In this thesis, the foundation for rate modulation and demodulation has been laid. Several unanswered questions remain and many new directions remain to be explored. For example, the perturbation expansion presented in Appendix A is more general than the manner in which it was used in this thesis. In particular, the perturbation expansion technique resulted in a systematic technique for tracking multiple unknown parameters that appear nonlinearly in a dynamical system that has a known exponentially convergent observer when the parameters are fixed and known. This presents two immediate avenues to explore. First, instead of modulating the rate of evolution, a parameter could be modulated proportional to an information signal and a demodulator could be constructed using the perturbation technique. Second, the perturbation technique allows for more than one parameter to be tracked, which suggests that some type of multiplexing scheme is possible for rate modulation systems.

Another new area to explore is the use of time-varying dynamical systems. In this thesis, only autonomous dynamical systems were used. Many of the ideas and results that were presented can be carried over to time-varying systems provided that the

modulator and demodulator are synchronized in time. Using time-varying systems could lead to a type of generalized frequency-hopping.

Yet another direction that could be pursued is one of analog channel coding. Rate modulation allows the carrier wave to be choosen from a large class of waveforms. Perhaps it is possible to search over the class waveforms to find a carrier wave that is in some sense optimal. For example, it may be possible to find an optimal carrier wave for a channel with a particular type of distortion.

In addition to these new directions, there are fundamental aspects of rate modulation that have yet to be analyzed. For example, in designing the demodulator, convergence was forced when the modulating signal was an unknown constant. It was then assumed that the demodulator would be able to track slowly varying signals, The ability to track non-constant signals was demonstrated, but this was not verified analytically. Also, the constraints on the rate at which the modulating signal can vary were not determined. Currently, these constraints are determined by trial and error.

As mentioned in the beginning of this chapter, this thesis constitutes the foundations for rate modulation and demodulation and there remain many unanswered questions regarding the practicality and potential benefits of rate modulation in comparison to standard modulation schemes.

Appendix A

Parameter Tracking by a Backwards Perturbation Expansion

Many systems have parameters that vary as a function of time. In this appendix, it is shown how parameter variations can be tracked when the dynamical system has a known exponentially convergent local observer for the case in which the parameters are fixed and known, and the observed output of the dynamical system satisfies an observability condition.

Perturbation Expansion The case in which there is only one unknown parameter is considered first. The system that is derived to track the unknown parameter is an augmentation of the known observer. The augmented observer is derived by expressing the state of the dynamical system as a perturbation expansion about the observer state in terms of the parameter estimate error. Specifically, the dynamical system is

$$\dot{\mathbf{x}} = \mathbf{F}(\mathbf{x}; \theta), \tag{A.1}$$

where θ is the unknown parameter and $\mathbf{x}$ is assumed to be confined to a region of $\mathbb{R}^N$, that is, $\mathbf{x} \in D \subset \mathbb{R}^N$. The observed output is a scalar function of the state variables,

$$y = h(\mathbf{x}). \tag{A.2}$$

and the exponentially convergent local observer when $\mathbf{x} \in D$ is

$$\dot{\mathbf{z}} = \hat{\mathbf{F}}(\mathbf{z}, y; \hat{\theta}). \tag{A.3}$$

The state of the dynamical system is expanded as

$$\mathbf{x} = \mathbf{z} + e_\theta \boldsymbol{\xi} + e_\theta^2 \boldsymbol{\zeta} + \cdots, \tag{A.4}$$

where $e_\theta = \hat{\theta} - \theta$. Expanding the dynamical system state variables in terms of the observer state variables results in expansion terms that depend only on variables local to the observer. These expansion variables are exploited to force the observer to converge to the unknown parameter.

Differentiating both sides of (A.4) results in

$$\begin{aligned} \dot{\boldsymbol{\varsigma}} + e_\theta \dot{\boldsymbol{\xi}} + \dot{e}_\theta \boldsymbol{\xi} + \cdots &= \mathbf{F}(\mathbf{x}; \theta) \\ &= \hat{\mathbf{F}}(\boldsymbol{\varsigma} + e_\theta \boldsymbol{\xi} + \cdots, y; \theta) \\ &= \hat{\mathbf{F}}(\boldsymbol{\varsigma} + e_\theta \boldsymbol{\xi} + \cdots, y; \hat{\theta} - e_\theta). \end{aligned} \tag{A.5}$$

In (A.5), the fact that $\mathbf{x}$ remains in the local observability region, D, was used along with the fact that $\mathbf{F}(\mathbf{x}; \theta) = \hat{\mathbf{F}}(\mathbf{x}, y; \theta)$ as described in Section 3.1.3. Expanding the right-hand side of (A.5) in a Taylor series with respect to e_θ results in

$$\dot{\boldsymbol{\varsigma}} + e_\theta \dot{\boldsymbol{\xi}} + \dot{e}_\theta \boldsymbol{\xi} + \cdots = \hat{\mathbf{F}}(\boldsymbol{\varsigma}, y; \hat{\theta}) + \left(\frac{\partial \hat{\mathbf{F}}}{\partial \boldsymbol{\varsigma}}(\boldsymbol{\varsigma}, y; \hat{\theta}) \boldsymbol{\xi} - \frac{\partial \hat{\mathbf{F}}}{\partial \hat{\theta}}(\boldsymbol{\varsigma}, y; \hat{\theta}) \right) e_\theta + \cdots. \tag{A.6}$$

It is assumed and verified later that $\dot{e}_\theta$ is of the form

$$\dot{e}_\theta = -K r(\boldsymbol{\varsigma}, \boldsymbol{\xi}) e_\theta, \tag{A.7}$$

where $r(\cdot, \cdot)$ is a scalar function of $\boldsymbol{\varsigma}$ and $\boldsymbol{\xi}$. Equating terms of equal power in e_θ and neglecting terms of higher order than first, two equations remain, namely

$$\dot{\boldsymbol{\varsigma}} = \hat{\mathbf{F}}(\boldsymbol{\varsigma}, y; \hat{\theta}) \tag{A.8}$$

and

$$\dot{\boldsymbol{\xi}} = \Big(\frac{\partial \hat{\mathbf{F}}}{\partial \boldsymbol{\varsigma}}(\boldsymbol{\varsigma}, y; \hat{\theta}) + Kr(\boldsymbol{\varsigma}, \boldsymbol{\xi})\Big)\boldsymbol{\xi} - \frac{\partial \hat{\mathbf{F}}}{\partial \theta}(\boldsymbol{\varsigma}, y, \hat{\theta}). \tag{A.9}$$

From (A.8), $\boldsymbol{\varsigma} = \mathbf{z}$. The equation in (A.9) generates the first-order term of the perturbation expansion. For the perturbation expansion to be valid, this expansion term must be bounded.

Boundedness of the Expansion The exponential stability of the observer is used to show that the perturbation term, $\boldsymbol{\xi}$, remains bounded. When there is no parameter mismatch, the error between the dynamical system and the observer evolves according to

$$\dot{\mathbf{e}}_{\mathbf{z}} = \hat{\mathbf{F}}(\mathbf{z}, y; \hat{\theta}) - \hat{\mathbf{F}}(\mathbf{z} - \mathbf{e}_{\mathbf{z}}, y; \hat{\theta}). \tag{A.10}$$

The assumption that the observer is exponentially stable is equivalent to (A.10) having an exponentially stable equilibrium point at $\mathbf{e}_{\mathbf{z}} = \mathbf{0}$. A nonlinear system has an exponentially stable equilibrium point at $\mathbf{e}_{\mathbf{z}} = \mathbf{0}$ if and only if the corresponding linearized system has an exponentially stable equilibrium point at $\mathbf{e}_{\mathbf{z}} = \mathbf{0}$ [6]. Therefore, the system given by

$$\dot{\mathbf{e}}_{\mathbf{z}} = \frac{\partial \hat{\mathbf{F}}}{\partial \mathbf{z}}(\mathbf{z}, y; \hat{\theta})\mathbf{e}_{\mathbf{z}} \tag{A.11}$$

has an exponentially stable equilibrium point at $\mathbf{e}_{\mathbf{z}} = \mathbf{0}$. The perturbed system given by

$$\dot{\mathbf{e}}_{\mathbf{z}} = \Big(\frac{\partial \hat{\mathbf{F}}}{\partial \mathbf{z}}(\mathbf{z}, y; \hat{\theta}) + Kr(\mathbf{z}, \mathbf{e}_{\mathbf{z}})\Big)\mathbf{e}_{\mathbf{z}} \tag{A.12}$$

is also exponentially stable for $0 < K < K_*$ for some sufficiently small K_* [6]. An exponentially stable linear system is bounded input–bounded output (BIBO) stable [9]. Since $\frac{\partial \hat{\mathbf{F}}}{\partial \theta}(\mathbf{z}, y; \hat{\theta})$ is bounded,

$$\dot{\mathbf{e}}_{\mathbf{z}} = \Big(\frac{\partial \hat{\mathbf{F}}}{\partial \mathbf{z}}(\mathbf{z}, y; \hat{\theta}) + Kr(\mathbf{z}, \mathbf{e}_{\mathbf{z}})\Big)\mathbf{e}_{\mathbf{z}} - \frac{\partial \hat{\mathbf{F}}}{\partial \theta}(\mathbf{z}, y; \hat{\theta}) \tag{A.13}$$

results in a bounded $\mathbf{e}_{\mathbf{z}}$. But (A.13) is identical to (A.9), which means that $\boldsymbol{\xi}$ is bounded and the perturbation expansion is valid. Moreover, $\boldsymbol{\xi}$ is determined by $\mathbf{z}$,

y, and $\hat{\theta}$, all of which are local to the observer, which means that each $\boldsymbol{\xi}$ can be generated at the observer.

Forcing the Parameter Error to Zero Because $\boldsymbol{\xi}$ is local to the observer, it can be generated in the observer and used to force convergence.

A signal is said to be persistently exciting if, for any $\delta > 0$,

$$\int_{t}^{t+\delta} \big(y(t)\big)^2 dt > 0 \tag{A.14}$$

for all t. In other words, a signal that is persistently exciting can cross zero, but cannot remain at zero for any length of time.

The difference between $y = h(\mathbf{x})$ and $\hat{y} = h(\mathbf{z})$ can be approximated as

$$\begin{aligned} \hat{y} - y &= h(\mathbf{z}) - h(\mathbf{x}) \\ &= h(\mathbf{z}) - h(\mathbf{z} + \boldsymbol{\xi} e_\theta + \cdots) \\ &= -\frac{\partial h}{\partial \mathbf{z}}(\mathbf{z}) \boldsymbol{\xi} e_\theta + \cdots . \end{aligned} \tag{A.15}$$

Since each $\boldsymbol{\xi}$ can be generated at the observer, $\hat{\theta}$ can be chosen to be

$$\dot{\hat{\theta}} = K(\hat{y} - y) g\Big(\frac{\partial h}{\partial \mathbf{z}}(\mathbf{z}) \cdot \boldsymbol{\xi}\Big), \tag{A.16}$$

where $g(\cdot)$ is a real-valued function that has the property $\operatorname{sgn}(g(a)) = \operatorname{sgn}(a)$, that is, $g(\cdot)$ has the same sign as its argument. This gives, to first-order,

$$\begin{aligned} \dot{\hat{\theta}} &= -K\Big(\frac{\partial h}{\partial \mathbf{z}}(\mathbf{z}) \cdot \boldsymbol{\xi}\Big) \cdot g\Big(\frac{\partial h}{\partial \mathbf{z}}(\mathbf{z}) \cdot \boldsymbol{\xi}\Big) e_\theta \\ \dot{\hat{\theta}} &= -K\Big(\frac{\partial h}{\partial \mathbf{z}}(\mathbf{z}) \cdot \boldsymbol{\xi}\Big) \cdot g\Big(\frac{\partial h}{\partial \mathbf{z}}(\mathbf{z}) \cdot \boldsymbol{\xi}\Big) (\hat{\theta} - \theta). \end{aligned} \tag{A.17}$$

To clarify the behavior of $\hat{\theta}$, its equation of motion can be written as

$$\dot{\hat{\theta}} = a(t)\big(\hat{\theta} - \theta\big), \tag{A.18}$$

where the time-varying coefficient, $a(t)$, is

$$a(t) = -K\Big(\frac{\partial h}{\partial \mathbf{z}}(\mathbf{z}) \cdot \boldsymbol{\xi}\Big) \cdot g\Big(\frac{\partial h}{\partial \mathbf{z}}(\mathbf{z}) \cdot \boldsymbol{\xi}\Big) \leq 0. \tag{A.19}$$

Rewriting (A.18) in terms of the error between $\hat{\theta}$ and θ results in

$$\dot{e}_\theta = a(t) e_\theta. \tag{A.20}$$

The solution to (A.20) is

$$e_\theta = c e^{\int_0^t a(\tau) d\tau}, \tag{A.21}$$

where $c = \hat{\theta}(0) - \theta$. Assuming that $\frac{\partial h}{\partial \mathbf{z}}(\mathbf{z}) \cdot \boldsymbol{\xi}$ is persistently exciting, $e^{\int_0^\infty a(\tau) d\tau}$ is a monotonically decreasing and goes to zero as $t \to \infty$. From (A.21), $e_\theta = 0$ is a uniformly asymptotically stable equilibrium point. A linear system that is uniformly asymptotically stable is also uniformly exponentially stable [9]. It follows that $\mathbf{z}$ converges to $\mathbf{x}$ exponentially as well [6]. This means that the augmented observer is an exponentially stable local observer of the dynamical system when θ is unknown. The assumption made during the derivation of the perturbation expansion that

$$\dot{e}_\theta = -K r(\mathbf{z}, \boldsymbol{\xi}) e_\theta \tag{A.22}$$

is valid with

$$r_1(\mathbf{z}, \boldsymbol{\xi}) = \Big(\frac{\partial h}{\partial \mathbf{z}}(\mathbf{z}) \cdot \boldsymbol{\xi}\Big) \cdot g\Big(\frac{\partial h}{\partial \mathbf{z}}(\mathbf{z}) \cdot \boldsymbol{\xi}\Big). \tag{A.23}$$

Since the augmented observer for one unknown is an exponentially convergent local observer, it can be used as the basis for a further augmented observers when there are additional unknown parameters.

Appendix B

Quasi-moment Neglect Applied to the PLL

In Chapter 4, a method called quasi-moment neglect closure (QMNC) was described for approximating the probability density function (pdf) and the low-order moments of the state variables of a dynamical system that is driven by a white noise process. In this appendix, the technique is demonstrated on a second-order phase-locked loop (PLL), which are often used FM demodulators.

Equivalent Model of PLL: A block diagram of a PLL is shown in Figure B-1. The voltage controlled oscillator (VCO) outputs a sinusoid whose frequency is

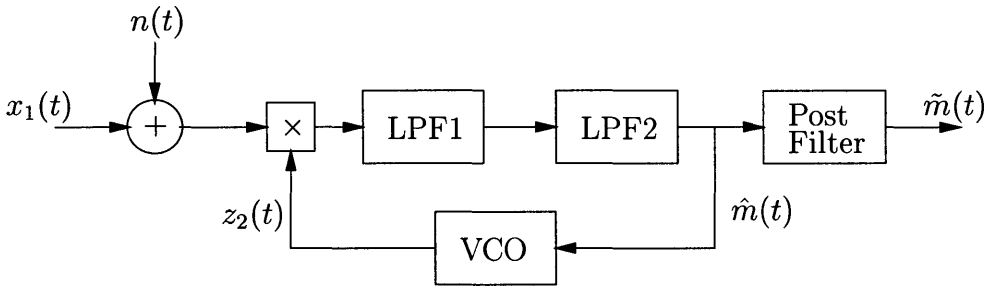

Figure B-1: The phase-locked loop.

proportional to the input. That is,

$$z_2(t) = \sin\big(\omega_c t + \int \hat{m}(\tau)d\tau\big), \tag{B.1}$$

where ω_c is the zero-input frequency of the VCO. The input to the first low-pass filter, labeled LPF1 in Figure B-1, is

$$\begin{aligned}(x_1(t)+n(t))z_2(t) &= K\sin\Big(\int(\beta m(\tau)-\hat{m}(\tau))d\tau\Big)\\ &+ K\sin\big(2\omega_c t+\int(\beta m(\tau)+\hat{m}(\tau))d\tau\big)\\ &- Kn_s(t)\sin(\int\hat{m}(\tau)d\tau)+Kn_c(t)\cos(\int\hat{m}(\tau)d\tau)\\ &+ Kn_s(t)\sin(2\omega_c+\int\hat{m}(\tau)d\tau)+Kn_c(t)\cos(2\omega_c t+\int\hat{m}(\tau)d\tau).\end{aligned} \tag{B.2}$$

The derivation of (B.2) uses the fact that a zero-mean Gaussian process that has a power density spectrum equal to $N_0/2$ for $|\omega| < B$ (rad/sec) and zero elsewhere can be represented as

$$n(t) = \sqrt{2}\big(n_s(t)\sin(\omega_c t) + n_c(t)\cos(\omega_c t)\big), \tag{B.3}$$

where $n_s(t)$ and $n_c(t)$ are independent, zero-mean Gaussian processes that also have a PSD that is equal to $N_0/2$ for $|\omega| < B$ (rad/sec) and negligible elsewhere [13].

The first low-pass filter, LPF1, has a cut-off frequency of ω_c and is assumed remove all components in (B.2) centered at $\omega = 2\omega_c$. Representing the noise terms that remain after filtering as

$$\tilde{n}(t) = -n_s(t)\sin(\int\hat{m}(\tau)d\tau) + n_c(t)\cos(\int\hat{m}(\tau)d\tau), \tag{B.4}$$

the output of the first low-pass filter is

$$r(t) = K\big\langle\sin\big(\int(\beta m(\tau)-\hat{m}(\tau))d\tau\big)+\tilde{n}(t)\big\rangle_L, \tag{B.5}$$

where $\langle\cdot\rangle_L$ represents the operation of the low-pass filter. It can be shown that

the power density spectrum of $\tilde{n}(t)$ is equal to $N_0/2$ over the bandwidth of the PLL. Therefore, $\langle \tilde{n}(t) \rangle_L$ can be treated as a Gaussian process with a power density spectrum level equal to $N_0/2$ [13]. The second low-pass filter, LPF2, smooths $r(t)$ before it is input into the VCO and has a transfer function of the form

$$H(s) = 1 + \frac{\alpha}{s}. \tag{B.6}$$

Using filter transfer function given in (B.6), the second order PLL is given by

$$\begin{aligned} d\psi &= \alpha K\big(\sin(\phi)dt + dW(t)\big), \\ d\phi &= \beta m dt - \big(\psi dt + K\sin(\phi)dt + K dW(t)\big), \\ d\varsigma &= A_p \varsigma dt + B_p \frac{1}{\beta}\big(\psi dt + K\sin(\phi)dt + K dW(t)\big), \\ \tilde{m} &= C_p \varsigma, \end{aligned} \tag{B.7}$$

where $dW(t)$ is a Gaussian white noise process with a power density spectrum level of $\eta^2$and A_p, B_p, and C_p correspond to the space-space implementation of the post-filter. The block diagram of the system given in (B.7) is shown in Figure B-2.

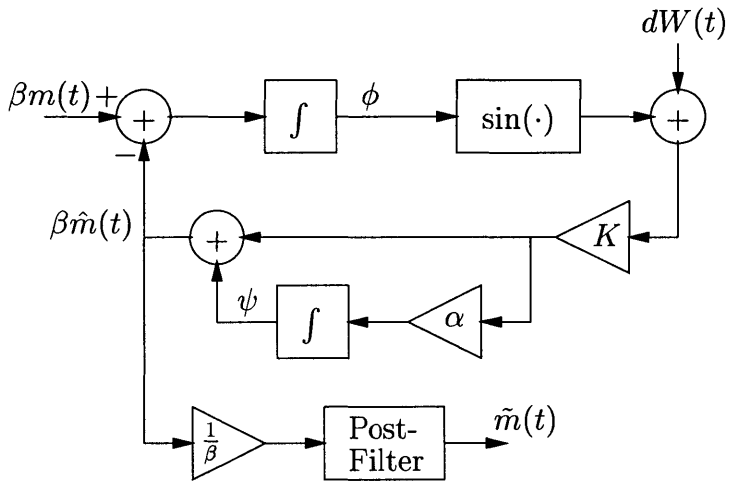

Figure B-2: A model of the phase-locked loop.

Quasi-moment Neglect Applied to the Two Dimensional PLL: To demonstrate the QMNC technique on the PLL, LPF1 and the post-filter are excluded. This makes the system equations

$$\begin{aligned} d\psi &= \alpha K\big(\sin(\phi)dt + dW(t)\big), \\ d\phi &= \beta m dt - \big(\psi dt + K\sin(\phi)dt + K dW(t)\big). \end{aligned} \tag{B.8}$$

The quasi-moment neglect technique allows only nonlinearities that are polynomials. Taking a fourth-order Taylor series expansion of the $\sin(\cdot)$ terms gives

$$\begin{aligned} d\psi &= \alpha K\big(\phi dt - \frac{1}{3!}\phi^3 dt + dW(t)\big), \\ d\phi &= \beta m dt - \big(\psi dt + K(\phi dt - \frac{1}{3!}\phi^3 dt) + K dW(t)\big). \end{aligned} \tag{B.9}$$

To generate the moment equations, (4.9) is used. $E[\psi]$ is obtained by setting $h(\psi,\phi) = \psi$ and substituting this into (4.9), giving

$$\frac{dE[\psi]}{dt} = \alpha K(E[\phi] - \frac{1}{3!}E[\phi^3]). \tag{B.10}$$

Similarly, $E[\phi]$ is obtained by setting $h(\psi,\phi) = \phi$, which gives

$$\frac{dE[\phi]}{dt} = \beta E[m] - E[\psi] - K(E[\phi] - \frac{1}{3!}E[\phi^3]). \tag{B.11}$$

The rest of the moments up to third order are obtained in a similar manner and they are listed in Table B.1. In the table, the notation used is

$$m_{kl} = E[\psi^k \phi^l]. \tag{B.12}$$

For example, $m_{11} = E[\psi\phi]$ and $m_{20} = E[\psi^2]$. The modulating signal, $m(t)$, was taken to be zero and η^2 is the level of the power density spectrum of the white noise process, $dW(t)$.

To close the moment equations in Table B.1, moments above third order must be expressed as moments at or below third order. The moments that are above

$h(\psi,\phi)$	Moment Equation
ψ	$\frac{dm_{10}}{dt} = \alpha K(m_{01} - \frac{1}{3!}m_{03})$
ϕ	$\frac{dm_{01}}{dt} = -m_{10} - K(m_{01} - \frac{1}{3!}m_{03})$
ψ^2	$\frac{dm_{20}}{dt} = \alpha K(2m_{11} - \frac{1}{3}m_{13}) + \alpha^2 K^2 \eta^2$
$\psi\phi$	$\frac{dm_{11}}{dt} = \alpha K(m_{02} - \frac{1}{6}m_{04}) - m_{20} + K(\frac{1}{6}m_{13} - m_{11})$
ϕ^2	$\frac{dm_{02}}{dt} = -2m_{11} + K(\frac{1}{3}m_{04} - 2m_{02}) + K^2\eta^2$
ψ^3	$\frac{dm_{30}}{dt} = \alpha K(3m_{21} - \frac{1}{2}m_{23}) + 3\alpha^2 K^2 \eta^2 m_{10}$
$\psi^2\phi$	$\frac{dm_{21}}{dt} = \alpha K(2m_{12} - \frac{1}{3}m_{14}) + K(\frac{1}{6}m_{23} - m_{21}) - m_{30} + \alpha^2 K^2 \eta^2 m_{01}$
$\psi\phi^2$	$\frac{dm_{12}}{dt} = \alpha K(m_{03} - \frac{1}{6}m_{05}) + K(\frac{1}{3}m_{14} - 2m_{12}) - 2m_{21} + K^2\eta^2 m_{10}$
ϕ^3	$\frac{dm_{03}}{dt} = K(\frac{1}{2}m_{05} - 3m_{03}) - 3m_{12} + 3K^2\eta^2 m_{01}$

Table B.1: Moment equations for the PLL.

third order that appear in the set of equations in Table B.1 are m_{13}, m_{04}, m_{23}, m_{14}, and m_{05}. The moment equations are closed by setting the quasi-moments above the third order to zero. Following the same procedure used in Section 4.3 to find the quasi-moment–moment relationships for a one dimensional system, the quasi-moment–moment relationships for a two dimensional system are shown in Table B.2 for m_{13}, m_{04}, m_{23}, m_{14}, and m_{05}. Setting all of the quasi-moments above order three to zero results in moment–quasi-moment relationships shown in Table B.3.

Just as with the one-dimensional case, the quasi-moments are expressed in terms of the moments by inverting the relationship established by (4.14) and (4.18). The relationships for up to third order are shown in Table B.4. The equations in Table B.4 are symmetric, meaning that b_{03} can be obtained from b_{30} be interchanging the first and second indices in every term, e.g.,

$$b_{03} = m_{03} - 3m_{01}m_{02} + 2m_{01}^3 \tag{B.13}$$

Substituting the quasi-moment–moment relationships shown in Table B.4 into the

$$
\begin{aligned}
m_{04} &= b_{04} + 4b_{03}b_{01} + 3b_{02}^2 + 6b_{02}b_{01}^2 + b_{01}^4 \\
m_{13} &= b_{13} + 3b_{12}b_{01} + 3b_{11}b_{02} + 3b_{11}b_{01}^2 + b_{01}b_{03} + 3b_{10}b_{02}b_{01} + b_{10}b_{01}^3 \\
m_{05} &= b_{05} + 5b_{04}b_{01} + 10b_{03}b_{02} + 10b_{03}b_{01}^2 + 15b_{02}^2b_{01} + 10b_{02}b_{01}^3 + b_{01}^5 \\
m_{14} &= b_{14} + 4b_{13}b_{01} + 6b_{12}b_{02} + 6b_{12}b_{01}^2 + 4b_{11}b_{03} + 12b_{11}b_{02}b_{01} \\
&\quad + 4b_{11}b_{01}^3 + b_{10}b_{04} + 4b_{10}b_{03}b_{01} + 3b_{10}b_{02}^2 + 6b_{10}b_{02}b_{01}^2 + b_{10}b_{01}^4 \\
m_{23} &= 3b_{20}b_{02}b_{01} + 3b_{21}b_{01}^2 + b_{10}^2b_{01}^3 + 3b_{10}^2b_{02}b_{01} + 6b_{10}b_{01}b_{12} \\
&\quad + 6b_{10}b_{02}b_{11} + b_{20}b_{01}^3 + b_{23} + 3b_{22}b_{01} + 3b_{21}b_{02} + b_{20}b_{03} + 6b_{11}b_{12} \\
&\quad + 6b_{11}^2b_{01} + 2b_{10}b_{13} + b_{10}^2b_{03} + 6b_{10}b_{01}^2b_{11}
\end{aligned}
$$

Table B.2: Moments expressed in terms of quasi-moments.

$$
\begin{aligned}
m_{04} &= 4b_{03}b_{01} + 3b_{02}^2 + 6b_{02}b_{01}^2 + b_{01}^4 \\
m_{13} &= 3b_{12}b_{01} + 3b_{11}b_{02} + 3b_{11}b_{01}^2 + b_{01}b_{03} + 3b_{10}b_{02}b_{01} + b_{10}b_{01}^3 \\
m_{05} &= 10b_{03}b_{02} + 10b_{03}b_{01}^2 + 15b_{02}^2b_{01} + 10b_{02}b_{01}^3 + b_{01}^5 \\
m_{14} &= 6b_{12}b_{02} + 6b_{12}b_{01}^2 + 4b_{11}b_{03} + 12b_{11}b_{02}b_{01} \\
&\quad + 4b_{11}b_{01}^3 + 4b_{10}b_{03}b_{01} + 3b_{10}b_{02}^2 + 6b_{10}b_{02}b_{01}^2 + b_{10}b_{01}^4 \\
m_{23} &= 3b_{20}b_{02}b_{01} + 3b_{21}b_{01}^2 + b_{10}^2b_{01}^3 + 3b_{10}^2b_{02}b_{01} + 6b_{10}b_{01}b_{12} \\
&\quad + 6b_{10}b_{02}b_{11} + b_{20}b_{01}^3 + 3b_{21}b_{02} + b_{20}b_{03} + 6b_{11}b_{12} \\
&\quad + 6b_{11}^2b_{01} + b_{10}^2b_{03} + 6b_{10}b_{01}^2b_{11}
\end{aligned}
$$

Table B.3: Moments expressed in terms of quasi-moments after applying third order quasi-moment neglect.

$$
\begin{aligned}
b_{30} &= m_{30} - 3m_{10}m_{20} + 2m_{10}^3 \\
b_{21} &= m_{21} - 2m_{10}m_{11} + 2m_{01}m_{10}^2 - m_{01}m_{20}
\end{aligned}
$$

Table B.4: Quasi-moments expressed in terms of moments.

$$
\begin{aligned}
\frac{dm_{10}}{dt} &= \alpha K(m_{01} - \frac{1}{6}m_{03}) \\
\frac{dm_{01}}{dt} &= -m_{10} - K(m_{01} - \frac{1}{6}m_{03}) \\
\frac{dm_{20}}{dt} &= 2\alpha K m_{11} - \frac{1}{3}\alpha K(3m_{01}m_{12} - 6m_{01}^2 m_{11} + 6m_{10}m_{01}^3 \\
&\quad - 6m_{01}m_{10}m_{02} + 3m_{11}m_{02} + m_{10}m_{03}) + \alpha^2 K^2 \eta^2 \\
\frac{dm_{11}}{dt} &= \alpha K m_{02} - \frac{1}{6}\alpha K(4m_{01}m_{03} - 12m_{01}^2 m_{02} + 6m_{01}^4 + 3m_{02}^2) - m_{20} \\
&\quad - K m_{11} + \frac{1}{6}K(3m_{01}m_{12} - 6m_{01}^2 m_{11} + 6m_{10}m_{01}^3 \\
&\quad - 6m_{01}m_{10}m_{02} + 3m_{11}m_{02} + m_{10}m_{03}) \\
\frac{dm_{02}}{dt} &= -2m_{11} - 2K m_{02} + \frac{1}{3}K(4m_{01}m_{03} - 12m_{01}^2 m_{02} + 6m_{01}^4 + 3m_{02}^2) + K^2\eta^2 \\
\frac{dm_{30}}{dt} &= 3\alpha K m_{21} - \frac{1}{2}\alpha K(-6m_{10}m_{11}m_{02} - 3m_{01}m_{20}m_{02} + 3m_{21}m_{02} \\
&\quad + 6m_{10}^2 m_{01}^3 + m_{20}m_{03} - 6m_{01}m_{11}^2 + 6m_{11}m_{12}) + 3\alpha^2 K^2 \eta^2 m_{10} \\
\frac{dm_{21}}{dt} &= 2\alpha K m_{12} - \frac{1}{3}\alpha K(6m_{12}m_{02} + 6m_{10}m_{01}^4 + 4m_{11}m_{03} - 3m_{10}m_{02}^2 \\
&\quad - 12m_{01}m_{11}m_{02}) - m_{30} - K m_{21} + \frac{1}{6}K(-6m_{10}m_{11}m_{02} \\
&\quad - 3m_{01}m_{20}m_{02} + 3m_{21}m_{02} + 6m_{10}^2 m_{01}^3 + m_{20}m_{03} - 6m_{01}m_{11}^2 + \\
&\quad 6m_{11}m_{12}) + \alpha^2 K^2 \eta^2 m_{01} \\
\frac{dm_{12}}{dt} &= \alpha K m_{03} - \frac{1}{6}\alpha K(10m_{03}m_{02} - 15m_{01}m_{02}^2 + 6m_{01}^5) - 2m_{21} + -2K m_{12} \\
&\quad + \frac{1}{3}K(6m_{12}m_{02} + 6m_{10}m_{01}^4 + 4m_{11}m_{03} - 3m_{10}m_{02}^2 - \\
&\quad 12m_{01}m_{11}m_{02}) + K^2\eta^2 m_{10} \\
\frac{dm_{03}}{dt} &= -3m_{12} - 3K m_{03} + \frac{1}{2}K(10m_{03}m_{02} - 15m_{01}m_{02}^2 + 6m_{01}^5) + 3K^2\eta^2 m_{01}
\end{aligned}
\tag{B.14}
$$

Table B.5: Closed moment equations for the PLL.

moments equations shown in Table B.3, the moments up to fifth order are expressed in terms of moments at or below third order. The differential equations for the moments are now closed and are shown in Table B.5.

Quasi-moment Neglect Applied to the PLL with the Post-filter: Adding the post-filter filter to the PLL results in the system given in (B.7). Using a third order Taylor series to approximate the $\sin(\cdot)$ function gives

$$d\psi = \alpha K\big(\phi dt - \frac{1}{6}\phi^3 dt + dW(t)\big) \tag{B.15}$$

$$d\phi = \beta m dt - \big(\psi dt + K\phi dt - K\frac{1}{6}\phi^3 dt + K dW(t)\big) \tag{B.16}$$

$$d\varsigma = A_p \varsigma dt + B_p \frac{1}{\beta}\big(\psi dt + K\phi dt - K\frac{1}{6}\phi^3 dt + K dW(t)\big) \tag{B.17}$$

$$\tilde{m} = C_p \varsigma, \tag{B.18}$$

where $dW(t)$ is a Gaussian white noise processand A_p, B_p, and C_p correspond to the space-space implementation of the post-filter. The post-filter has a dimension of five, making the entire PLL system have a dimension of seven. Second order QMNC requires the first and second order moments. The second order moments correspond to a symmetric seven by seven covariance matrix, which has twenty-eight unique entries. There are seven first order moments, bringing the total dimension of the differential moment equations to thirty-five.

Bandwidth of Modulated Signal: The bandwidth of the FM signal is, from Carson's rule described in Chapter 2, approximately $2(\beta+1)\omega_m$ when $y(t) = \cos(\omega_c + \beta\sin(\omega_m t))$. The input signal is $m(t) = \omega_m \cos(\omega_m t)$, which makes $P_m = \overline{m^2(t)} = \omega_m^2/2$. The baseband SNR is

$$\mathrm{SNR_b} == 10\log_{10}\left(\frac{\pi\omega_m}{2\eta^2}\right)\ \mathrm{dB}. \tag{B.19}$$

$\mathrm{SNR_b}$ corresponds to the output SNR when the information signal, $m(t)$, is sent directly through the additive white noise channel and then filtered with a low-pass

filter with a cut-off frequency of ω_m. Therefore, plotting SNR_{out} as a function of SNR_{b} shows how rate modulation compares to using no modulation. The SNR at the output of the post filter is

$$\text{SNR}_{\text{out}} = 10 \log_{10} \frac{\overline{\hat{m}^2}}{\overline{(\hat{m} - m)^2}} \text{ dB}. \tag{B.20}$$

Results: In presenting the results, the noise output of the demodulator is assumed to be independent of the modulating signal, $m(t)$, which was shown by Sakrison [10]. This assumption allows the modulating signal to be set to zero to simplify the numerical simulations. Figure B-3 shows the demodulator output SNR versus the baseband output SNR for $\beta = 2$, 5, and 10. From the plot, increasing β increases the noise

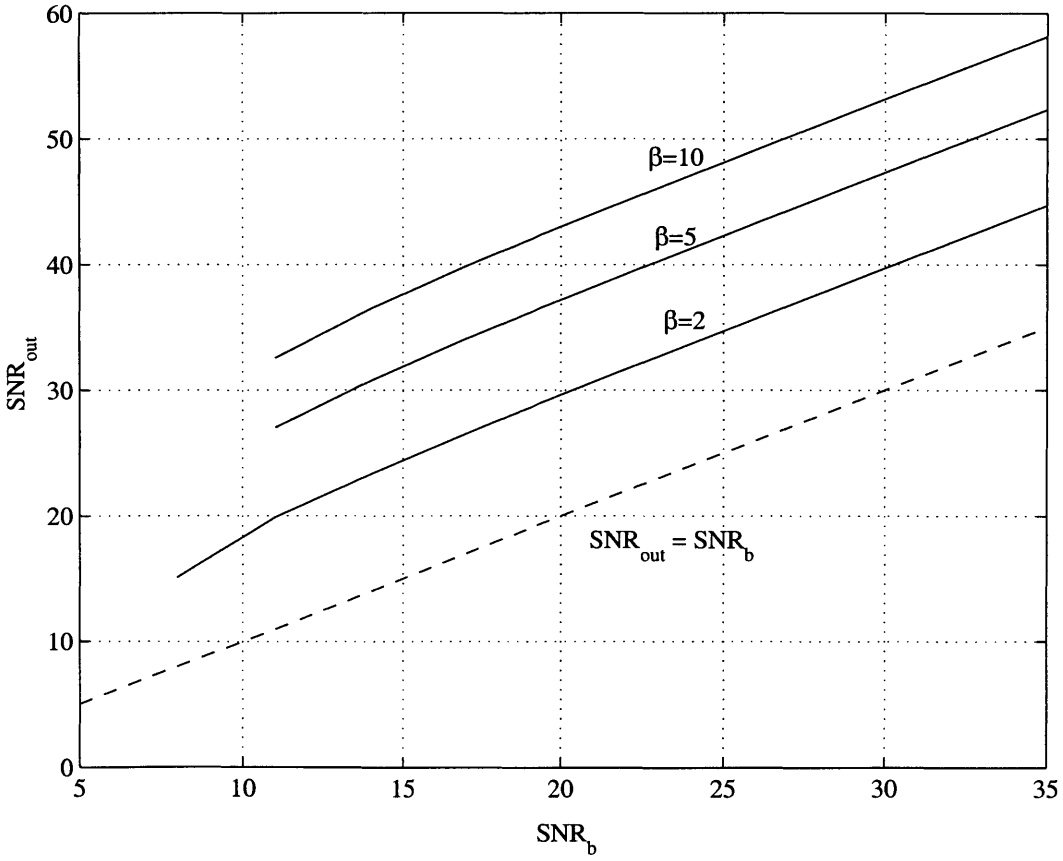

Figure B-3: SNR_{out} vs. SNR_{b} for $\beta = 2$, 5, and 10 for the PLL.

immunity.

The results of the QMNC technique are compared with a direct simulation of the SDE. The direct simulation corresponds to $\beta = 2$ and $SNR_b = 14$ dB, which corresponds to the data point marked with a star in Figure B-3. From the direct simulation, the estimated output SNR is 23.24 dB and the QMNC technique estimates the output SNR to be 23.35 dB. The pdf of the output noise process estimated from the direct simulation and the pdf estimated from the QMNC technique are compared in Figure B-4.

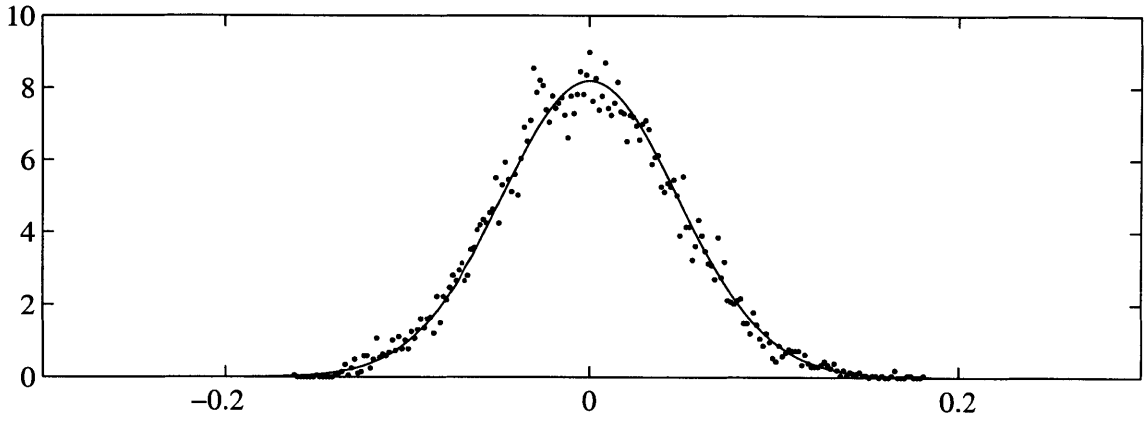

Figure B-4: A comparison of the pdfs for the PLL obtained from the QMNC technique (solid line) and a direct simulation (dots).

Threshold: The PLL exhibits a threshold [11]. At the threshold, the SNR output of the PLL drops of dramatically as $\mathrm{SNR_b}$ is decreased. Second order QMNC is not capable of capturing this phenomenon. Instead the moment equation become unstable. In Figure B-3, the points where the SNR curves terminate are the points at which the equations became unstable. However, these points do not necessarily correspond to the threshold points.

Comparison of QMNC and Analytical Results: For the high input SNR case, the relationship between $\mathrm{SNR_{out}}$ and $\mathrm{SNR_b}$ for a linearization of the PLL model shown in Figure B-2 is [11]

$$\mathrm{SNR_{out}} = \frac{3}{2}\beta^2 \mathrm{SNR_b}. \tag{B.21}$$

Table B.6 compares the output SNR predicted by the QMNC technique to the output SNR predicted by the linearized PLL.

	β					
	2		5		10	
SNR_b	QMNC	Linear	QMNC	Linear	QMNC	Linear
35	43.92	42.78	51.60	50.74	57.90	56.76
32	40.92	39.78	48.88	47.74	54.90	53.76
29	37.91	36.78	45.87	44.74	51.89	50.76
26	34.89	33.78	42.84	41.74	48.87	47.76
23	31.84	30.78	39.80	38.74	45.82	44.76
20	28.75	27.78	36.71	35.74	42.73	41.76

Table B.6: A comparison of the PLL output SNR predicted by QMNC and that predicted by a linearized model of the PLL.

Bibliography

[1] F. Bowman. *Introduction to Bessel Functions.* Dover Publications, New York, 1958.

[2] R. W. Brockett. Notes on stochastic control. Course notes., 2000.

[3] Leon W. Couch. *Digital and Analog Communication Systems.* Prentice-Hall, Upper Saddle River, NJ, sixth edition, 2000.

[4] C. W. Gardiner. *Handbook of Stochastic Methods for Physics, Chemistry and the Natural Sciences.* Springer Series in Synergetics. Springer-Verlag, Berlin, Germany, second edition, 1985.

[5] A. H. Jazwinski. *Stochastic Processes and Filtering Theory.* Mathematics in Science and Engineering. Academic Press, New York, New York, 1970.

[6] H. K. Khalil. *Nonlinear Systems.* Prentice-Hall, Upper Saddle River, NJ, second edition, 1996.

[7] E. N. Lorenz. Deterministic nonperiodic flow. *Journal of the Atmospheric Sciences*, 20:130–141, March 1963.

[8] J. B. Roberts and P. D. Spanos. *Random Vibration and Statistical Linearization.* John Wiley & Sons, New York, New York, 1990.

[9] W. J. Rugh. *Linear System Theory.* Prentice-Hall, Upper Saddle River, NJ, second edition, 1996.

[10] D. Sakrison. *Communication Theory.* John Wiley & Sons, Inc., New York, New York, 1968.

[11] H. Taub and D. Schulling. *Principles of Communication Systems.* McGraw Hill, New York, New York, second edition, 1986.

[12] M. Unser, A. Aldroubi, and M. Eden. B-spline signal processing: Part i – theory. *IEEE Trans. on Sig. Proc.*, 41(2):821–833, February 1993.

[13] Andrew J. Viterbi. *Principles of Coherent Communication.* McGraw-Hill Series in Systems Science. McGraw-Hill, New York, New York, 1966.

[14] A. Wolf, J. B. Swift, H. L. Swinney, and J. A. Vastano. Determining lyapunov exponents from a time series. *Physica D*, 16D(3):285–317, July 1985.